2012-02-06

Dynamics of the Solvent Exchange Reaction of Weakly Bound Organic Solvents to Group 6 Transition Metal Carbonyls and the Molybdenum Hexacarbonyl Mediated Pauson-Khand Reaction

Richard J. Gates
Brigham Young University - Provo

Dynamics of the Solvent Exchange Reaction of Weakly Bound Organic Solvents to Group 6 Transition Metal Carbonyls and the Molybdenum Hexacarbonyl Mediated Pauson-Khand Reaction

Richard J Gates

A dissertation submitted to the faculty of
Brigham Young University
in partial fulfillment of the requirements for the degree of

Doctor of Philosophy

Matthew C. Asplund, chair
Jaron C. Hansen
Roger G. Harrison
Eric T. Sevy
Randall B. Shirts

Department of Chemistry and Biochemistry

Brigham Young University

April 2012

ABSTRACT

Dynamics of the Solvent Exchange Reaction of Weakly Bound
Organic Solvents to Group 6 Transition Metal Carbonyls
and the Molybdenum Hexacarbonyl Mediated
Pauson-Khand Reaction

Richard J Gates
Department of Chemistry and Biochemistry, BYU
Doctor of Philosophy

Many organometallic reactions are solvent-dependent, suggesting solvent molecules interact with reaction intermediates. Studies of the solvent exchange reaction of group 6 transition metal carbonyls with moderately binding ligands have provided insight into these interactions, however, studies of the mechanism for this reaction with weakly binding ligands have not been performed. Experiments were conducted on the nanosecond time scale in methylcyclohexane over the temperature range of 4 to 44 ^{0}C using Step Scan FTIR (SS FTIR) spectroscopy with weakly binding ligands benzene and mesitylene. Upon photolysis of the metal hexacarbonyls, the kinetically favored product ($M(CO)_5$(solv)), decays following pseudo-first-order kinetics to the thermodynamical favored product, $M(CO)_5$(L). The decay is fit using a single exponential decay with a single exponential instrument response function, time zero and an offset. An Arrhenius plot yielded activation energies of 23.7 kJ/mol (M = Mo, L = benzene), 35.1 kJ/mol (M = W, L = benzene) and 29.8 kJ/mol (M = Mo, L = mesitylene). DFT calculations using NWCHEM gave binding energies of 45.8 and 54.3 kJ mol^{-1} for $Mo(CO)_5C_6H_{12}$ and $W(CO)_5C_6H_{12}$. The experimental and computational results suggest the exchange mechanism proceeds through an associative pathway, were slightly negative values of the entropy of reaction denote that the transition state has greater metal solvent bond breaking character then the more moderately binding ligands in the literature.

Density Functional theory was used to calculate C-O vibrational frequencies of metal carbonyl complexes measured in our work and other complexes from the literature, with density functionals B3LYP, M06 and M06-L. Measured and computational frequencies were compared to obtain both an overall vibrational shift and a scaling factor. Scaling factors were found to be 0.9519±0.0095 for B3LYP, 0.9429 ± 0.0087 for M06 and 0.9565 ± 0.0095 for M06-L with overall shifts of 102 ± 16, 121 ± 15, 93 ± 17 cm^{-1}, respectively.

The molybdenum mediated Pauson-Khand reaction, a [2+2+1] cyclo-addition begins very similarly to the solvent exchange reaction on molybdenum. The initial product, the solvated complex, decays away with pseudo-first-order kinetics as the solvent is replaced by the C-C triple bond in 2-(2-propen-1-yl)-2-(2-propyn-1-yl)-,1,3-diethyl ester. An Arrhenius plot over the temperature range of -8 to 20^o C yielded an energy of activation of 15.6 kJ/mol.

Keywords: [Kinetics; molybdenum; tungsten; group six metal carbonyls;]

ACKNOWLEDGEMENTS

First, I am grateful for the environment of learning at Brigham Young University, for funding from the Department of Chemistry and Biochemistry, and for the use of the Fulton Supercomputing Lab. In the Asplund lab, I have learned that research is not something one does between the hour you show up in the morning and when you go home in the evening; rather you must work at it, until it becomes a part of who you are. I am thankful for Dr. Matthew Asplund for allowing me the time to come to understand this and for the many undergraduates who have worked on our research projects: Carolyn (who also earned her Masters degree in the Asplund lab), Elliot, Bryon, Andrew, Nick, Jacob, Chris, and Nathan. I also owe special thanks for the NSF grant which purchased the Continuum Precision II and Continuum Panther OPO in the laser lab in the Benson Building and to Nick for helping me rediscover my excitement for research, without either of these the data within this dissertation would not have been collected.

In addition to those in the chemistry department, I would like to thank my family for being there to share in the triumphs and the trials. I look forward to having many more “sciency” discussions with you. I am grateful for my fiancé, Elisabeth, for helping me look forward to the finish; you are wonderful.

Table of Contents

List of Equations

List of Fiqures

List of Tables

Chapter 1: A Review of Group 6 Transition Metal Exchange Dynamics

1.1 Introduction

Upon photolysis, $M(CO)_6$ loses a CO leaving the "naked" pentacarbonyl complex. Lian et al.[1] found this complex to form within the 240 fs time resolution of their experiments. The "naked" $M(CO)_5$ is solvated within 25 ps,[2] and in neat organic solutions, this complex lasts for microseconds.[3] A solvent exchange reaction occurs with the addition of a more strongly binding secondary solvent (see **Equation 1.1**, where the secondary solvent is denoted as L)

$$M(CO)_5(solv) + L \rightarrow M(CO)_5(L) + solv \qquad \textbf{Equation 1.1}$$

Our interest in looking at ligand exchange reactions has grown out of the results of ultrafast transient IR studies of transition metal carbonyl chemistry. Asplund et al.,[4] studied C-H bond activation dynamics on the femtosecond time scale using a home built amplified Ti:Saphire laser for times up to 1 ns. For longer times, they used a FTIR spectrometer (Bruker model IFS 88) modified for Step Scan FTIR (SS FTIR) spectroscopy with a fast IR detector and electronics capable of 25 ns time slices. Loss of CO after photolysis of $Tp^*Rh(CO)_2$ (Tp^* = HB-$(Pz)_3$, Pz = 3,5-dimethyl pyrazolyl) yields a monocarbonyl species on time scale of 350 fs, which quickly complexes with a solvent alkane molecule, vibrationally cools in 20 ps and converts to a second monocarbonyl through dechelation of the Tp* ligand from η^3 to η^2 in 200 ps. Ligands bond to transition metals by donate electron character to the metal center, an η^1 bond is donation through a single electron while and η^3 bond is donation through a pair of electrons or a π cloud. SS FTIR spectroscopy

measurements of this second monocarbonyl performed on a 25 ns time scale show that this transient has an approximate 230 ns lifetime in cyclohexane, after which it converts into the final C-H bond activated product. Asplund et al., saw solvation almost instantaneously, in 20 ps, after photolysis of the metal carbonyl complex and formation of the reactive intermediate. With a similar UV pump IR probe experiment, To and coworkers[5] studied the chelation dynamics of ligands with tethered thioethers on a chromium metal center. Tethering these groups allows for two separate reaction pathways, a fast metal-sulfur chelation, which occurs in the first 100 ps after photolysis, and a slower solvation pathway. The solvated complex converts to the chelated form in about 30 ns. The ratios of the fast metal-S chelation and slower solvation pathway were measured in different solvents. The chelation dynamics for the complexes studied are similar for n-heptane and THF (ratios of 1:2 and 1:2 for n-heptane and 1:3 and 1:1 for THF), except for THF, the chelation pathway through the Cr-THF solvated complex dominates. Experiments in acetonitrile only yield the solvated complex.

While studying Si-H bond activation by manganese and rhenium complexes in neat triethylsilane using femtosecond and nanosecond UV pump-IR probe spectroscopy, Yang et al.[6] also observed the reaction proceeding through two separate pathways; initial solvation of the metal carbonyls through the Si-H bond or an ethyl group of the solvent.

Organometallic reactions are important in catalysis and the synthesis of organic molecules. Many of these reactions begin with the creation of a highly

reactive coordinatively unsaturated metal center that coordinates with a nearby solvent molecule before reacting further to form desired products; therefore, the choice of solvent has the ability to drive the chemistry. **Equation 1.1** is a simplified test reaction for these types of reactions using group 6 metal carbonyls. However, the mechanism of this reaction has been of some debate over the last few decades. If the solvent exchange reaction in **Equation 1.1** follows a dissociative mechanism, the enthalpy of reaction would be the same magnitude as the metal solvent dissociation energy of $M(CO)_5(solv)$ and the transition state would be the "naked" $M(CO)_5$ complex. The exchanging ligand would have to wait in the solvation shell of the solvated metal carbonyl complex until the dissociation of the solvent.

If the enthalpy of reaction was much lower, with a more energetically favorable transition state, the reaction would follow an associative reaction. The transition state would be more ordered and contain both metal-solvent and metal-ligand bonding character. The binding strength of entering ligand and exiting solvent would both play a role in the energy and geometry of the transition state. For either dissociative or associative mechanisms, the choice of solvent affects the rate of reaction, reaction yields and activation energies.

Group 6 metal hexacarbonyls are used as a prototype system in this work to probe solvation and chelation dynamics. Although group 6 metal carbonyls are not widely used in industry or for synthetic purposes, studies of these complexes can be used to provide greater understanding for more general chemical principles. They

make great test molecules because they are unreactive at ambient temperatures until photolysis, their carbonyl vibrational frequencies are particularly easy to identify in the IR region of approximately 1800 to 2250 cm^{-1}, and their spectrum is prone to shifting due to changing chemistry around the metal center. This effect is caused by electron density on the metal d *t2g* orbitals backbonding into the π* antibonding orbitals of the carbonyl, thus weakening the C-O triple bond. Upon photolysis of $M(CO)_6$ (M = Cr, Mo, W) in solution, a CO is lost, followed by solvation of the highly reactive coordinatively unsaturated metal. This kinetically favorable product can continue to react further to form a more thermodynamically favorable product, either through internal rearrangement, or through exchange with other solution phase ligands. Understanding the single-step formation of these solvated intermediates and the exchange with a secondary organic solvent is important in understanding the reaction dynamics of overall reactions.

Chemists have studied the kinetics of these reactions with matrix isolation,[7] in the gas phase,[8] in unreactive liquid noble gases[9] and in the solution phase using NMR,[10] photoacoustic calorimetry (PAC),[11] UV[11e, 12] and IR[7a, 8, 12c, d, 13] detection. These experiments have focused on the measurement of strong to moderately binding organic solvents to group 6 transition metal carbonyls.

1.2 Matrix Isolation

Matrix isolation is a technique of trapping a material inside an unreactive host matrix, usually a frozen liquid or gas. These trapped materials, called guest particles, are isolated within a continuous solid phase host matrix. George C.

Pimentel, often referred to as the father of matrix isolation, used inert gases like xenon and nitrogen as a host material. Matrix isolation often refers to the trapping of gases in low temperature solids, a guest particle usually being diluted within the gas phase before cooling to approximately 10 K. These low temperatures allow for easy identification and observation of otherwise short-lived or highly reactive species using spectroscopic methods.

Building upon the work by Rest[14] with polymer matrices, Goff and coworkers[7b] developed a miniature high pressure cell attached to a modified matrix isolation apparatus. The result is an apparatus which can be cooled to cryogenic temperatures (T < 30 K) and filled to high pressure (P > 34 MPa). The organometallic compounds being studied were impregnated into a polymer film before being surrounded by high pressure gas. UV photolysis of $M(CO)_6$ under pressures of N_2 leads to the formation of $M(CO)_5N_2$ and $M(CO)_{(6-n)}(N_2)_n$ complexes. UV photolysis of $M(CO)_6$ under pressures of H_2 only leads to the formation of the single substituted $M(CO)_5(\eta^2\text{-}H_2)$ or the doubly substituted cis-$M(CO)_4(\eta^2\text{-}H_2)_2$. Goff and coworkers also observed the formation of H_2 and N_2 complexes upon the photolysis of $W(CO)_5CS$ and $M(CO)_3(\eta^6\text{-mesitylene})$. For these experiments they observed the reactivity followed the order Mo > Cr > W. We will discuss the significance of this in Chapter 5.

1.3 Gas Phase

Gas phase kinetic measurements for the recombination of $Cr(CO)_5^*$ with CO following dissociation of L = H_2, CH_4, C_2H_4, C_2F_4, C_6H_6 and C_6F_6 were conducted

by Wells[15] at chromium hexacarbonyl partial pressures of 65–130 mTorr and ligand partial pressures of 0.7–80 Torr were studied a CaF_2 capped 16 cm Pyrex cell. The metal carbonyl was pumped using a frequency tripled Nd:YAG (355 nm) or a XeF eximer laser (351nm) and probed by a home built, line tunable CO_2 laser. Reactions were monitored using a fast InSb detector. Bond enthalpies for $Cr(CO)_5L$ with L = H_2 (15.2 kcal/mol), C_2H_4 (24.7 kcal/mol), C_2F_4 (19.7 kcal/mol) and C_6H_6 (13.7 kcal/mol) were calculated from kinetic data and estimated for L = CH_4 (8 kcal/mol) and C_6F_6 (8 kcal/mol).

1.4 Liquid Noble Gases

Turner and coworkers[9b] investigated the substitution of carbonyls by N_2 on $Cr(CO)_6$ by UV photolysis using a Philip HPK- 125W medium-pressure Hg arc in a N_2 doped liquid Kr solution (~183 K). IR spectra were recorded by a Perkin-Elmer 283B spectrometer or Nicolet MX-3600 FT IR spectrometer with a resolution of 0.6 cm^{-1}. In addition to IR detection, UV-Vis spectra were recorded with a Perkin-Elmer Lambda 5 UV-Vis spectrometer. The low temperature, high pressure cell needed to conduct liquid noble gas experiments designed by Maier and Stewart[16], consists of a copper block with windows sealed in place with lead gaskets; the one cm path length cell is cooled by pulses of liquid nitrogen. The length of the pulses needed to control the temperature of the cell is monitored by a thermocouple calibrated by the freezing point of liquid Xe. IR absorptions for $Cr(CO)_5N_2$ were recorded at 1913.3, 1938.5, 1975.5, and 2073.9 cm^{-1}. In addition, this liquid noble gas data was used to

compare and analyze previously acquired matrix isolation data, which was otherwise unyielding of information.

1.5 Solution Phase

1.5.1 Photoacoustic Calorimetry

Photoacoustic Calorimetry (PAC) is an important technique in studying the kinetics of **Equation 1.1** because it can measure both the absolute enthalpy of a reaction (ΔH_{rxn}) and enthalpy of activation ($\Delta H^{\ddagger}$), where techniques using UV-Vis or IR detection only measure the latter. The basic operation of PAC as explained by Yang,[11h] Jiao[11d] and in more detail by Peters and coworkers[11f, g] is as follows. Photolysis of a sample solution generates an acoustic signal dependent upon the heats, volumes, and rates of reaction. The response of a transducer to an acoustic wave is modeled as a point source and a point detector. For a 1 MHz transducer, the acoustic wave gives rise to a waveform for transients with lifetimes of 50 ns to 50 μs. The measured time-resolved photoacoustic waveform, $C_{exp}(t)$, is a convolution of a time-dependent heat source, $E(t)$, and the transducer response function, $T(t)$. The deconvolution procedure described by Peters[11f, g] involves the calculating of a heat wave, $C_{calc}(t)$ with parameters T_k, the transients' decay lifetime, and Φ_k, a representation of the fraction of heat released as the transient k decays. The calculated and measured waveforms are compared; minimizing residuals results in the best fit values for T_k and Φ_k.

Studies on the effects of reaction volumes on reaction enthalpies of **Equation 1.1** with L = straight chain alkanes using PAC were conducted by Jiao[11d] and

coworkers. $Mo(CO)_6$ was chosen to be studied over $Cr(CO)_6$ because the quantum yields of the latter are dependent upon the length of a straight chain alkane. This effect can be attributed to sterics; the larger molybdenum is able to bind more similarly with primary and secondary hydrocarbons compared to the smaller chromium. This can be explained by an analysis of the hydrogen reaction volume of primary and secondary hydrocarbons; an increase in the length of a straight hydrocarbon chain increases the number and therefore volume of secondary hydrogens, while the primary hydrogens remains constant. A Cr-alkane interaction probability decreases as the length of the hydrocarbon chain length increases due to sterics around the smaller Cr atom, and therefore the probability of CO recombination increases. The enthalpies for the formation of $Mo(CO)_5$(alkane) from the photolysis of $Mo(CO)_6$ in alkane, and the solvent exchange reaction with L = THF were measured to be 30 kcal/mol and 14 kcal/mol respectively.

1.5.2 UV Studies

With both UV spectroscopy and photoacoustic calorimetry, Morse and coworkers[11e] measured the bond enthalpies of $M(CO)_5$(solv) (M=Cr, Mo, W and solv=alkane). They noted the way to determine if these types of weak metal-ligand bonds play an important role in ligand exchange reactions (**Equation 1.1**) is to measure the metal-solvent bond enthalpy. A bond enthalpy on the order of 4.1 kJ/mole indicates the weakly bound metal-ligand complex is in equilibrium with the coordinatively unsaturated metal complex. If it is stronger, the weakly bound-metal solvent complex dominates. Although they could not rule out a dissociative

pathway, they concluded that the formation of $M(CO)_5$(solv) occurs through an associative process. They found the $Cr(CO)_5C_6H_{12}$ bond enthalpy to be 24.2 kcal/mol.

Dobson and Zhang[12b] measured the kinetics and deduced the mechanism for **Equation 1.1** for M = Cr, solv = n-heptane and L = a series of ligands (piperidine, tetrahydrofuran, pyridine, acetonitrile, 2-picoline, ethanol, 1-hexene, chlorobenzene and 2,6-lutidine) with pulsed laser flash photolysis and UV detection. The reaction takes place with a competition between associative and dissociative mechanisms. The overall mechanism is dependent on the identity of the solvent and L,[12e, 17] where ligands with greater steric hindrance predominantly followed a dissociative pathway. PAC experiments conducted by Peters et al.[11h] on this reaction with various ligands bonding through N, O and P atoms or π orbitals, showed a 10-fold variation in the rate of exchange for acetonitrile to 1-hexene as ligands. This suggests that **Equation 1.1** proceeds through an interchange mechanism where the transition state has "a high degree of heptane-Cr bond lengthening concurrent with the association of the incoming ligand".[11h] Dobson found for the solvent 1-hexene the reaction proceeds through a purely dissociative ligand exchange; however, acetonitrile has competing dissociative and a late transition state associative mechanism. The activation energies for the series of pyridine, 2-picoline and 2,6-lutidine shifts from an interchange to dissociative pathways with increasing sterics. Less sterically hindered ligands are more likely to proceed through a late transition state associative mechanism, where ligands with greater sterics are likely to

proceed by a dissociative mechanism. A plot of $\Delta S^{\ddagger}$ vs. $\Delta H^{\ddagger}$ shows values of $\Delta S^{\ddagger}$ increase regularly as $\Delta H^{\ddagger}$ values increase. Dobson presumes that the mechanism changes from associative interchange to dissociative to as the ligand changes from unhindered to hindered, where the upper limit of $\Delta H^{\ddagger}$ is the bond dissociation energy of Cr-(solv) (solv = n-heptane in this experiment), determined by Dobson to be 8 kcal/mole. This energy was measured by Burkey to be 11.62 kcal/mole.[11a]

1.5.3 IR Studies

Until the use of an IR detection system by Hermann and coworkers,[13d] the study of transients using flash photolysis was restricted to the use of UV-Vis detection. The observed electronic absorption bands allowed for little information about structural properties of the molecules. The use of an IR detector system permitted the recording of IR absorptions and kinetics of transients with lifetimes ≥ 5 μs in solution. A standard IR system consists of two quartz capillary flash lamps passing through a sample cell on the same side as an IR globar source. The IR is directed through a double monochromator with two gratings of 150 grooves per mm. Due to the low intensity of the globar source, the monochromator slits were left open to 1.25 mm, which results in a resolution of 0.01 to 0.02 microns. Measurements were carried out with an InSb photodiode; however, there was a large drop in signal from 5 to 6 μm, and, therefore, a mercury cadmium telluride (HgCdTe) photodiode, which also has a faster response, was used in this range. The system was tested by studying the solvent exchange reaction (**Equation 1.1**) with M = Cr, Mo, W in neat solvent (solv = cyclohexane) as well as in solutions with the

addition of a secondary ligand (L = acetone, benzene, and methanol). $M(CO)_5$(solv) disappeared with a first-order rate constant, *k*, whose inverse increases linearly with concentration of the secondary ligand. First observed by Kelly et al.,[12e] Herman also observed $M(CO)_5$(L) (the product of **Equation 1.1**) to further react with a trace contaminant X, identified to be water[13c, d] by the addition of H_2O to tungsten hexacarbonyl solutions. This accelerated the decay of $W(CO)_5$(solv) and the formation of $W(CO)_5$(X).

Using SS FTIR spectroscopy, Krav-Ami and Shultz[18] measured the rates of reaction of the **Equation 1.1** with $W(CO)_5$ in cyclohexane for a series of ligands. The rate of reaction was observed to linearly increase with a larger red shift in the IR spectrum of $W(CO)_5$L for L = pyrrolidine to furan. Increased backbonding from the metal center into the CO π* antibonding orbitals weakens the CO bond strength, creating a red shift in the CO vibrational spectra. This, in turn, can be interpreted as an increase in electron donating ability of the ligand. Thus, the larger the CO red shift, the greater the electron donating ability of the ligand, and, therefore, the better able it is to stabilize the transition state. This analysis lead Krav-Ami and coworkers to propose an associative mechanism with a transition state which has the solvent cyclohexane still within the coordination sphere of tungsten.

Shagal and coworkers[13k] investigated the linkage isomerization reaction

$$M(CO)_5(\eta^1\text{-}L) \rightarrow M(CO)_5(\eta^2\text{-}L) \qquad \textbf{Equation 1.2}$$

with M = Cr, Mo, W and L = 2-methyl-2,3-dihydrofuran or 2,3-dihydropyran with time-resolved infrared absorption spectroscopy and SS FTIR in cyclohexane solution. Photolysis of the metal hexacarbonyl produced the oxygen bound η^1-complex which further reacted intramolecularly to form an equilibrium mixture of the η^1 and η^2 complex (bound through C-C double bond). For sufficiently high concentrations of L, the solvent cage of the "naked" $M(CO)_5$ formed after photolysis of $M(CO)_6$ would contain some molecules of L. Therefore, following photolysis, "naked" $M(CO)_5$ would sometimes react with L to form the η^1 and η^2 product. However, while Shagal observed the formation of the η^1 product, no evidence of the η^2 product was found, which is in agreement with experiments performed by Dobson and coworkers[17d] on the linkage isomerization of $Cr(CO)_5$ with 5-chloropent-1-ene. The preference of the "naked M(CO)5 to react to form the η^1 product over the η^2 occurs even though "naked" $M(CO)_5$ does not tend to discriminate between potential reaction partners.[13k, 19] Shagal and coworkers also discussed the order of reactivity of the solvated group 6 metal pentacarbonyls, which follows Mo>Cr>W. The higher reactivity of Mo is explained as being primarily an enthalpic effect; whereas the difference between W and Cr is entropic (a further discussion of this order can be found in Chapter 4). The reactivity of a set ligand is dependent upon the geometry of the $M(CO)_5(\eta^1$-L) complex with the complex that requires the least rearrangement from η^1 to η^2 occurring most rapidly.

1.6 Determination of the Mechanism of Solvent Exchange

The mechanism of solvent exchange in group 6 transition metal carbonyls (**Equation 1.1**) has been a point of discussion for the last few decades. The dissociative pathway could be generalized by thinking of the solvent on the solvated intermediate as randomly detaching and reattaching. The ligand would need to wait until solvent detaches before it could bond with the metal pentacarbonyl. For the coordinatively unsaturated metal pentacarbonyl to be in equilibrium with the solvated complex, the bond enthalpy would have to be approximately 1 kcal/mole, and the coordinatively unsaturated metal pentacarbonyl is not likely to form for stronger binding solvents as the energy to break this agostic bond is not available at room temperature.[11e] The associative pathway could be generalized as the entering ligand being strong enough to push the solvent away from the metal as it enters. Either mechanism should appear to have a measurable transient species, one with a decreased coordination number and the other with an increased coordination number. However, we only see the reaction as going from the solvated complex to the weakly bound ligand complex with no intermediates. I believe, because of this, the identification of the reaction mechanism has been an issue of debate in the literature.

While the formation of $M(CO)_5(L)$ in **Equation 1.1** is dependent upon the concentrations of $M(CO)_5(solv)$ and the ligand, because the ligand is in such excess, the reaction rate follows pseudo-first-order kinetics. A second-order rate constant for a given temperature, independent of ligand concentration, can be determined by

measuring the reaction rate over a range of ligand concentrations. Using SS FTIR spectroscopy, Krav-Ami and Schultz[18] investigated **Equation 1.1** with L equal to a series of five-membered N and O containing heterocyclic rings. They observed a correlation between rate constants and product properties, namely, the red shift in the CO stretching frequencies of the product, $W(CO)_5(L)$ complex increases as the room temperature ligand (L) independent rate constants increases, indicating the exchange reaction occurs with a late transition state. For more strongly binding or better Lewis base character the incoming ligands has, the more electron density is donated to the metal center and the more associative the reaction is. When more electron density is donated into the metal, there is greater π backbonding into the π* antibonding orbital of the carbonyls, weakening the CO bonds and shifting their stretches to lower frequencies.

Paur-Afshari et al.[13h] studied the exchange kinetics of **Equation 1.1** with L = tetrahydrofuran (THF). They measured the enthalpy of activation for $W(CO)_5THF$ in cyclohexane solution to be considerably lower than the bond dissociation energy of $W(CO)_5C_6H_{12}$ of 15 kcal/mole. If the solvent exchange reaction were purely dissociative, the reaction would proceed first by the leaving or dissociation of cyclohexane and second by the entering of the secondary solvent (in Paur-Afshari's studies this would be THF). Because the enthalpy of activation is much smaller than the literature value of the bond dissociation energy of cyclohexane, a more energetically favorable transition state must exist. They also observed that the reaction proceeds more slowly in C_6D_{12} even though $\Delta H^{\ddagger}$ is smaller than for

cyclohexane. This observation suggests that the solvent has a large entropic contribution to the reaction energetics, possibly due to low frequency metal solvent hindered rotations.

In continuation of the Schultz group's work with THF, Lugovskoy and coworkers[13f] measured the rates of **Equation 1.1** with L = furan, 2-3,dihydrofuran and 2,5-dihydrofuran using SS FTIR spectroscopy. The low enthalpies of activation support the findings of the THF data (for L = furan, $\Delta H^{\ddagger} = 7.1 \pm 0.7$ kcal mol^{-1} and $\Delta S^{\ddagger} = -7.1 \pm 5.1$ eu; for L = 2,3-dihydrofuran, $\Delta H^{\ddagger} = 5.9 \pm 0.5$ kcal mol^{-1} and $\Delta S^{\ddagger} = -8.9 \pm 7.3$ eu; for L = 2,5-dihydrofuran, $\Delta H^{\ddagger} = 3.8 \pm 0.2$ kcal mol^{-1} and $\Delta S^{\ddagger} = -14.0 \pm 3.5$ e.u.; and for L = THF, $\Delta H^{\ddagger} = 3.6 \pm 0.2$ kcal mol^{-1} and $\Delta S^{\ddagger} = -13.7 \pm 2.5$ eu). They also observed large negative values for the entropies of activation, providing evidence that the rate determining step is not solvent dissociation. Lacking evidence of an intermediate of increased coordination sphere around the central metal, Lugovskoy calls the solvent exchange reaction shown by group 6 transition metal carbonyls an associative interchange (I_a) mechanism. An associative interchange mechanism is analogous to an associative mechanism that occurs through a late transition state.

1.7 Conclusions

Solvation of coordinatively unsaturated metal carbonyls occurs in the first 20 ps after the photolysis of the parent metal hexacarbonyl. Because solvents interact with reaction intermediates, they may play an important role in organometallic reactions. The solvent exchange reaction of group 6 metal carbonyls (**Equation 1.1**)

is used to test these noncovalent interactions with weakly bound organic solvents. **Equation 1.1** proceeds through an associative mechanism with a late transition state for ligands with strong to moderate binding strength, with a transition state that has less metal-solvent bond breaking than metal-ligand (secondary solvent) bond forming. While some measurements of the pseudo-first-order rate constants for more weakly binding ligands have been measured, a full-temperature resolved analysis and calculation of the activation energy and enthalpy of reaction have not been conducted. We have measured these thermodynamical values for the exchange of methylcyclohexane by benzene and mesitylene for the group six transition metal carbonyls of molybdenum and tungsten. In addition, we have measured the activation energy of first step in the molybdenum mediated Pauson-Khand reaction and identified the time constant and vibrational frequencies of the second step in this mechanism.

Our work to determine the mechanism of **Equation 1.1** has been divided into the following chapters. Chapter 2 is a detailed summary of the methods we used to measure the reaction in **Equation 1.1**, extract the kinetic data from each temperature resolved run and calculate thermodynamic properties of the reaction using an Arrhenius plot and Eyring analysis. This chapter will also include a section describing the computational techniques we have used to calculate theoretical carbonyl vibrational frequencies and bond dissociation energies of $M(CO)_5$(solv) and $M(CO)_5L$ (M =Cr, Mo, W). Chapter 3 will address the need of a computational method for identifying short-lived intermediates using carbonyl

vibrational frequencies. We calculated a scaling factor and overall vibrational shift in wavenumbers to scale computational frequencies to be compared with measured frequencies. The measured frequencies came from our work with the exchange reaction **Equation 1.1** of and other metal carbonyl complexes found in the literature. Our work on the solvent exchange reaction is found in Chapter 4. We will evaluate the dynamics of the solvent exchange reaction with the weakly binding ligands benzene and mesitylene using Step Scan FTIR spectroscopy and calculate the activation energy, enthalpy of reaction and entropy of reaction of these reactions. As a continuation of the solvent exchange reaction, Chapter 5 will introduce the kinetics of the Pauson-Khand reaction, a [2 + 2 + 1] cycloaddition of an alkyne, alkene and carbon dioxide to form a cyclopentanone. Chapter 6 will include a summary of the results of the previous 5 chapters, additional work to be completed and ending conclusions.

In addition to these chapters I have also included an appendix with detailed instructions and standard operating procedures for the benefit of future researchers in the Asplund laboratory.

.

1.8 References

1. Lian, T. Q.; Bromberg, S. E.; Asplund, M. C.; Yang, H.; Harris, C. B., Femtosecond Infrared Studies of the Dissociation and Dynamics of Transition Metal Carbonyls in Solution. *J. Phys. Chem.* **1996,** *100*, 11994–12001.

2. Welch, J. A.; Peters, K. S.; Vaida, V., Medium Effects on the Photodissociation of Hexacarbonylchromium ($Cr(CO)_6$). *J. Phys. Chem.* **1982,** *86*, 1941–1947.

3. Sheffield, C. Time-Resolved Infrared Spectroscopy and Density Functional Theory Study of Weak Interactions of Metal Carbonyls and Organic Solvents. Brigham Young University, Provo, 2010.

4. Asplund, M. C.; Yang, H.; Kotz, K. T.; Bromberg, S. E.; Wilkens, M. J.; Harris, C. B., Femtosecond Infrared Studies of Chemical Bond Activation. *Laser Chem.* **1999,** *19*, 253–262.

5. To, T. T.; Heilweil, E. J.; Duke, C. B.; Burkey, T. J., Solvent and Structural Effects on Ultrafast Chelation Dynamics of Arene Chromium Tricarbonyl Sulfide Derivatives. *J. Phys. Chem. A* **2007,** *111*, 6933–6937.

6. Yang, H.; Asplund, M. C.; Kotz, K. T.; Wilkens, M. J.; Frei, H.; Harris, C. B., Reaction Mechanism of Silicon-Hydrogen Bond Activation Studied Using Femtosecond to Nanosecond IR Spectroscopy and Ab Initio Methods. *J. Am. Chem. Soc.* **1998,** *120*, 10154–10165.

7. (a) Burdett, J. K.; Downs, A. J.; Gaskill, G. P.; Graham, M. A.; Turner, J. J.; Turner, R. F., Characterization by Infrared and Raman Spectroscopy of Matrix-Isolated $M(CO)_5N_2$ (M = Chromium, Molybdenum, or Tungsten) Produced by Photolysis of $M(CO)_6$. *Inorg. Chem.* **1978,** *17*, 523–532; (b) Goff, S. E. J.; Nolan, T. F.; George, M. W.; Poliakoff, M., Chemistry of Reactive Organometallic Compounds at Low Temperatures and High Pressures: Reactions of $M(CO)_6$ (M = Cr, Mo, W), $(\eta^6\text{-}C_6H_3Me_3)M(CO)_3$ (M = Cr and Mo), and $W(CO)_5CS$ with H_2 and N_2 in Polyethylene Matrices. *Organometallics* **1998,** *17*, 2730–2737; (c) Graham, M. A.; Poliakoff, M.; Turner, J. J., Photochemistry of the Group VI Hexacarbonyls in Low Temperature Matrices. Part I. The Pentacarbonyls of Chromium, Molybdenum, and Tungsten. *J. Chem. Soc. A* **1971**, 2939–2948.

8. Ishikawa, Y.; Hackett, P. A.; Rayner, D. M., Coordination of Molecular Hydrogen and Nitrogen to Coordinatively Unsaturated Tungsten Carbonyls in the Gas Phase. *J. Phys. Chem.* **1989,** *93*, 652–657.

9. (a) Turner, J. J.; Simpson, M. B.; Poliakoff, M.; Maier, W. B., Synthesis and Decay Kinetics of Tricarbonyldinitrogennickel ($Ni(CO)_3N_2$) in Liquid Krypton: Approximate Determination of the Nickel-Dinitrogen ($Ni\text{-}N_2$) Bond Dissociation Energy. *J. Am. Chem. Soc.* **1983,** *105*, 3898–3904; (b) Turner, J. J.; Simpson, M. B.; Poliakoff, M.; Maier, W. B.; Graham, M. A., Mixed Carbonyl-Dinitrogen Compounds: Synthesis and Thermal Stability of $Cr(CO)_{6\text{-}x}(N_2)_x$ in Liquid Xenon Solution and Low-Temperature Matrixes. *Inorg. Chem.* **1983,** *22*, 911–920.

10. (a) Matthews, S. L.; Pons, V.; Heinekey, D. M., Dihydrogen Complexes of Electrophilic Metal Centers: Observation of $Cr(CO)_5(H_2)$, $W(CO)_5(H_2)$ and $[Re(CO)_5(H_2)]+$. *J. Am. Chem. Soc.* **2004,** *127*, 850–851; (b) Shimoi, M.; Nagai, S.-i.; Ichikawa, M.; Kawano, Y.; Katoh, K.; Uruichi, M.; Ogino, H., Coordination Compounds of Monoborane−Lewis Base Adducts: Syntheses and Structures of $[M(CO)_5(\eta^1\text{-}BH_3\text{-}L)]$ (M = Cr, Mo, W; L = NMe_3, PMe_3, PPh_3). *J. Am. Chem. Soc.* **1999,** *121*, 11704–11712.

11. (a) Burkey, T. L., *Energetics of Organometallic Species*. Kluwer Academic Publishers: Drodrecht, The Netherlands, 1992; (b) Shulin, Z.; Dobson, G. R., Octahedral Metal Carbonyls. 74. Estimates of Solvent-Metal Bond Strengths in (Solvent)$M(CO)_5$ Complexes (Solvent = benzene (M = Mo, W) and Tetrachloromethane (M = Cr)). *Inorg. Chim. Acta* **1991,** *181*, 103–109; (c) Gittermann, S. M.; Letterman, R. G.; Jiao, T.; Leu, G.-L.; DeYonker, N. J.; Webster, C. E.; Burkey, T. J., Bond Energies, Reaction Volumes, and Kinetics for σ- and π-Complexes of $Mo(CO)_5L$. *J. Phys. Chem. A* **2011**, 9004–9013; (d) Jiao, T.; Leu, G.-L.; Farrell, G. J.; Burkey, T. J., Photoacoustic Calorimetry and Quantum Yields of $Mo(CO)_6$ Ligand Exchange in Linear Alkanes: Determination of Volume of Reaction, Energetics, and Kinetics of Nucleophile Displacement of Alkane from $Mo(CO)_5$(Alkane). *J. Am. Chem. Soc.* **2001,** *123*, 4960–4965; (e) Morse, J. M.; Parker, G. H.; Burkey, T. J., Enthalpy of Carbonyl Dissociation from Metal Hexacarbonyls $M(CO)_6$ (M = Chromium, Molybdenum, Tungsten) in Alkane Solvent: Determination of Intermolecular Agostic Bond Strengths. *Organometallics*

1989, *8*, 2471–2474; (f) Rothberg, L. J.; Simon, J. D.; Bernstein, M.; Peters, K. S., Pulsed Laser Photoacoustic Calorimetry of Metastable Secies. *J. Am. Chem. Soc.* **1983,** *105*, 3464–3468; (g) Rudzki, J. E.; Goodman, J. L.; Peters, K. S., Simultaneous Determination of Photoreaction Dynamics and Energetics Using Pulsed, Time-Resolved Photoacoustic Calorimetry. *J. Am. Chem. Soc.* **1985,** *107*, 7849–7854; (h) Yang, G. K.; Vaida, V.; Peters, K. S., Application of Time-Resolved Photoacoustic Calorimetry to Cr-L Bond Enthalpies in $Cr(CO)_5$-L. *Polyhedron* **1988,** *7*, 1619–1622; (i) Zhang, S.; Bajaj, H. C.; Zang, V.; Dobson, G. R.; Vaneldik, R., Volumes of Acitvation for Solvent Displacement-Reactions on Pentacarbonyl Chromium(0) - Comparison of Data for Pure and Mixed-Solvents. *Organometallics* **1992,** *11*, 3901–3903.

12. (a) Bonneau, R.; Kelly, J. M., Flash Photolysis of Chromium Hexacarbonyl in Perfluorocarbon Solvents. Observation of a Highly Reactive Chromium Pentacarbonyl. *J. Am. Chem. Soc.* **1980,** *102*, 1220–1221; (b) Dobson, G. R.; Zhang, S. L., Mechanism of Displacement of Alkanes from Photogenerated (Alkane) $Cr(CO)_5$ Complexes. *J. Coord. Chem.* **1999,** *47*, 409–416; (c) Grills, D. C.; Huang, K.-W.; Muckerman, J. T.; Fujita, E., Kinetic Studies of the Photoinduced Formation of Transition Metal-Dinitrogen Complexes Using Time-Resolved Infrared and UV-vis Spectroscopy. *Coord. Chem. Rev.* **2006,** *250*, 1681–1695; (d) Lees, A. J.; Adamson, A. W., Reaction Kinetics of the Intermediate Produced in the Laser Pulse Photolysis of Tungsten Hexacarbonyl in Fluid Solution. *Inorg. Chem.* **1981,** *20*, 4381–4384; (e) Kelly, J. M.; Bent, D. V.; Hermann, H.; Schultefrohlinde, D.; von Gustorf, E. K.,

Pentacarbonylchromium-Solvent Complexes : Flash-Spectroscopic Determination of Rate Constants of Formation and of Stability Constants and Their Application as Solvent Parameters to Catalytic Butadiene Oligomerisation. *J. Organomet. Chem.* **1974,** *69*, 259–269.

13. (a) Banno, M.; Iwata, K.; Hamaguchi, H.-o., Intra- and Intermolecular Vibrational Energy Transfer in Tungsten Carbonyl Complexes $W(CO)_5(X)$ (X = CO, CS, CH_3CN, and CD_3CN). *J. Chem. Phys.* **2007,** *126*; (b) Barré, C.; Boudot, P.; Kubicki, M. M.; Moiese, C., Synthesis, Spectroscopy, Bonding and Structure in Phosphido Bridged Bimetallics Derived from Bent Metallocenes of Molybdenum and Tungsten and from Group 6 Metal Carbonyls. *Inorg. Chem.* **1995,** *34*, 284–291; (c) Church, S. P.; Grevels, F. W.; Hermann, H.; Schaffner, K., Fast Infrared Detection of Pentacarbonyldinitrogenchromium ($Cr(CO)_5N_2$) in Room-Temperature Solution. *Inorg. Chem.* **1984,** *23*, 3830–3833; (d) Hermann, H.; Grevels, F. W.; Henne, A.; Schaffner, K., Flash Photolysis with Infrared Detection. The Photochemistry and Secondary Thermal Reactions of $M(CO)_6$ [M = Cr, Mo, and W]. *J. Phys. Chem.* **1982,** *86*, 5151–5154; (e) Krishnan, R.; Schultz, R. H., Electronic and Steric Effects in Ligand Substitution at a Transient Organometallic Species: The Reaction of $W(CO)_5$(Cyclohexane) with $(CH_3)_n$THF and $(CH_3)_n$Furan (n = 1, 2). *Organometallics* **2001,** *20*, 3314–3322; (f) Lugovskoy, A.; Paur-Afshari, R.; Schultz, R. H., Reaction of the Transient Species $W(CO)_5$(Cyclohexane) with Cyclo-C_4H_nO (n = 4, 6, 8) Studied by Time-Resolved Infrared Absorption Spectroscopy†. *J. Phys. Chem. A* **2000,** *104*, 10587–10593; (g) Lugovskoy, A.; Shagal, A.; Lugovskoy, S.;

Huppert, I.; Schultz, R. H., Reaction of the Transient Species $W(CO)_5$(Cyclohexane) with Pyrrolidine and with Pyrrole. *Organometallics* **2003,** *22*, 2273–2278; (h) Paur-Afshari, R.; Lin, J.; Schultz, R. H., An Unusual Solvent Isotope Effect in the Reaction of $W(CO)_5$(solv) (solv = Cyclohexane or Cyclohexane-d12) with THF. *Organometallics* **2000,** *19*, 1682–1691; (i) Schoonover, J. R.; Strouse, G. F., Time-Resolved Vibrational Spectroscopy of Electronically Excited Inorganic Complexes in Solution. *Chem. Rev.* **1998,** *98*, 1335–1356; (j) Schultz, R. H.; Biber, L.; Reuvenov, D.; Revzin, T.; Sinai, T.; Zahavi, A., Reactions of the Transient Species $Cr(CO)_5$(cyclohexane) with C_4H_nE (n=4, 8; E = O, NH, S) studied by Time-Resolved IR Absorption Spectroscopy. *J. Chem. Soc., Dalton Trans.* **2007**, 41–51; (k) Shagal, A.; Schultz, R. H., Steric and Electronic Effects in Linkage Isomerization Reactions of $M(CO)_5$(L) (M = Cr, Mo, W; L = 2-methyl-2,3-dihydrofuran, 2,3-dihydropyran). *Organometallics* **2007,** *26*, 4896–4903.

14. Rest, A. J., Infra Dig Matrix Media. *J. Mol. Struct.* **1990,** *222*, 87–93.

15. Wells, J. R.; House, P. G.; Weitz, E., Interaction of H_2 and Prototypical Solvent Molecules with $Cr(CO)_5$ in the Gas Phase. *J. Phys. Chem.* **1994,** *98*, 8343–8351.

16. (a) Morris, D. E.; Basolo, F., Kinetics and Mechanism of Substitution Reactions of Dinitrosyldicarbonyliron(0). *J. Am. Chem. Soc.* **1968,** *90*, 2531–2535; (b) Rest, A. J., IR Evidence for Tricarbonyl(dinitrogen) Nickel, $Ni(CO)_3(N_2)$, in a Nitrogen Matrix at 20 K. *J. Organomet. Chem.* **1972,** *40*, C76–C78.

17. (a) Kelly, J. M.; Long, C.; Bonneau, R., Laser Flash-Photolysis of $Cr(CO)_6$, $Mo(CO)_6$, $W(CO)_6$ in Perfuoromethylcyclohexane - The Generation of Highly Reactive Coordinatively Unsaturated Species. *J. Phys. Chem.* **1983,** *87*, 3344–3349; (b) Ladogana, S.; Dobson, G. R.; Smit, J. P., Bonding of Halogenated Arenes in Photogenerated (Arene)$M(CO)_5$ Complexes (M = Cr, Mo, W). *Inorg. Chim. Acta* **1998,** *278*, 202–208; (c) Ladogana, S.; Nayak, S. K.; Smit, J. P.; Dobson, G. R., Kinetics and Mechanism of Ligand Exchange in Photogenerated (η^2-Monoalkylarene)$Cr(CO)_5$ Complexes with Alkenes: Evidence for Involvement of Aliphatic Chains in the Arene and Alkene in the Exchange Process. *Organometallics* **1997,** *16*, 3051–3054; (d) Ladogana, S.; Nayak, S. K.; Smit, J. P.; Dobson, G. R., Mechanism of Linkage Isomerization in (η1-5-Chloropentene)pentacarbonylchromium(0). *Inorg. Chem.* **1997,** *36*, 650–655; (e) Zhang, S.; Dobson, G. R., Octahedral Metal-Carbonyls. 73. Displacement of Aromatic Solvents (solv) from (solv)$Cr(CO)_5$ Complexes Generated After Flash-Photolysis - Modes of Bonding and Mechanism. *Polyhedron* **1990,** *9*, 2511–2516; (f) Zhang, S. L.; Dobson, G. R.; Zang, V.; Bajaj, H. C.; Vaneldik, R., Octahedral Metal-Carbonyls. 71. Kinetics and Mechanism of Benzne Displacement from Photogenerated (η^2-Benzene)$Cr(CO)_5$. *Inorg. Chem.* **1990,** *29*, 3477–3482.

18. Krav-Ami, S.; H. Schultz, R., When the Ligands Go Marching in: A Step-Scan Fourier Transform Infrared Spectroscopic Study of Ligand Attack at the Transient Species $W(CO)_5$(CyH). *J. Chem. Soc., Dalton Trans.* **1999**, 115–118.

19. (a) Xie, X.; Simon, J. D., Photodissociation of Chromium Hexacarbonyl and Hexakis(Phenyl Isocyanide)Chromium in Tetrahydrofuran. *J. Phys. Chem.* **1989,** *93*, 4401–4404; (b) Simon, J. D.; Peters, K. S., Picosecond Photochemistry of $Cr(CO)_6$: Solvation and Dynamics of the Primary Intermediate. *Chem. Phys. Lett.* **1983,** *98*, 53–56; (c) Lee, M.; Harris, C. B., Ultrafast Studies of Transition Metal Carbonyl Reactions in the Condensed Phase. Solvation of Coordinatively Unsaturated Pentacarbonyls. *J. Am. Chem. Soc.* **1989,** *111*, 8963–8965; (d) Joly, A. G.; Nelson, K. A., Metal Carbonyl Photochemistry in Organic Solvents: Femtosecond Transient Absorption and Preliminary Resonance Raman Spectroscopy. *Chem. Phys.* **1991,** *152*, 69–82.

Chapter 2: Methods

2.1 Reagents

Metal carbonyls were obtained from Aldrich with purities of 97% for $W(CO)_6$, 99% for $Cr(CO)_6$ and 98% for $Mo(CO)_6$ and were stored as received. Solvents used in measuring the thermodynamical properties of the exchange reaction were obtained from; Fisher, HPLC grade cyclohexane and spectranalyzed benzene, Sigma Aldrich, reagent plus 99% methylcyclohexane and Acros, 99% extra pure mesitylene. Reagents used to synthesize the molecules needed to observe the kinetics for the Pauson-Khand reaction were obtained from: Alfa Aesar, 97% diethyl allylmalonate and propargyl bromide 97%, 80% w/w in toluene, Decon Laboratories, Inc., 200 proof ethanol and CCI, ACS grade sodium metal lumps. All solvents were also stored over activated molecular sieves and under argon. Sodium metal lumps were stored under argon.

2.2 Sample Preparation

Metal carbonyl samples were prepared by dissolving 2.5 to 5 mM $M(CO)_6$ (M = Cr, W, and Mo) in methylcyclohexane. Three cycles of freezing at liquid nitrogen temperature, pumping down to approximately 1 mTorr using a diffusion pump and thawing, followed by back filling with argon, were performed to remove any dissolved gasses. Methylcyclohexane was used in replacement of cyclohexane as the primary solvent for all temperature-resolved experiments due to its higher boiling point and lower freezing point. In addition to solutions of metal carbonyls in neat

methylcyclohexane, samples were also prepared with a secondary solvent, 1% to 4% of either benzene or mesitylene.

Reactions were initialized by pumping the Metal to Ligand Charge Transfer (MLCT) bands on the metal carbonyls with a YAG (Continuum Precision II) pumped OPO (Optical Parametric Oscillator, Continuum Panther). Transient species were followed with an FTIR (Bruker IFS/66S) spectrometer equipped with a Mercury Cadmium Telluride (MCT) detector and modified for step scan experiments. A band pass IR filter (1600 to 2600 cm^{-1}) was placed in front of the MCT detector to reduce the number of interferometer points needed to complete each step scan measurement. The timing pulse from the Continuum Precision II was sent through a Stanford Research Digital Delay Pulse Generator (model DG535) to sync the FTIR with the laser pulse. Sample preparation and experiments were carried out under a positive argon pressure of slightly greater than 1 atmosphere.

We discovered some difficulties while understanding the best procedures for preparing samples. First, we observed degradation of samples when they were left under a positive argon pressure overnight. We therefore only made a sample on the day it was needed. We also noticed benzophenone was being introduced as a contaminant, prior to sample preparation during the distillation of our solvents over sodium metal lumps and benzophenone. Benzophenone reacted in much the same way as benzene; the vibrational frequencies for $M(CO)_5$(benzophenone) and $M(CO)_5$(benzene) are equivalent within the frequency resolution of spectra.

Therefore, we could no longer use this distillation process. Finally found that the signal-to-noise of our spectra was greatly improved when we pumped the frozen sample down to 1–2 mTorr the first and second rather than only the third pump.

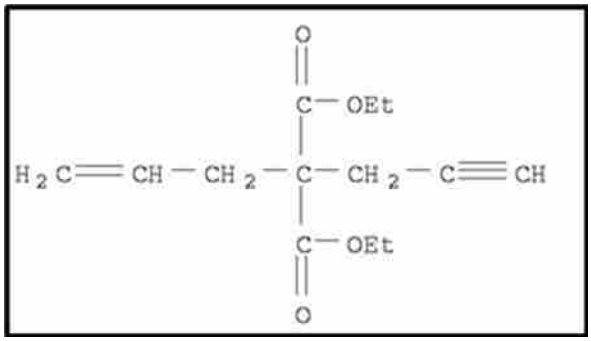

Figure 2.1 **Structure of the Enyne.** Figure produced with the drawing tool in SciFinder.

2.3 Enyne Synthesis

A detailed procedure for the synthesis of 2-(2-propen-1-yl)-2-(2-propyn-1-yl)-, 1,3-diethyl ester (Enyne, see Figure 2.1) solution can be found in Appendix A.[1] Sodium ethoxide was prepared by adding equal molar quantities of sodium metal and 100% ethanol. Sodium metal lumps were carefully trimmed of any sodium hydroxide and cut into small pieces. A solution of diethyl allylmalonate in diethyl ether was prepared and the previously prepared sodium ethoxide was slowly added dropwise to this solution. The sodium ethoxide removes the acidic hydrogen from the diethyl allylmalonate, turning the solution a pale yellow color. Addition of propargyl bromide slowly, over the course of an hour, reacts with the open site on the diethyl allylmalonate. The remaining organics were extracted with a sodium chloride brine solution and washed with ether to remove any enyne. The enyne oil was then dried with magnesium sulfate to remove the aqueous layer and rotovaped to remove excess ether and ethanol.

2.4 Step Scan Spectroscopy

In a standard FTIR spectrometer light from a broadband IR source, typically a glow bar, is split into two parts by a beam splitter (see **Figure 2.2**). Approximately one half is sent to a mirror on a translation stage and the second half is reflected into a stationary mirror. The scanning of the translation stage creates constructive and destructive interference of the waves as the two halves are

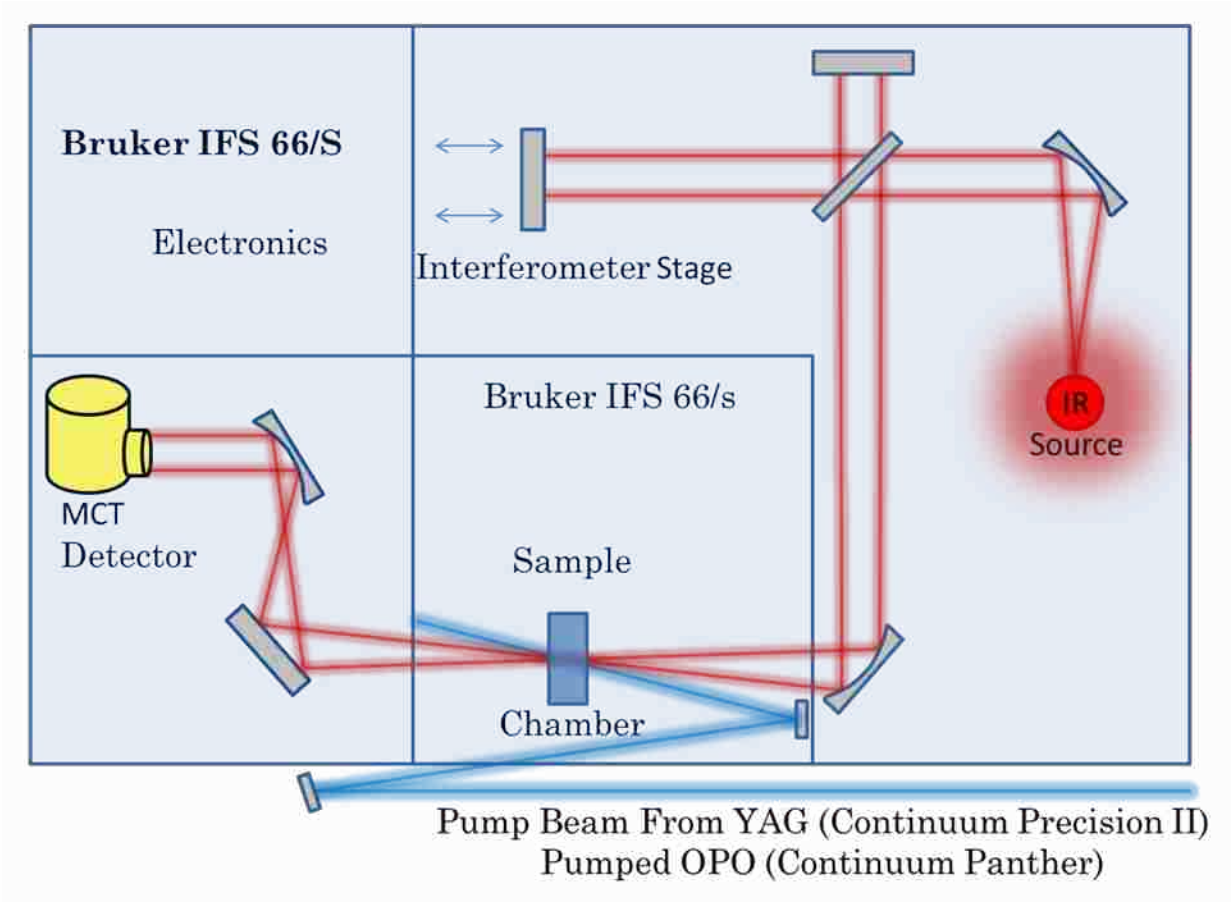

Figure 2.2 Step Scan FTIR step up. A pump beam(blue) from a Continuum Precision II YAG pumped Continuum Panther OPO photolyzes a metal carbonyl in the sample compartment. The photolyzed sample is then monitored in time by a Bruker IFS 66/s FTIR (red).

recombined. The absorption of light by the sample further modifies IR beam. The signal from the detector is then sent to the computer where it is digitized and Fourier Transformed into frequency space. Due to the relatively slow speed of the translation stage, this technique can only collect data on a millisecond time domain. This is not fast enough to observe many chemical reactions.

First described by Uhmann et al.,[2] Step Scan Fourier Transform Infrared (SS FT-IR, see **Figure 2.2**) spectroscopy collects data at n discreet interferometer points, stopping to collect m time traces at each point. Time traces are averaged over multiple coadds to improve signal to noise in a spectrum. Time traces are collected over linearly increasing time slices p. In this way, data is collected in time for each interferometer point and, it is not until all interferometer points are collected that a plot of n verses the intensity ($I_{n,p}$) for each n value yields an interferogram for each time slice p. These interferograms can then be Fourier Transformed to produce a raw 3 dimensional (n, p, $I_{n,p}$) spectrum. Data is collected with a Mercury Cadmium Telluride (MCT) detector and a high speed transient digitizer.

The signal consists of a time-dependent AC and time-independent DC signals. These unprocessed signals are used to calculate the change in absorption of the sample.

$$A = -log\left(\frac{I}{I_0}\right) \qquad \textbf{Equation 2.1}$$

An absorption spectrum can be calculated using **Equation 2.1** where I is equivalent to the sum of the AC and DC scans, and I_0 is equal to the DC scan. A

factor of 4 must also be included due to the preamplifier in the MCT detector; in past experiments, we have also added an external amplifier box to the electronics. Inserting these into **Equation 2.1** with some rearranging, yields:

$$A = -\log\left(1 + \frac{4AC}{DC}\right) \qquad \textbf{Equation 2.2}$$

Even though SS FTIR has advantages over traditional transient IR spectroscopy, which requires a spectrum to be collected at one frequency or time slice at a time, it is not without difficulties. For instance, the number of laser shots necessary to acquire a kinetic trace at a single frequency is the product of the number of interferogram points, n, and the number of coadds, m. The required number of interferogram positions for a 4 cm^{-1} resolution, 1700 cm^{-1} to 2600 cm^{-1} SS FTIR scan is 666, therefore the number of laser shots to complete a single 10 coadd AC scan is 6,660.

Due to the way traditional transient IR spectra are acquired, sample degradation of the sample over the scan may show up in the spectrum, making interpretation of the collected data difficult. In SS FTIR, any sample degradation during a scan is reflected over the entire collected frequency range rather than a subset of frequencies. In addition, the center of the interferogram is collected first and outer tails later, therefore peak positions are unaffected, and only spectral resolution is degraded.

Another difficulty in measuring transient IR signal is the change in refractive index occurring when the temperature of the sample cell increases upon absorption of UV light. This perturbation of η in turn causes a change in the number of IR

photons hitting the detector, which appears as a change in absorption in the 3D spectrum. Often these changes are relatively frequency independent and the overall absorption change occurs across the entire interferogram. Once the Fourier Transform is done the offset is constant and therefore goes to zero. However, in many of our spectra, this is not the case.

Photoinitiated reactions are followed using a Bruker IFS 66 FTIR spectrometer modified for step scan spectroscopy. A Stanford Research Digital Delay Pulse Generator (DDG, model number DG535) is used to synchronize the pump pulse and probe digitization. Detailed instrument settings on the Bruker IFS 66/S FTIR and DDG can be found in **Appendix C**.

To avoid obscuring the SS FTIR spectrum by photolysis of previously formed photoproducts, each laser pulse must photolyze fresh sample; the sample must continuously flow. Directly connecting a pump to the input or output of the FTIR cell would create too much noise in the SS FTIR spectra, therefore, to continuously flow sample, we have created a complex temperature-controlled pump-flow system (see **Figure 2.3**) consisting of two sample glass cells, produced in house, connected by a peristaltic (Masterflex Easy-load II) pump. Several ml of sample is held in the upper glass cell until it is gravity feed through the FTIR cell and into a lower glass cell and is pumped back to the upper glass cell. Temperature control is achieved by flowing ethylene glycol solution through outer jackets on upper and lower glass cells and the FTIR cell.

Reactions are photoinitiated by exciting the MLCT band of $M(CO)_6$ (for M = Mo, λ = 290 nm and for M = W, λ = 290 nm) using a Coherent Precision II laser pumping a Coherent Panther Optical Parametric Oscillator (OPO). 1064 nm light is produced by the Precision II YAG oscillator rod and amplified by an additional two YAG rods. This 1064 nm laser light is then tripled to 355 nm laser light. These 355 nm photons enter into the Panther OPO, where they are used to produce tunable visible laser light. Before this visible light exits the Panther, it is further doubled to the UV range. This laser light is used to pump the MLCT band of the metal carbonyls.

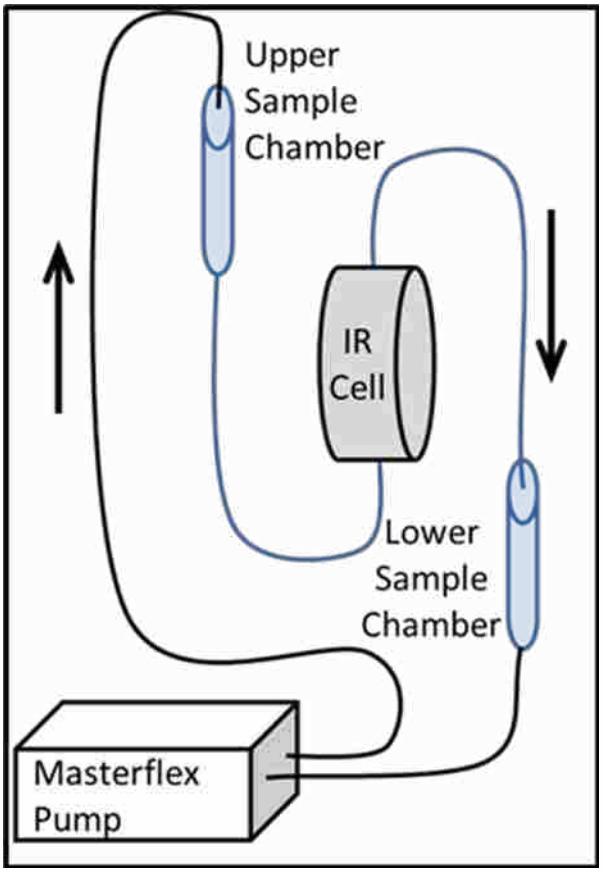

Figure 2.3 Sample Flow System. Sample solutions are inserted into the upper sample chamber and allowed to flow in the direction indicated by the arrows through Teflon tubing through the IR sample cell to the lower sample chamber. The solution is then pumped back to the upper chamber via a Masterflex Easy-Load II Pump equipped with #14 Masterflex tubing.

To determine the optimal pumping frequency for the MLCT band, we acquired a UV-Vis spectrum for each metal carbonyl. This was accomplished using an UV-Vis spectrophotometer (Agilent

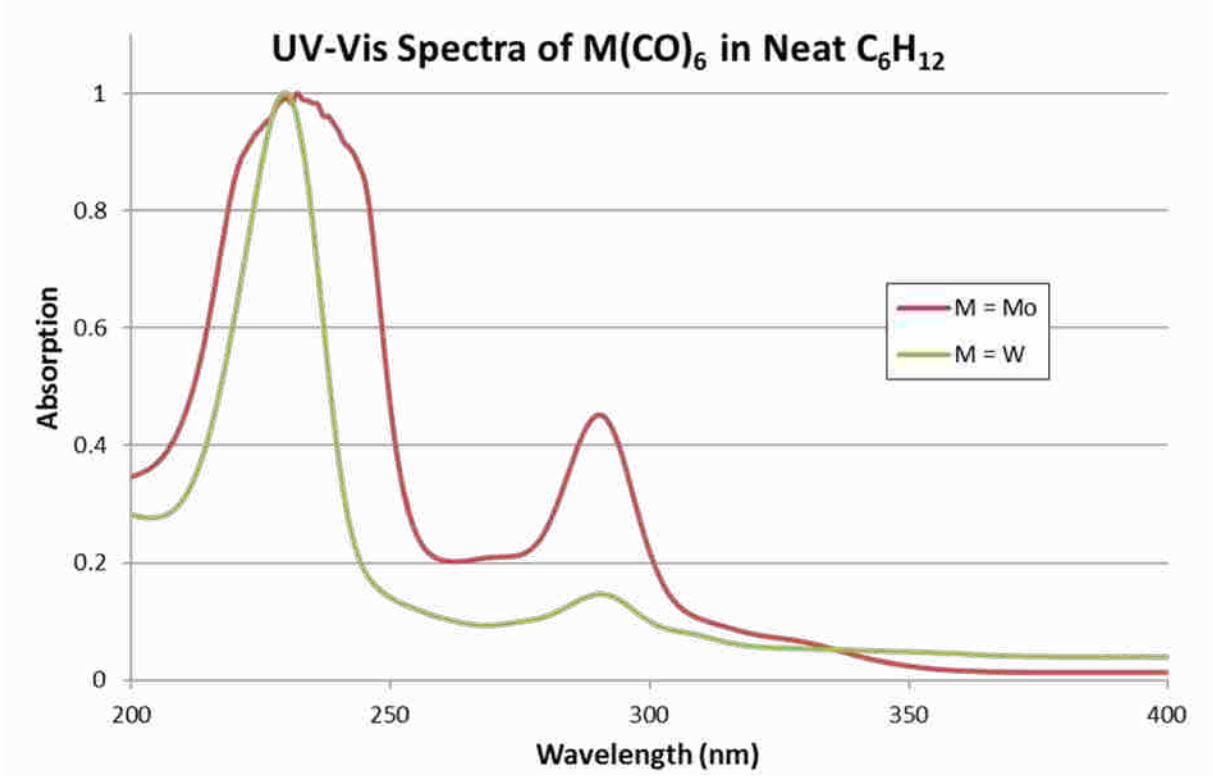

Figure 2.4 UV-Vis Spectra of $Mo(CO)_6$ and $W(CO)_6$ in Neat Cyclohexane. MLCT band maximum is at approximately 290 nm for both metal carbonyls.

8453) equipped with a photodiode array (PDA), allowing for collection of the entire UV-Vis range in less than one second. **Figure 2.4** shows a plot of UV-Vis spectrum for $M(CO)_6$ (M = Mo, W). In previous experiments, we were limited by our laser (YAG Coherent Infinity) to pumping experiments with either 355 nm or 266 nm UV light, as seen in **Figure 2.4** little radiation is absorbed at these frequencies. This introduced difficulties in acquiring reproducible results; as you can see in **Figure 2.5** the signal-to-noise ratio is drastically different pumping at 290 nm vs. 355 nm.

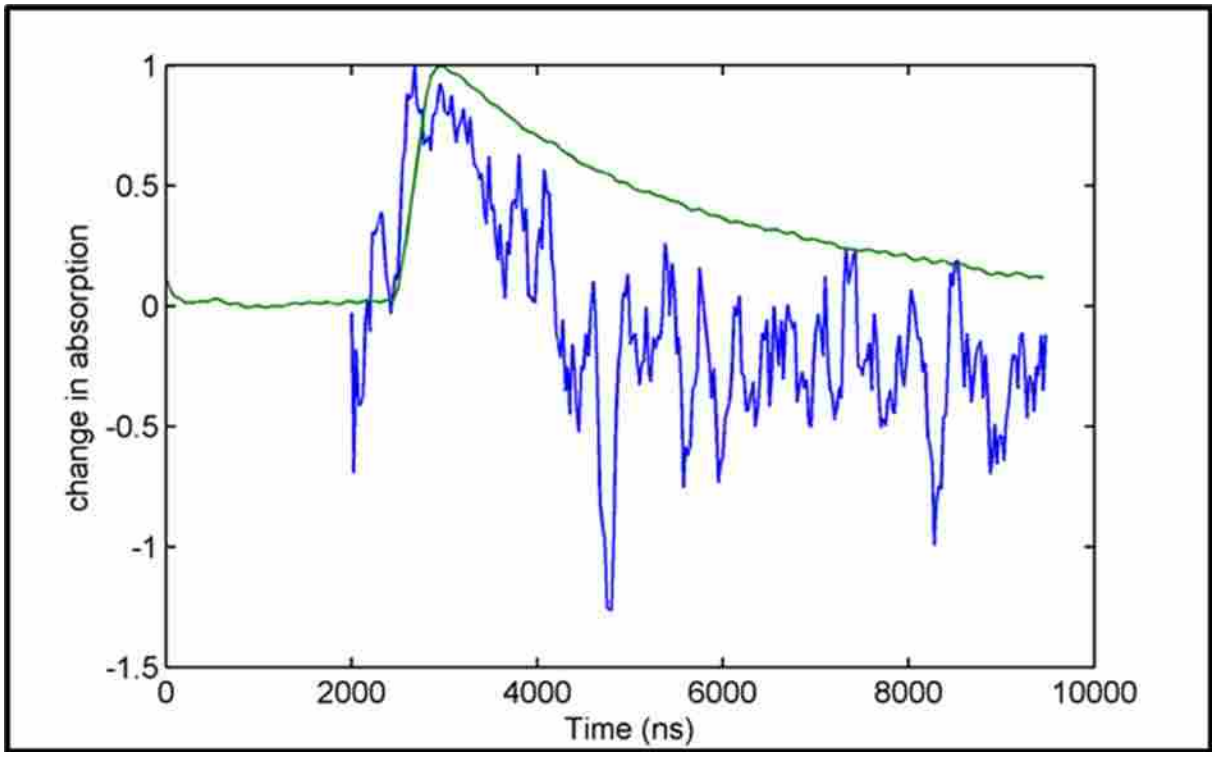

Figure 2.5 Pumping at 355 nm vs. 290 nm Photons. (a) The blue single frequency time trace is the decay of $W(CO)_5C_6H_{12}$ produced by pumping 2.5 mM $W(CO)_6$ with 355 nm photons from Coherent Infinity. Note the large glitch in the time trace at approximately 5,000 ns. (b) The green single frequency time trace is the decay of $W(CO)_5C_6H_{12}$ produced by pumping 2.5 mM $W(CO)_6$ with 290 nm photons from Continuum Precision II/Panther OPO.

Pumping at 355 nm required collecting and averaging 5 scans at 30 coadds each, versus one scan at 10 coadds when pumping with 290 nm light.

2.5 Density Functional Theory Calculations

Recent improvements in computational chemistry techniques for transition metal complexes, primarily in the use of density functional theory (DFT), may be of use in predicting the vibrational frequencies for comparison with experimental data and therefore the identification of these short lived intermediates.[3]. The use of DFT

calculations to study these transition metal complexes owes much of its success to the development of hybrid functionals that contain some of the exact exchange in the exchange functional.[4] One of the more common functionals, that has gained much popularity with main group chemistry is the combination of Becke's three parameter exchange functional[5] with Lee-Yang-Parr correlation functional[6] to form the B3LYP density functional. The use of B3LYP for transition metal chemistry, however, has shortcomings as many hybrid functionals give unreliable results for transition metal chemistry.[7] It is better for main group chemistry, but does not accurately account for medium range correlation energy such as van der Waals forces and aromatic stacking, and it overestimates reaction barrier heights and, therefore, is not as accurate for calculations containing weak transition metal solvent interactions.[8] In understanding the weak solvent complexes in organometallic reactions, it is necessary to be able to calculate properties which involve these weak interactions. It is common for DFT calculations of bond energies and heats of formation to deviate by 10 kcal mol^{-1}.[7b] Two relatively new functionals M06,[8] a hybrid Meta functional and M06-L,[9] a meta-GGA exchange-correlation functional, have been developed by Truhlar and coworkers to correct for these shortcomings in B3LYP and, therefore, should give better answers for transition metal complexes. However, M06 and M06-L have remained mostly untested for vibrational frequencies of moderate to weakly bound transition metal carbonyl complexes with organic solvents. In addition to using B3LYP and M06 to calculate the binding energy of these complexes, one of our purposes in this study is to test

these three density functionals against each other in the complexes of transition metal carbonyls with moderate to weakly bound organic solvent molecules.

2.5.1 Calculations of Vibrational Frequencies

Calculations were performed with the NWChem[10] computational chemistry program and the Extensible Computational Chemistry Environment (ECCE) developed by Pacific Northwest Laboratories using a mixed basis set of Los Alamos National Laboratory 2 double-ζ (LAN2DZ) basis function for transition metals and 6-31G*, a Pople-type split valence double-ζ polarized basis set, for all remaining main group atoms. All calculations were run using density functional level of theory.

We have studied transition metal carbonyls with weakly bound solvent metals using FTIR step scan techniques. IR frequencies measured in these studies were compared with the NWCHEM[10] calculations obtained from each of the mentioned density functionals. Scaling factors were calculated by taking the ratio of the measured to computational values, and overall vibrational shifts by the difference of these values; standard deviations for these two factors were also calculated.

2.5.2 Calculations of Binding Energies

Calculations of bond enthalpies were conducted using density functional level of theory using NWCHEM[10] and Gaussian 09.[11] Jobs were built using ECCE[12] and submitted to Brigham Young University's Fulton Supercomputing Lab to run calculations. The bond enthalpies are calculated by:

$$E_{bond} = E_{complex} - \Sigma\, E_{fragments} \qquad \textbf{Equation 2.3}$$

Some troubles exist comparing calculated bond enthalpies to measured energies. The calculated bond enthalpies are the energy differences between geometrically relaxed, weakly-bound ligand metal carbonyls and the individual ligand and metal carbonyl pieces. When using DFT to calculate the energy of a molecule, all of the Gaussian functions for all of the atoms in each fragment of the molecule are used to determine the energy minimum; however, when we calculate the energy of a single fragment, we use fewer Gaussian functions because each fragment contains fewer atoms. Variational theory tells us that the more Gaussian functions used the closer to the actual energy we will get and that our calculations will always be higher than this energy and, therefore, the result of **Equation 2.3** will be lower than expected. This is called Basis Set Superposition Error (BSSE). The energy calculations in this work are adjusted for BSSE. In NWCHEM,[10] BSSE can be fixed by assigning some atoms to be "ghost atoms" to use the basis set from the whole on each of the parts. The NWCHEM[10] approach at solving the BSSE problem cannot be used to calculate the energy of relaxed fragments and therefore will not give accurate answers for a purely dissociative process. Not allowing the geometries to relax, over-estimates the energies of these fragments. Using **Equation 2.3** would then under-estimate the binding energy of a weakly-bound solvent molecule to the metal center. Gaussian 09[11] however differs, directly calculating the BSSE energy of the two weakly bound fragments, ligand and metal

carbonyl, using the counterpoise keyword. This enables us to calculate the relaxed energies of the two fragments independent of the whole complex.

For NWCHEM calculations, an adjustment for the zero point energy (ZPE) cannot be done on the fragments of the metal carbonyl complex. The energy for each fragment can only be calculated when atoms of the other fragment are ghosted. And a geometry minimization, and therefore, a zero point energy for the fragment cannot be calculated with the full basis set. Gaussian 09, however, can do a geometry minimization with a counterpoise correction, and therefore, it can be used to do a ZPE correction.

Sample input files for NWCHEM[10] and Gaussian 09[11] calculations are included in **Appendix** F.

2.6 Data Analysis

All data was acquired using OPUS 2.0 software on a computer running OS/2 Warp. Using a newer version of OPUS running on a windows XP box, data was converted into comma separated text files to be used in Matlab. All the time slices in the DC files were averaged together and saved as a single text file. Unlike static DC scans, it is necessary to extract each AC time slice individually. A macro (found in appendix E) was therefore created in OPUS to extract each time slice and save it as a text file with a numerically increasing file name. These text files are then imported into Matlab using scripts **loaddc.m** and **loadac.m** produced in-house (these scripts are included in **Appendix E**). The Matlab script **loaddc.m** is used to import the single DC comma separated text file and create a three dimensional DC

spectrum in which every frequency slice is identical to the original DC intensities. The Matlab script **loadac.m** is used to import the entire array of AC comma separated text files and create a three dimensional AC spectrum where time slices come from the individual text files created in OPUS. The **loadac.m** script also calculates the absorption spectrum using **Equation 2.2** and smooths the absorption spectrum with a seven-point moving average.

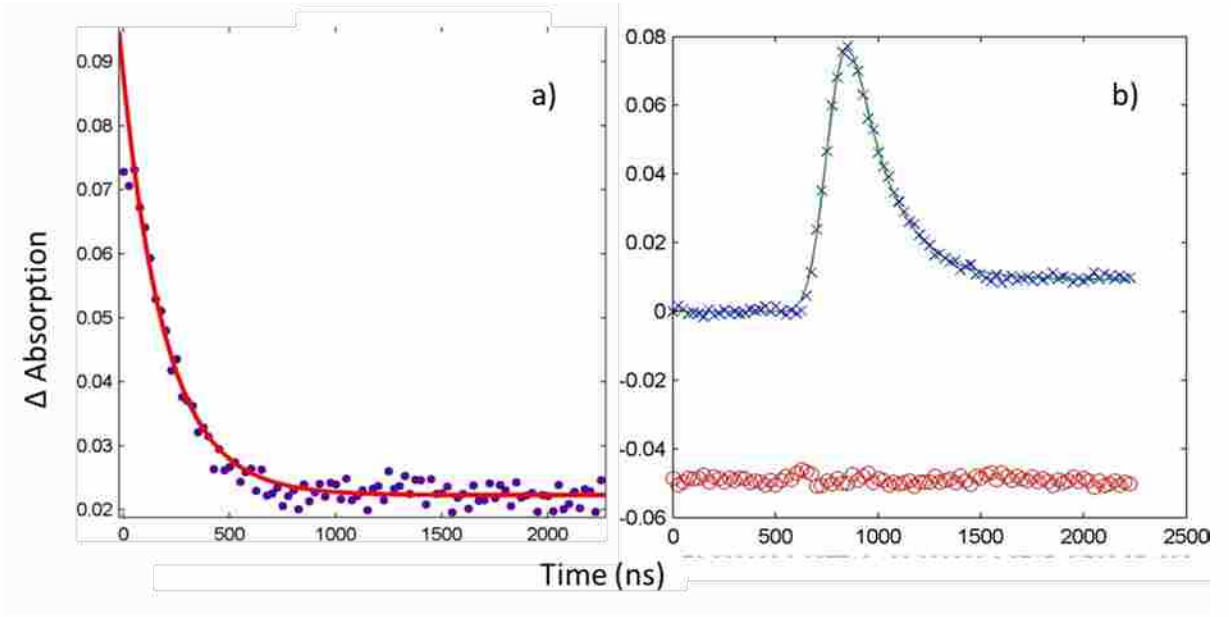

Figure 2.6. Data Fitting. The same data of the decay of Mo(CO)5(methylcyclohexane) at 1963 cm-1 to Mo(CO)5(benzene) at 35 0C is fit with two methods: (a) the data is cut off from time zero and the decay is fit with a single exponential with an offset, (b) the entire frequency slice is fit using an instrument resoponce function, single exponential decay, time zero and an offset, yielding decay times (τ) of 205 ns for (a) and 182 ns for (b). Fitting the rise time of the detector lowers τ by approximately 10%, due to the decay being near the same rate as the rise time of the detector, adding an additional decay time to (a).

We have used two methods to fit our data to an exponential decay (see **Figure 2.6**). In both methods, the time and absorption vectors for the decaying $M(CO)_5$:C_6H_{12} peak are extracted from the smoothed absorption spectrum and plotted for evaluation of the associated rate constants. First, we fit the decay to a single exponential and offset, ignoring the rise of the signal before t_0 using the Matlab's curve fitting tool (cftool). This method is less accurate for decay times on the same order of magnitude as our instrument response time because the signal after t_0 is affected by the rise. The second fit method simultaneously fitS a single exponential instrument response function, t_0, a single exponential decay of the $M(CO)_5$(solv) peak and an offset using the Matlab scripts **jfit.m** and **jmexp.m** (included in **Appendix E**, created by Jason McNeill). Rate constant values are then

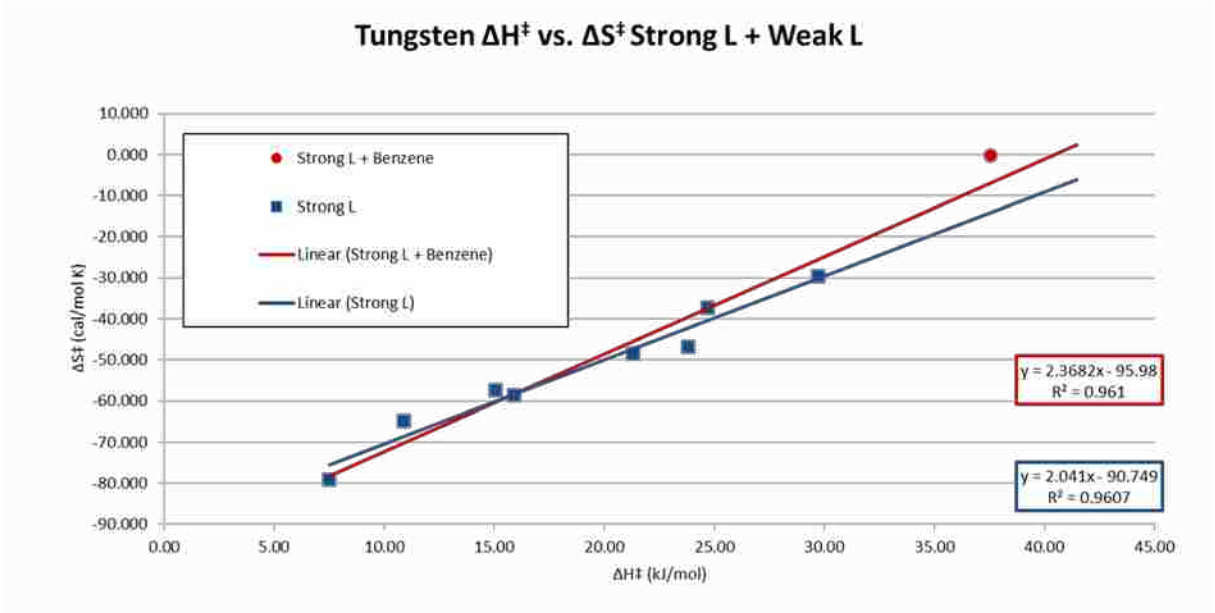

Figure 2.7 Linear relationship of ΔH‡ and ΔS‡ for moderate to weakly binding ligands to tungsten pentacarbonyl.

imported into an Excel spreadsheet to create an Arrhenius plot. The slope of the Arrhenius plot is used to determine the energy of activation for the exchange reaction. An Eyring analysis provides the enthalpy and entropy of reaction.

2.7 Conclusions

The measurement of the vibrational frequencies of transition metal complexes using SS FTIR is a useful method to follow the kinetics of the solvent exchange reaction. Carbonyl vibration frequencies are sensitive to the electronic environment around the metal center due to metal to ligand backbonding into the π^* molecular orbital on CO. These vibrational frequencies are also useful in the identification of transition metal carbonyl complexes.

A plot of enthalpy of reaction vs. entropy of reaction for the solvent exchange reaction with M = W and solv = cyclohexane was observed by Schultz et al.[13] to follow a linear relationship. To compare our experimental data with the data taken by Schultz and coworkers,[13] we included our data points on the same graph, see **Figure 2.7**. This figure shows that, with the addition of our data for ligand exchange reaction, the R squared value or goodness of the linear fit to the data is equal to within three significant figures. Only data for W could be included in this analysis because the experiments involving Mo were not pursued by Schultz, and chromium was not a part of this work.

2.8 References

1. Castle, S. L., Personal Communication. 2011.

2. Uhmann, W.; Becker, A.; Taran, C.; Siebert, F., Time-Resolved FT-IR Absorption Spectroscopy Using a Step-Scan Interferometer. *Appl. Spectrosc.* **1991,** *45*, 390–397.

3. Jonas, V.; Thiel, W., Theoretical Study of the Vibrational Spectra of the Transition-Metal Carbonyl Hydrides $HM(CO)_5$ (M=Mn, Re), $H_2M(CO)_4$ (M=Fe, Ru, Os), and $HM(CO)_4$ (M=Co, Rh, Ir). *J. Chem. Phys.* **1996,** *105*, 3636–3648.

4. Gonzalez-Blanco, O.; Branchadell, V., Density Functional Study of the Fe–CO Bond Dissociation Energies of $Fe(CO)_5$. *J. Chem. Phys.* **1999,** *110*, 778–783.

5. Becke, A. D., Density-Functional Thermochemistry. III. The Role of Exact Exchange. *J. Chem. Phys.* **1993,** *98*, 5648–5652.

6. Lee, C.; Yang, W.; Parr, R. G., Development of the Colle-Salvetti Correlation-Energy Formula into a Functional of the Electron Density. *Phys. Rev. B* **1988,** *37*, 785–789.

7. (a) Reiher, M.; Salomon, O.; Artur Hess, B., Reparameterization of Hybrid Functionals Based on Energy Differences of States of Different Multiplicity. *Theor. Chim. Acta* **2001,** *107*, 48–55; (b) Harvey, J. N., On the Accuracy of Density Functional Theory in Transition Metal Chemistry. *Annu. Rep. Prog. Chem. Sect. C: Phys. Chem.* **2006,** *102*, 203–226; (c) Schultz, N. E.; Zhao, Y.; Truhlar, D. G., Density

Functionals for Inorganometallic and Organometallic Chemistry. *J. Phys. Chem. A* **2005,** *109*, 11127–11143.

8. Zhao, Y.; Truhlar, D. G., Density Functionals with Broad Applicability in Chemistry. *Acc. Chem. Res.* **2008,** *41*, 157–167.

9. Zhao, Y.; Truhlar, D. G., A New Local Density Functional for Main-Group Thermochemistry, Transition Metal Bonding, Thermochemical Kinetics, and Noncovalent Interactions. *J. Chem. Phys.* **2006,** *125*, No. 194101.

10. Valiev, M.; Bylaska, E. J.; Govind, N.; Kowalski, K.; Straatsma, T. P.; Van Dam, H. J. J.; Wang, D.; Nieplocha, J.; Apra, E.; Windus, T. L.; de Jong, W. A., NWChem: A comprehensive and Scalable Open-Source Solution for Large Scale Molecular Simulations. *Comput. Phys. Commun.* **2010,** *181*, 1477–1489.

11. Frisch, M. J.; Trucks, G. W.; Schlegel, H. B.; Scuseria, G. E.; Robb, M. A.; Cheeseman, J. R.; Scalmani, G.; Barone, V.; Mennucci, B.; Petersson, G. A.; Nakatsuji, H.; Caricato, M.; Li, X.; Hratchian, H. P.; Izmaylov, A. F.; Bloino, J.; Zheng, G.; Sonnenberg, J. L.; Hada, M.; Ehara, M.; Toyota, K.; Fukuda, R.; Hasegawa, J.; Ishida, M.; Nakajima, T.; Honda, Y.; Kitao, O.; Nakai, H.; Vreven, T.; Jr., J. A. M.; Peralta, J. E.; Ogliaro, F.; Bearpark, M.; Heyd, J. J.; Brothers, E.; Kudin, K. N.; Staroverov, V. N.; Kobayashi, R.; Normand, J.; Raghavachari, K.; Rendell, A.; Burant, J. C.; Iyengar, S. S.; Tomasi, J.; Cossi, M.; Rega, N.; Millam, J. M.; Klene, M.; Knox, J. E.; Cross, J. B.; Bakken, V.; Adamo, C.; Jaramillo, J.; Gomperts, R.; Stratmann, R. E.; Yazyev, O.; Austin, A. J.; Cammi, R.; Pomelli, C.; Ochterski, J. W.; Martin, R. L.; Morokuma, K.; Zakrzewski, V. G.; Voth, G. A.;

Salvador, P.; Dannenberg, J. J.; Dapprich, S.; Daniels, A. D.; Farkas, Ö.; Foresman, J. B.; Ortiz, J. V.; Cioslowski, J.; Fox, D. J. *Gaussian 09*, Gaussian, Inc.: Wallingford CT, 2009, 2009.

12. G.Black; Chase, J.; Chatterton, J.; Daily, J.; Elsethagen, T.; Feller, D.; Gracio, D.; Jones, D.; Keller, T.; Lansing, C.; Matsumoto, S.; Palmer, B.; Peterson, M.; Schuchardt, K.; Stephan, E.; Sun, L.; Swanson, K.; Taylor, H.; Thomas, G.; Vorpagel, E.; Windus, T.; Winters, C. *ECCE, A Problem Solving Environment for Computational Chemistry*, Software Version 6.0 Pacific Northwest National Laboratory: Richland, Washington 99352-0999, USA, 2009.

13. Schultz, R. H.; Biber, L.; Reuvenov, D.; Revzin, T.; Sinai, T.; Zahavi, A., Reactions of the Transient Species $Cr(CO)_5$(cyclohexane) with C_4H_nE (n=4, 8; E = O, NH, S) studied by Time-Resolved IR Absorption Spectroscopy. *J. Chem. Soc., Dalton Trans.* **2007**, 41–51.

Chapter 3: Carbonyl Vibrational Scaling Factors for Weakly-Bound Transition Metal Carbonyl, Organic Solvent Intermediates.

3.1 Introduction

Organometallic reactions are important in industry and research. Many of these reactions begin with the creation of a highly reactive, coordinatively unsaturated metal center followed by coordination with a nearby solvent molecule. This kinetically favorable product reacts further to form the desired product. Understanding the single-step formation of these solvated intermediates is important in understanding the dynamics of the overall reaction. The choice of solvent may affect the rate of reaction, yield and activation energy. A study by Church et al.[1] of the transition metal carbonyl $Cr(CO)_5N_2$ noted that the activated species $Cr(CO)_5$ would react readily with many ligands. Upon flash photolysis, the first observed absorption was the complex with the solvent cyclohexane, reported to form within 25 ps by Welch et al. and no photolysis study of $Cr(CO)_6$ dissolved in neat cyclohexane has observed the formation of an earlier complex than $Cr(CO)_5(C_6H_{12})$.[2] The isolation and further identification of these intermediates is difficult because they readily react with trace contaminants in solution on the microsecond time scale.

Recent improvements in computational chemistry techniques for transition metal complexes, primarily the use of density functional theory (DFT), may be of use in predicting the carbonyl vibrational frequencies for comparison with experimental data and therefore, the identification of short-lived transition metal

intermediates.[3] The use of DFT calculations to study transition metal complexes owes much of its success to the development of hybrid functionals which contain some exact exchange in the exchange functional.[4] One of the more common functionals, which has gained much popularity with main group chemistry, is the combination of Becke's three parameter exchange functional[4-5] with Lee-Yang-Parr correlation functional[6] to form the B3LYP density functional. The use of B3LYP for transition metal chemistry, however, does have shortcomings as many hybrid functionals give unreliable results for transition metal chemistry.[7] B3LYP is better for main group chemistry, however, it does not accurately account for medium range correlation energy such as van der Waals forces and aromatic stacking and overestimates reaction barrier heights and therefore, is not as accurate for calculations containing weak transition metal solvent interactions.[8] In understanding the weak solvent complexes in organometallic reactions, it is necessary to calculate properties which involve these weak interactions. Density Functional Calculations of bond energies and heats of formation commonly deviate by 10 kcal mol^{-1}.[7b] Two relatively new functionals M06,[8] a hybrid Meta functional and M06-L,[9] a meta-GGA exchange-correlation functional, have been developed by Truhlar and coworkers in order to correct for these shortcomings in B3LYP. Our purpose in this study is to test these three density functionals against complexes of $M(CO)_5$ with weakly bound organic solvent molecules.

3.2 Methods

3.2.1 Reagents

Samples were prepared by dissolving 2.5 mM $M(CO)_6$ (M = Cr, W, Mo) in methylcyclohexane., To reduce any oxygen contamination, the samples undergo 3 cycles of freeze, pump, thawing and followed by back filling with argon. In addition to neat methylcyclohexane samples were also prepared with a secondary solvent, 1% to 4% of either benzene or mesitylene. Metal carbonyls were obtained from Aldrich with purities of 97% for $W(CO)_6$, 99% for $Cr(CO)_6$ and 98% for $Mo(CO)_6$, and stored as received. Reagent plus 99% methylcyclohexane obtained from Sigma Aldrich, spectranalyzed benzene from Fisher and 99% extra pure mesitylene from Acros. Solvents were stored with the addition of molecular sieves and under argon.

3.2.2 Step Scan Spectroscopy

Vibrational frequencies were measured using Step Scan FTIR (SS FTIR) spectroscopy. Samples were continuously flowed to ensure fresh sample for each laser pulse. Reactions where initialized by pumping the Metal to Ligand Charge Transfer (MLCT) band of the metal carbonyl with a tripled YAG (Continuum Precision II) pumped OPO (Optical Parametric Oscillator, Continuum Panther). Transient species were followed with a Bruker model IFS/66S FTIR, modified for step scan experiments and equipped with a mercury cadmium telluride (MCT) detector. A band pass IR filter (1600 to 2600 cm^{-1}) was placed in front of the MCT detector to reduce the number of interferometer points needed to complete each step scan measurement. The timing pulses from the YAG were sent through a Stanford

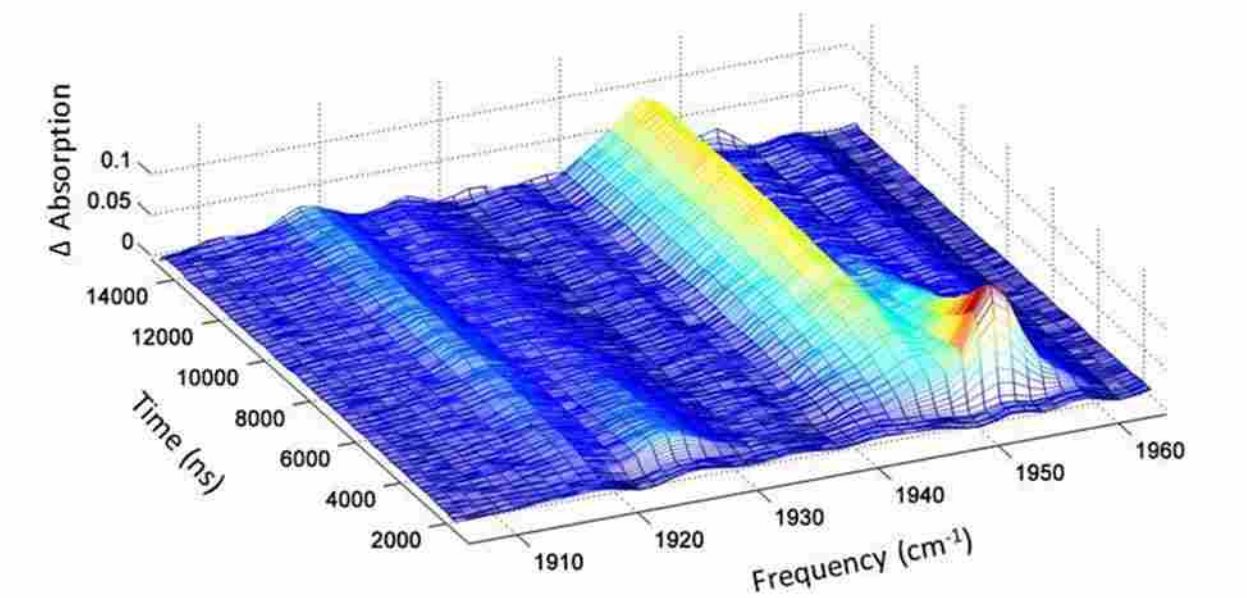

Figure 3.1 Step Scan FTIR data of the exchange reaction of $W(CO)_5$(methylcyclohexane) to form $W(CO)_5(C_6H_6)$. At time zero there is a quick rise over the instrument response time at 1954 cm^{-1}, the strongest carbonyl frequency of the $W(CO)_5$(methylcyclohexane) complex, which slowly decays away into the more thermodynamically favorable product $W(CO)_5(C_6H_6)$ at 1946 cm^{-1}.

Research Digital Delay Pulse Generator to synchronize the FTIR with the laser pulse. Sample preparation and experiments were carried out under a positive argon pressure of slightly greater than one atmosphere. The sample SS FTIR spectra in **Figure 3.1** shows the rise of the tungsten pentacarbonyl methylcyclohexane complex peak within the time resolution of our detector and its decay as the formation of the thermodynamical favorable tungsten pentacarbonyl benzene complex forms.

3.2.3 Density Functional Theory Calculations of Transition Metal Carbonyl Frequencies

Vibrational frequencies were calculated with the NWChem[10] computational chemistry program and the Extensible Computational Chemistry Environment (ECCE), developed by Pacific Northwest Laboratories. Calculations were performed using a mixed basis set, Los Alamos National Laboratory 2 double-ζ (LAN2DZ) basis set for transition metals and 6-31G* a Pople-type split-valence double-ζ polarized basis set for all remaining main group atoms. All calculations were run using density functional level of theory.

The B3LYP density functional general works well with main group atoms but, does not account well for exchange and correlation energies which are important when dealing with transition metal complexes. M06[8] (Minnesota 2006) and M06-L[9] (Minnesota 2006 local functional) developed more recently by Truhlar were designed to address these problems in the B3LYP functional and ,therefore, should give better answers for transition metal complexes but have remained mostly untested for vibrational frequencies of weakly bound transition metal carbonyl complexes with organic solvents.

We have studied transition metal carbonyls with weakly bound solvent metals using FTIR step scan techniques. IR frequencies measured in these studies were compared with the NWCHEM[10] calculations obtained from each of the before mentioned density functionals. Scaling factors and overall vibrational shifts in addition to standard deviations for these factors have been calculated.

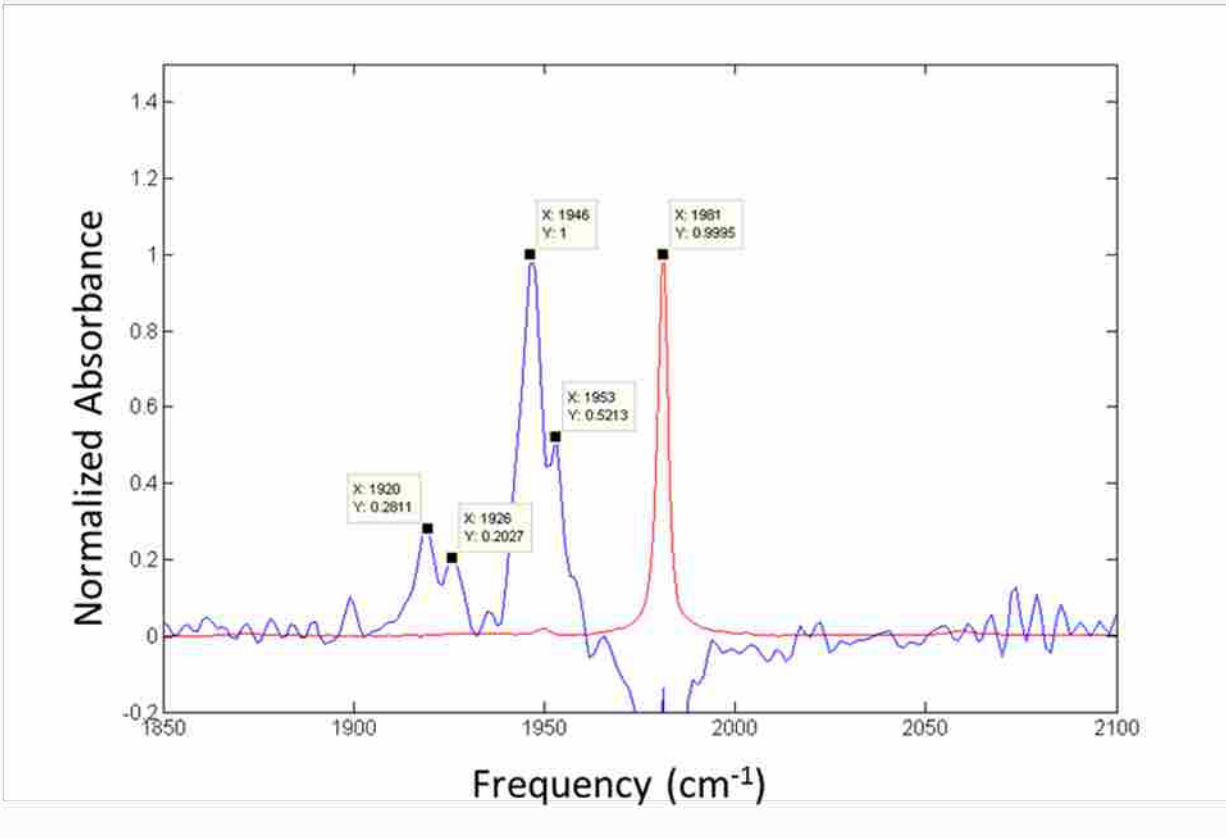

Figure 3.2 Normalized sum of one step scan of the exchange reaction of $W(CO)_5$(methylcyclohexane) to $W(CO)_5(C_6H_6)$ (blue) and the parent $W(CO)_6$ (red). The peaks due $W(CO)_5$(methylcyclohexane) to at 1953 cm^{-1} and 1926 cm^{-1} decay away to form $W(CO)_5(C_6H_6)$ with carbonyl peaks at 1943 cm^{-1} and 1920 cm^{-1}.

3.3 Results and Discussion

DFT calculations show that each $M(CO)_5(L)$ complex has five vibrational frequencies assigned to carbonyls; the lowest frequency vibrational mode is predicted to have a medium IR intensity, followed by two nearly degenerate peaks of high predicted IR intensity, one peak of very low predicted IR intensity and the highest energy vibrational mode has a weak predicted IR intensity. The exception to this is $W(CO)_5(CS)$ where the lowest energy vibrational frequency is predicted to be

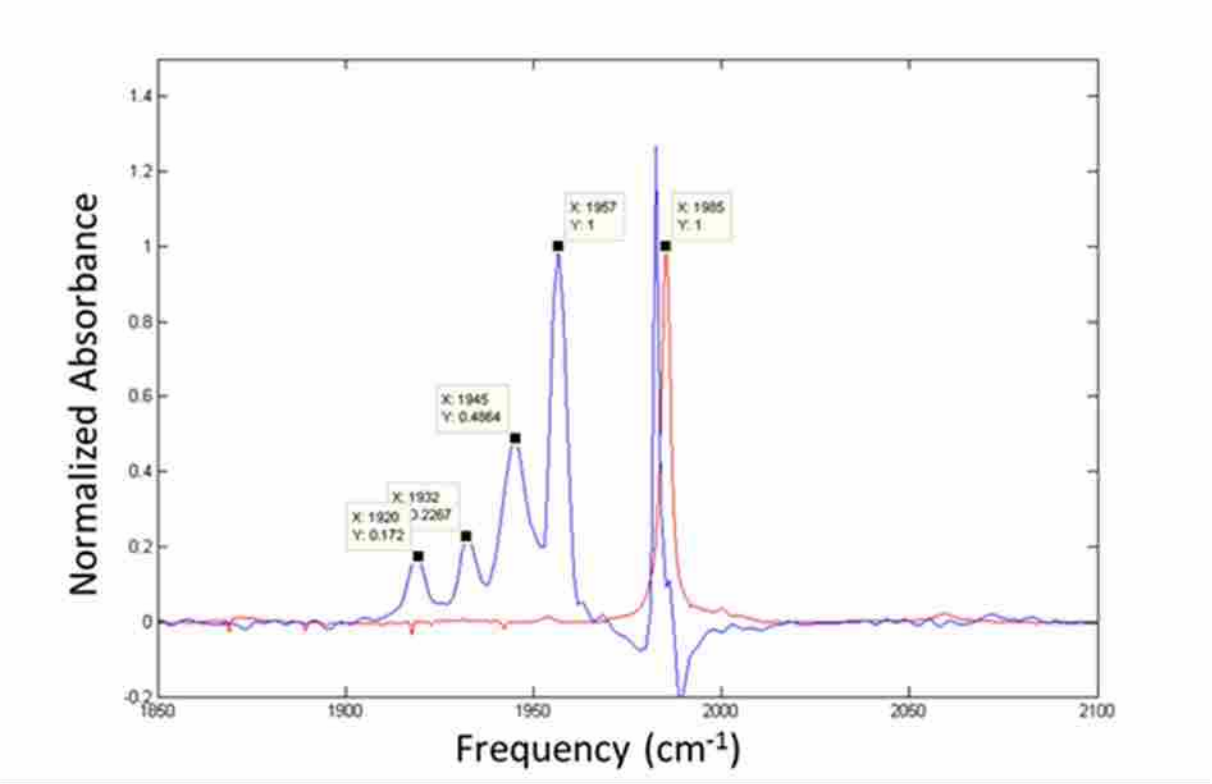

Figure 3.3 Normalized sum of one step scan of the exchange reaction of $Cr(CO)_5(C_6H_{12})$ to $Cr(CO)_5(C_6H_6)$(blue) and the parent $Cr(CO)_6$ (red). Carbonyl peaks at 1957 cm^{-1} and 1932 cm^{-1} as $Cr(CO)_5(C_6H_{12})$ decays to form $Cr(CO)_5(C_6H_6)$ with peaks 1945 cm^{-1} and 1920 cm^{-1}.

the most intense and the third lowest energy vibrational frequency is predicted to be of medium intensity.

The "naked" $M(CO)_5$ fragment has C_{4v} symmetry where the $M(CO)_5(L)$ complexes with the exception of the bound ligand retain a C_{4v}-like symmetry. To determine the symmetries of each vibrational frequency in these C_{4v}-like complexes, we calculated the frequencies of the $W(CO)_5Ar$ complex, using Gaussian 03, with density functional level of theory. The highest vibrational frequency is of A_1 symmetry, where all 5 CO vibrations are completely symmetric. The next highest is

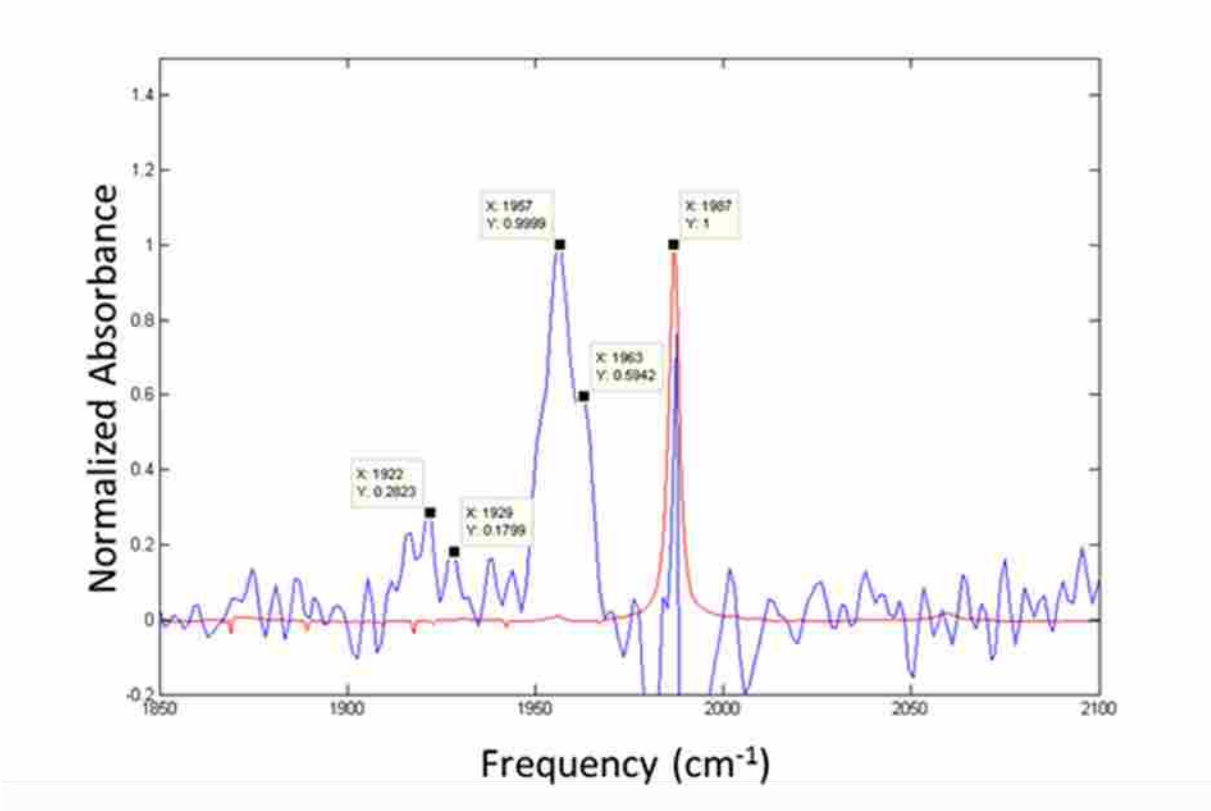

Figure 3.4 Normalized Sum of One Step Scan of the Exchange Reaction of $Mo(CO)_5(C_6H_{12})$ to $Mo(CO)_5(C_6H_6)$ (blue) and Parent $Mo(CO)_6$ (red). Carbonyl peaks at 1963 cm^{-1} and 1929 cm^{-1} from $Mo(CO)_5(C_6H_{12})$ decay away as peaks at 1957 cm^{-1} and 1922 cm^{-1} grow in to form $Mo(CO)_5(C_6H_6)$.

of B_2 symmetry in which the carbonyl along the Z axis, along the Ar-W-CO bonds, does not vibrate and the carbonyls along the Y axis and X axis vibrate opposite of each other. The next two frequencies are doubly degenerate and have E character; the carbonyl along the Z axis does not vibrate in either E mode, the carbonyls along X axis vibrate symmetrically for one E and those along the Y axis vibrate symmetrically for the second E. The lowest frequency is A_1 where the only carbonyl that vibrates is along the Z axis.

Most metal carbonyl solvent complexes react rapidly with oxygen, water, or other impurities or can undergo spontaneous decomposition. Therefore, they must be measured either at very low temperatures, or very short time-scales. **Figure 3.1** shows a 3-dimentioanl SS FTIR spectrum of tungsten pentacarbonyl cyclohexane, the statistical product being exchanged for more thermodynamically stable product $W(CO)_5$mesitylene. **Figure 3.2**, **Figure 3.3** and **Figure 3.4** are the average of similar step scan plots of additional group 6 transition metal carbonyls (M = Cr, W, Mo respectively) with vibrational peaks labeled.

Density Functional Theory tends to predict vibrational frequencies that are too high. We will compare experimentally measured frequencies to DFT calculated frequencies to determine a frequency difference (calculated – experimental) and scaling factor (experimental/calculated) for each of the density functionals used. **Table 3.1** includes experimental data for $Cr(CO)_5L$, **Table 3.2** data for $Fe(CO)_4L$ and $Mo(CO)_5L$ and **Table 3.3** and **Table 3.4** for $W(CO)_5L$, where L stands for ligand. Using these results we have assigned calculated peaks to each of the experimentally determined IR frequencies. Our data shows three peaks, the lowest energy is of medium intensity and will therefore be correlated with the lowest energy calculated vibrational frequency. The next highest in energy is the most intense peak and will therefore be assigned to the second vibrational frequency. The transient step scan experiments used to obtain the IR spectrum of these weakly bound organometallic intermediates was obtained with 4 cm^{-1} resolution and therefore the second and third calculated vibrational peaks could not be resolved.

Table 3.1 Experimental and computational vibrations for $Cr(CO)_5L$ (L=denoted ligand).

Complex	Functionals	Calculated										Experimental			References
$Cr(CO)_5$:THF	B3LYP	2038	m	2044	s	2054	s	2074	w	2154	w				KBr[11]
	m06	2055	m	2060	s	2067	s	2099	w	2178	w	1877	1933	2059	
	m06-L	2026	m	2034	s	2036	s	2061	w	2143	w				
	B3LYP	2038	m	2044	s	2054	s	2074	w	2154	w				THF[12]
	m06	2055	m	2060	s	2067	s	2099	w	2178	w	1895	1937	2073	
	m06-L	2026	m	2034	s	2036	s	2061	w	2143	w				
$Cr(CO)_5$:N_2	B3LYP	2079	m	2081	s	2081	s	2103	vw	2167	w				C_6H_{12}[1]
	m06	2093	m	2096	s	2097	s	2126	vw	2189	w	1966	1976		
	m06-L	2061	m	2067	s	2068	s	2092	vw	2153	w				
	B3LYP	2079	m	2081	s	2081	s	2103	vw	2167	w				PE[13]
	m06	2093	m	2096	s	2097	s	2126	vw	2189	w	1960	1972	2084	
	m06-L	2061	m	2067	s	2068	s	2092	vw	2153	w				
$Cr(CO)_5$:C_6H_{12}	B3LYP	2054	m	2063	s	2064	s	2088	w	2163	w				C_6H_{12}[14]
	m06	2068	m	2079	s	2079	s	2111	w	2188	w	1932	1957		
	m06-L	2039	m	2047	s	2048	s	2071	w	2151	w				
$Cr(CO)_5$:C_6H_6	B3LYP	2045		2054		2058		2082		2157					C_6H_{12}[14]
	m06	2064		2069		2072		2105		2178		1925	1950	2075	
	m06-L	2032		2039		2044		2069		2144					
$Cr(CO)_5$:H_2O	B3LYP	2044		2051		2054		2081		2159					C_6H_{12}[14]
	m06	2059		2066		2070		2107		2182		1913	1943	1950	
	m06-L	2030		2038		2041		2067		2149					

Table 3.2 Experimental and computational vibrations for $Mo(CO)_5L$ (L=denoted ligand). (Met = mesitylene)

Complex	Functional	Calculated												Experimental			References
$Fe(CO)_4:N_2$	B3LYP	2090	s	2091	s	2111	mw	2163	mw					1984	1992		Gas phase [15]
	M06	2116	s	2116	s	2130	mw	2185	mw								
	M06-L	2071	s	2072	s	2089	mw	2146	mw								
$Mo(CO)_5$:THF	B3LYP	2030	m	2046	s	2049	s	2070	vw	2156	w			1959	1982	2080	THF [11]
	M06	2053	m	2064	s	2068	s	2096	vw	2181	w						
	M06-L	2023	m	2028	s	2029	s	2064	vw	2146	w						
$Mo(CO)_5:N_2$	B3LYP	2070	m	2075	s	2075	s	2098	vw	2169	w			1959	1974	2089	PE [13]
	M06	2091	m	2098	s	2098	s	2125	vw	2194	w						
	M06-L	2059	m	2066	s	2066	s	2088	vw	2157	w						
	B3LYP	2070	m	2075	s	2075	s	2098	vw	2169	w			1964	1978	2092	Gas phase [16]
	M06	2091	m	2098	s	2098	s	2125	vw	2194	w						
	M06-L	2059	m	2066	s	2066	s	2088	vw	2157	w						
$Mo(CO)_5:C_6H_6$	B3LYP	2035	m	2051	s	2054	s	2085	vw	2158	w			1920	1957		This work
	M06	2049	m	2067	s	2072	s	2101	vw	2178	w						
	M06-L	2025	m	2043	s	2047	s	2066	vw	2149	w						
$Mo(CO)_5:C_6H_{12}$	B3LYP	2040	m	2065	s	2066	s	2093	vw	2166	w			1927	1963	2089	This work
	M06	2060	m	2084	s	2084	s	2118	vw	2191	w						
	M06-L	2035	m	2047	s	2048	s	2071	vw	2154	w						
$Mo(CO)_5$:Met	B3LYP	2030	m	2047	s	2069	s	2077	vw	2155	w			1916	1952	2078	This work
	M06	2047	m	2064	s	2067	s	2097	vw	2176	w						
	M06-L	2030	m	2047	s	2056	s	2067	vw	2150	w						

Table 3.3 Experimental and computational vibrations for $W(CO)_5L$ (L=denoted ligand).

Complex	Functional	Calculated									Experimental			References
$W(CO)_5$:THF	B3LYP	2030	m	2033	s	2036	s	2070	vw	2154	w			C_6H_{12}[17]
	M06	2047	ms	2052	s	2054	s	2092	vw	2177	w	1912	1933	
	M06-L	2022	s	2025	s	2026	s	2057	vw	2145	w			
	B3LYP	2030	m	2033	s	2036	s	2070	vw	2154	w			KBr[11]
	M06	2047	ms	2052	s	2054	s	2092	vw	2177	w	1941	1972 2069	
	M06-l	2022	s	2025	s	2026	s	2057	vw	2145	w			
$W(CO)_5$:CH_3CN	B3LYP	2041	ms	2045	s	2045	s	2079	vw	2155	w			C_7H_{16}[18]
	M06	2063	ms	2066	s	2066	s	2101	vw	2179	w	1926	1944 2077	
	M06-L	2036	ms	2037	s	2037	s	2067	vw	2148	w			
$W(CO)_5$:CS	B3LYP	2084	s	2084	s	2099	m	2109	vw	2178	w			C_7H_{16}[18]
	M06	2104	s	2105	s	2121	m	2130	vw	2201	w	1988	2006 2096	
	M06-L	2079	s	2080	s	2086	m	2094	vw	2172	w			
	B3LYP	2084	s	2084	s	2099	m	2109	vw	2178	w			PE[13]
	M06	2104	s	2105	s	2121	m	2130	vw	2201	w	1985	2005 2096	
	M06-L	2079	s	2080	s	2086	m	2094	vw	2172	w			
$W(CO)_5$:N_2	B3LYP	2071	s	2071	s	2072	m	2100	vw	2167	w			Gas phase[15]
	M06	2093	s	2093	s	2095	m	2125	vw	2194	w	1974	1985	
	M06-L	2063	m	2066	s	2067	s	2085	vw	2158	w			
	B3LYP	2071	s	2071	s	2072	m	2100	vw	2167	w			PE[13]
	M06	2093	s	2093	s	2095	m	2125	vw	2194	w	1959	1967 2086	
	M06-L	2063	m	2066	s	2067	s	2085	vw	2158	w			

Table 3.4 Continuation of the Vibration frequencies in Table 3.4.

Complex	Functional	Calculated										Experimental			References
$W(CO)_5$:C_6H_{12}	B3LYP	2042	m	2052	s	2054	s	2086	w	2164	w				This work
	M06	2063	m	2072	s	2074	s	2108	w	2190	w	1927	1953	2086	
	M06-L	2034	m	2035	s	2036	s	2067	w	2152	w				
$W(CO)_5$:C_6H_6	B3LYP	2033	m	2041	s	2042	s	2081	w	2156	w				This work
	M06	2052	m	2060	s	2061	s	2098	w	2177	w	1921	1948	2079	
	M06-L	2030	m	2030	s	2040	s	2069	w	2148	w				
$W(CO)_5$:H_2O	B3LYP	2034	m	2037	s	2043	s	2078	w	2159	w				C_6H_{12}[14]
	M06	2053	m	2059	s	2064	s	2099	w	2183	w	1908	1933	1948	
	M06-L	2031	m	2037	s	2039	s	2061	w	2151	w				

Assignment of the highest intensity experimental peak to the second, third (which are nearly degenerate) or the average of the second and third computational peaks does not change the scaling factor until the ten thousandths place nor the standard deviation of the scaling factor until the hundred thousandths place, so we will assign the second experimental peak to the average of the two nearly degenerate peaks. Due to the fourth calculated peak being of a predicted very low intensity, it will not be assigned to one of the three experimentally measured vibrations. The third experimental peak, which was not observable in all spectra, will be assigned to the highest energy calculated peak. The scaling factors for the solution phase literature data contained in **Tables 3.1–3.3** and our experimentally determined peaks for $Cr(CO)_5$ bonded with C_6H_{12}, C_6H_6 and H_2O, $Mo(CO)_5$ bonded with C_6H_{12}, C_6H_6, and mesitylene and $W(CO)_5$ bonded with C_6H_{12}, C_6H_6 and H_2O , KBr and

Table 3.5 Scaling Factors for Group 6 Transition Metal Carbonyl Complexes.

Difference of calculated vs. experimental carbonyl frequencies and scaling factors for data found in **Tables 3.1–3.3**; organized by solution phase frequencies, matrix isolation, gas phase and the combination of all carbonyl vibrational frequencies found in **Tables 3.1–3.3**.

	Calc-Exp Freq. (cm^{-1})			Scaling Factor = Exp/Calc		
	B3LYP	M06	M06-L	B3LYP	M06	M06-L
Solution Phase	102 ± 16	121 ± 15	93 ± 17	0.9513 ± 0.0084	0.9423 ± 0.0080	0.9548 ± 0.0092
Matrix Isolation	99 ± 22	120 ± 20	89 ± 21	0.953 ± 0.011	0.943 ± 0.010	0.957 ± 0.011
Gas Phase	98 ± 14	121 ± 13	86 ± 11	0.951 ± 0.006	0.941 ± 0.006	0.957 ± 0.003
Literature	98 ± 20	119 ± 18	87 ± 19	0.9529 ± 0.0100	0.9436 ± 0.0093	0.9578 ± 0.0098
This Work	104 ± 15	122 ± 14	94 ± 16	0.9497 ± 0.0081	0.9408 ± 0.0074	0.9546 ± 0.0086
All Freq.	100 ± 18	120 ± 17	90 ± 18	0.9519 ± 0.0095	0.9429 ± 0.0087	0.9565 ± 0.0095

polyethylene matrix isolation data in **Tables 3.1–3.3**, gas phase data contained in **Tables 3.1–3.3** and a combined scaling factor for all the carbonyl vibrations in **Tables 3.1–3.3** are contained in **Table 3.5**. The overall scaling factors are 0.9519 for B3LYP, 0.9429 for M06 and 0.9565 for M06-L with an overall shift of 100 cm^{-1}, 120 cm^{-1} and 90 cm^{-1}, respectively.

3.4 Conclusions

Using density functional theory with functionals, B3LYP, M06 and M06-L we have calculated the vibrational frequencies of transition metal carbonyl complexes; the use of M06 and M06-L have not previously been tested for the prediction of vibrational frequencies of short-lived transition metal carbonyl intermediates. The use of the functional M06 to calculate the energy of metal carbonyls has been shown to be more accurate than B3LYP,[8] therefore, we would expect M06 to also be more accurate in predicting carbonyl vibrational frequencies; however, neither of these functionals are going to be accurate in predicting the measured vibrational frequencies, therefore, we calculated a vibrational scaling factor and an overall vibrational shift for each functional. The scaling factors are 0.9519±0.0095 for B3LYP, 0.9429 ± 0.0087 for M06 and 0.9565 ± 0.0095 for M06-L and overall shifts are 102 ± 16, 121 ± 15, 93 ± 17 cm^{-1}, respectively. To compare the precision of each calculated scaling factor, the magnitude is not important, only the standard deviation. Even ignoring solvation, each functional does a reasonable job determining the vibrational frequencies of the intermediates found in **Table 3.1** through **Table 3.4**. While there is some improvement using M06, surprisingly

B3LYP has nearly identical accuracy in predicting transition metal carbonyl complexes.

3.5 References

1. Church, S. P.; Grevels, F. W.; Hermann, H.; Schaffner, K., Fast Infrared Detection of Pentacarbonyldinitrogenchromium ($Cr(CO)_5N_2$) in Room-Temperature Solution. *Inorg. Chem.* **1984,** *23*, 3830–3833.

2. Welch, J. A.; Peters, K. S.; Vaida, V., Medium Effects on the Photodissociation of Hexacarbonylchromium ($Cr(CO)_6$). *J. Phys. Chem.* **1982,** *86*, 1941–1947.

3. Jonas, V.; Thiel, W., Theoretical Study of the Vibrational Spectra of the Transition-Metal Carbonyl Hydrides $HM(CO)_5$ (M=Mn, Re), $H_2M(CO)_4$ (M=Fe, Ru, Os), and $HM(CO)_4$ (M=Co, Rh, Ir). *J. Chem. Phys.* **1996,** *105*, 3636–3648.

4. Gonzalez-Blanco, O.; Branchadell, V., Density Functional Study of the Fe–CO Bond Dissociation Energies of $Fe(CO)_5$. *J. Chem. Phys.* **1999,** *110*, 778–783.

5. Becke, A. D., Density-Functional Thermochemistry. III. The Role of Exact Exchange. *J. Chem. Phys.* **1993,** *98*, 5648–5652.

6. Lee, C.; Yang, W.; Parr, R. G., Development of the Colle-Salvetti Correlation-Energy Formula into a Functional of the Electron Density. *Phys. Rev. B* **1988,** *37*, 785–789.

7. (a) Reiher, M.; Salomon, O.; Artur Hess, B., Reparameterization of Hybrid Functionals Based on Energy Differences of States of Different Multiplicity. *Theor. Chim. Acta* **2001,** *107*, 48–55; (b) Harvey, J. N., On the Accuracy of Density Functional Theory in Transition Metal Chemistry. *Annu. Rep. Prog. Chem. Sect. C:*

Phys. Chem. **2006,** *102*, 203–226; (c) Schultz, N. E.; Zhao, Y.; Truhlar, D. G., Density Functionals for Inorganometallic and Organometallic Chemistry. *J. Phys. Chem. A* **2005,** *109*, 11127–11143.

8. Zhao, Y.; Truhlar, D. G., Density Functionals with Broad Applicability in Chemistry. *Acc. Chem. Res.* **2008,** *41*, 157–167.

9. Zhao, Y.; Truhlar, D. G., A New Local Density Functional for Main-Group Thermochemistry, Transition Metal Bonding, Thermochemical Kinetics, and Noncovalent Interactions. *J. Chem. Phys.* **2006,** *125*, No. 194101.

10. Valiev, M.; Bylaska, E. J.; Govind, N.; Kowalski, K.; Straatsma, T. P.; Van Dam, H. J. J.; Wang, D.; Nieplocha, J.; Apra, E.; Windus, T. L.; de Jong, W. A., NWChem: A comprehensive and Scalable Open-Source Solution for Large Scale Molecular Simulations. *Comput. Phys. Commun.* **2010,** *181*, 1477–1489.

11. Karahan, S.; Kose, P.; Subasi, E.; Alp, H.; Temel, H., Photochemical Reactions of $M(CO)_5THF$ (M = Cr, Mo, W) with Thio Schiff bases. *Transition Met. Chem*. **2008,** *33*, 849–854.

12. Barré, C.; Boudot, P.; Kubicki, M. M.; Moiese, C., Synthesis, Spectroscopy, Bonding and Structure in Phosphido Bridged Bimetallics Derived from Bent Metallocenes of Molybdenum and Tungsten and from Group 6 Metal Carbonyls. *Inorg. Chem*. **1995,** *34*, 284–291.

13. Goff, S. E. J.; Nolan, T. F.; George, M. W.; Poliakoff, M., Chemistry of Reactive Organometallic Compounds at Low Temperatures and High Pressures: Reactions of $M(CO)_6$ (M = Cr, Mo, W), $(\eta^6\text{-}C_6H_3Me_3)M(CO)_3$ (M = Cr and Mo), and

$W(CO)_5CS$ with H_2 and N_2 in Polyethylene Matrices. *Organometallics* **1998,** *17*, 2730–2737.

14. Sheffield, C. Time-Resolved Infrared Spectroscopy and Density Functional Theory Study of Weak Interactions of Metal Carbonyls and Organic Solvents. Brigham Young University, Provo, 2010.

15. Grills, D. C.; Huang, K.-W.; Muckerman, J. T.; Fujita, E., Kinetic Studies of the Photoinduced Formation of Transition Metal-Dinitrogen Complexes Using Time-Resolved Infrared and UV-vis Spectroscopy. *Coord. Chem. Rev.* **2006,** *250*, 1681–1695.

16. Ishikawa, Y.; Hackett, P. A.; Rayner, D. M., Coordination of Molecular Hydrogen and Nitrogen to Coordinatively Unsaturated Tungsten Carbonyls in the Gas Phase. *J. Phys. Chem.* **1989,** *93*, 652–657.

17. Paur-Afshari, R.; Lin, J.; Schultz, R. H., An Unusual Solvent Isotope Effect in the Reaction of $W(CO)_5$(solv) (solv = Cyclohexane or Cyclohexane-d12) with THF. *Organometallics* **2000,** *19*, 1682–1691.

18. Banno, M.; Iwata, K.; Hamaguchi, H.-o., Intra- and Intermolecular Vibrational Energy Transfer in Tungsten Carbonyl Complexes $W(CO)_5(X)$ (X = CO, CS, CH_3CN, and CD_3CN). *J. Chem. Phys.* **2007,** *126*.

Chapter 4: Solvent Exchange Dynamics of Weakly Bound Organic Solvents to Group 6 Metal Carbonyls

4.1 Introduction

Solvent exchange reactions involving group 6 transition metal carbonyls have been of considerable interest over the last few decades. This interest stems from the importance of transition metals as catalysts in industry and in the synthesis of organic molecules and natural products. Ultrafast studies have shown these types

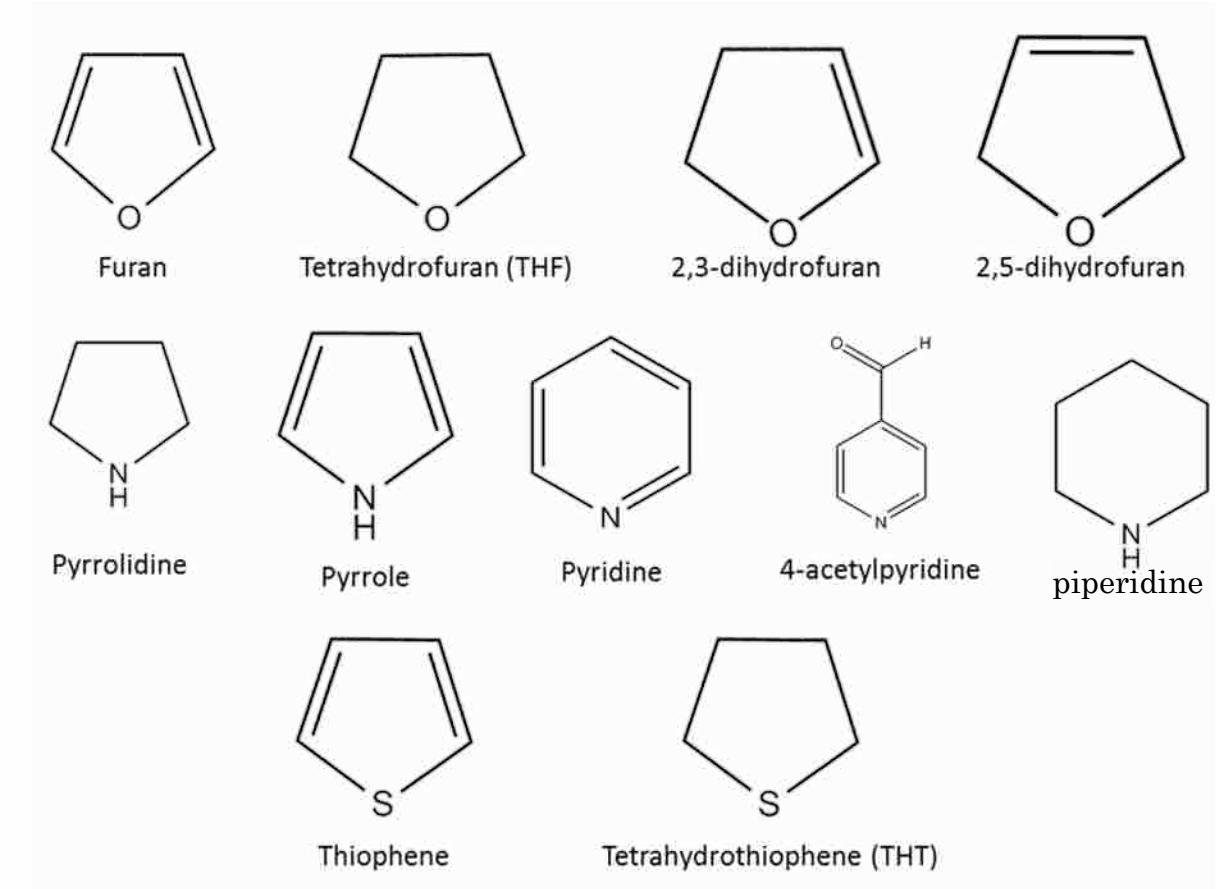

Figure 4.1. Moderate Binding Ligands Previously Studied in the Solvent Exchange Reaction.

of reactions proceed through the formation of a solvated complex in the first 20 ps.[1] This solvated complex then reacts with a secondary ligand in solution as depicted in **Equation 4.1**; where solv denotes solvent, L for ligand and M = Cr, Mo and W.

$$M(CO)_5(solv) + L \rightarrow M(CO)_5L + solv \qquad \textbf{Equation 4.1}$$

$$Rate = k[M(CO)_5(solv)][L] \qquad \textbf{Equation 4.2}$$

The rate law for **Equation 4.1** predicts a reaction that is first-order in the solvated metal carbonyl and first-order in the entering ligand (see **Equation 4.2**). The decay of the solvated metal pentacarbonyl however, follows pseudo-first-order kinetics and is fit with a single exponential. The concentration of the ligand is in such excess that the solvent exchange reaction can be modeled as:

$$Rate = k'[M(CO)_5(solv)] \qquad \textbf{Equation 4.3}$$

Previous studies of these exchange reactions include gas phase,[2] unreactive liquid noble gases,[3] matrix isolation[4] and solution phase.[2, 4a, 5] The development of fast Time-Resolved Fourier Transform IR spectroscopy (TR-FTIR) and Photoacoustic Calorimetry (PAC) has enabled us to better probe these solvent exchange reactions. Thermodynamical properties have been measured for **Equation 4.1** with L = THF,[5b, 6] furan,[5b, 5f] pyridine,[6] acetonitrile,[6] 2-picoline,[6] pyrrolidine,[5b] pyrrole,[5b] THT,[5b] thiophene,[5b] 4-acetylpyridine,[7] 1-hexene,[6, 8] carbon monoxide,[9] 2,3-dihydrofuran,[5f] piperidine,[6, 8] and 2,5-dihydrofuran.[5f] These strong to moderately binding ligands (see **Figure 4.1**) proceed by an associative mechanism with a late transition state.[5f]

We now for the first time have carried out these measurements for the weakly binding ligands, benzene and mesitylene to chromium, molybdenum and tungsten pentacarbonyl and compare our results with the more strongly binding ligands previously studied.

4.2 Methods

4.2.1 Reagents

Metal carbonyls were obtained from Aldrich with purities of 97% for $W(CO)_6$, 99% for $Cr(CO)_6$ and 98% for $Mo(CO)_6$ and were stored as received. Solvents were obtained from; Fisher, HPLC grade cyclohexane and spectranalyzed benzene, Sigma Aldrich, reagent plus 99% methylcyclohexane and Acros, 99% extra pure mesitylene. All solvents were stored over activated molecular sieves and back filled with argon upon opening and after each use.

4.2.2 Sample Preparation

Sample solutions of metal carbonyls were prepared by dissolving 2.5 to 5 mM $M(CO)_6$ (M = Cr, W, Mo) in methylcyclohexane. To reduce contamination by water and oxygen, all glassware was stored in an oven, and samples were prepared by three cycles of freeze, pump, thawing followed by back-filling with argon. In addition to methylcyclohexane, samples were prepared with a secondary solvent, 1% to 4% of either benzene or mesitylene. Sample preparation and experiments were carried out under a positive argon pressure of slightly greater than one atmosphere.

4.2.3 Step Scan Spectroscopy

During data collection, samples were continuously flowed through an IR cell to a lower return cell where a peristaltic pump (Masterflex Easy-load II) returned the sample back to an upper holding cell. Return and holding glass cells were produced in-house with an outer jacket to facilitate flowing ethylene glycol from a temperature bath. Reactions were photoinitialized by pumping the metal to ligand charge transfer (MLCT) bands on the metal carbonyls with a tripled YAG (Continuum Precision II) pumped OPO (Optical Parametric Oscillator, Continuum Panther). Intermediates were monitored with a Bruker model IFS/66S FTIR equipped with a mercury cadmium telluride (MCT) detector modified for step scan experiments. A band pass IR filter (1600 to 2600 cm^{-1}) was placed in front of the MCT detector to reduce the number of interferometer points needed to complete each step scan measurement. The timing pulse from the Continuum Precision II was sent through a Stanford Research Digital Delay Pulse Generator (model number DG535) to sync the FTIR and laser.

4.2.4 DFT Calculations

Calculations of bond enthalpies was conducted using density functional level of theory using NWCHEM[10] and Gaussian 09.[11] Jobs were built using ECCE[12] and run on a single 12 processor node (Marylou 4, Brigham Young University Fulton Supercomputing Lab).

Calculations of binding energies were further adjusted for Basis Set Superposition Error (BSSE), however, because of the way NWCHEM handles this

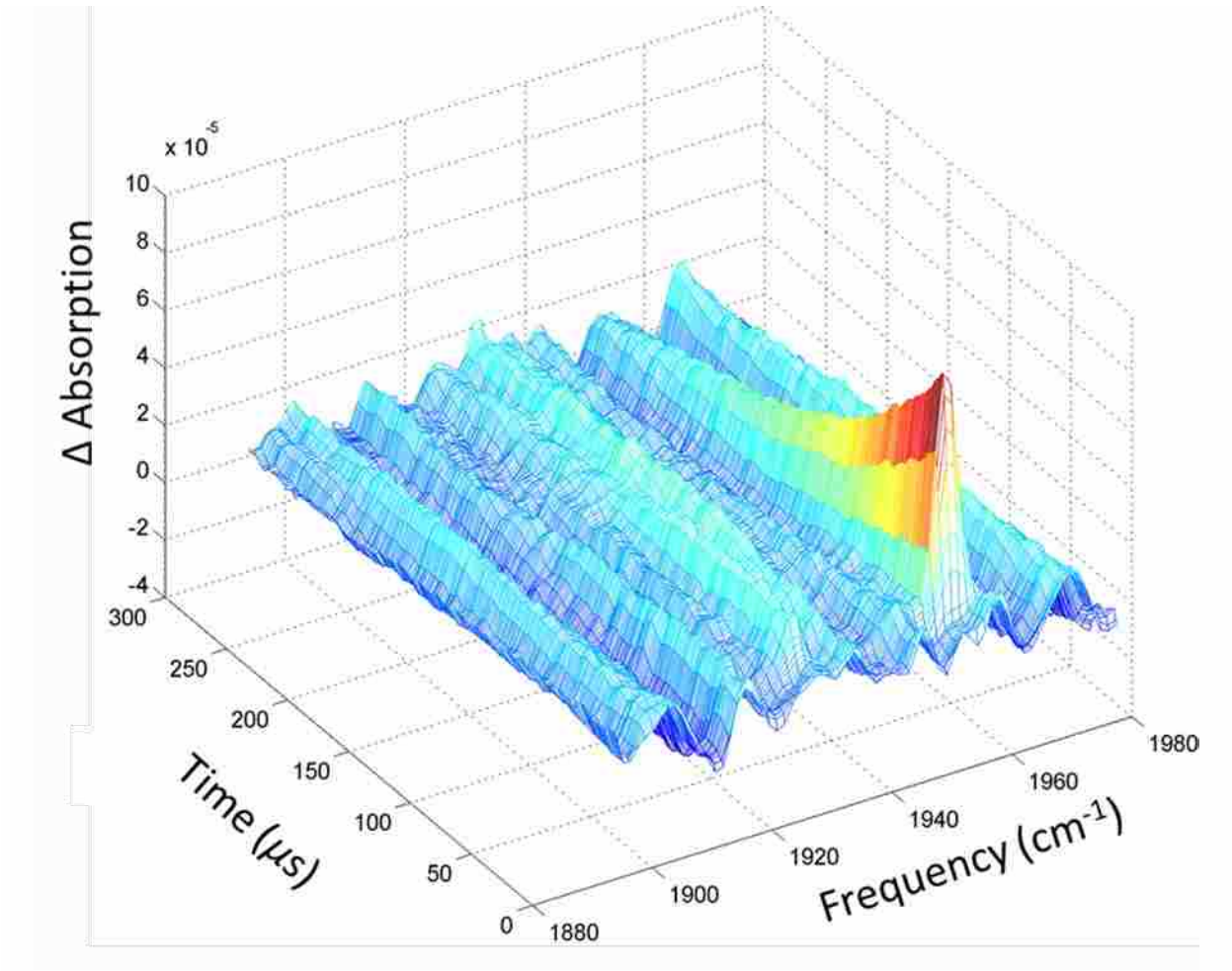

Figure 4.2 Decay of Photogenerated $W(CO)_5$(methylcyclohexane) at 1953 cm^{-1} from 2.5 mM $W(CO)_6$ in methylcyclohexane in 200 to 250 μs.

correction, we could not correct for Zero Point Energy (ZPE). In NWCHEM BSSE is fixed by assigning orbitals which do not belong to the fragment being calculated as "ghost atoms" to use the basis set from the whole complex to calculate the energy of the fragment, therefore, you cannot do a geometry relaxation before the energy calculation. The calculated bond enthalpies are the energy differences between relaxed weakly bound ligand metal carbonyls and the unrelaxed ligand and metal carbonyl fragments:

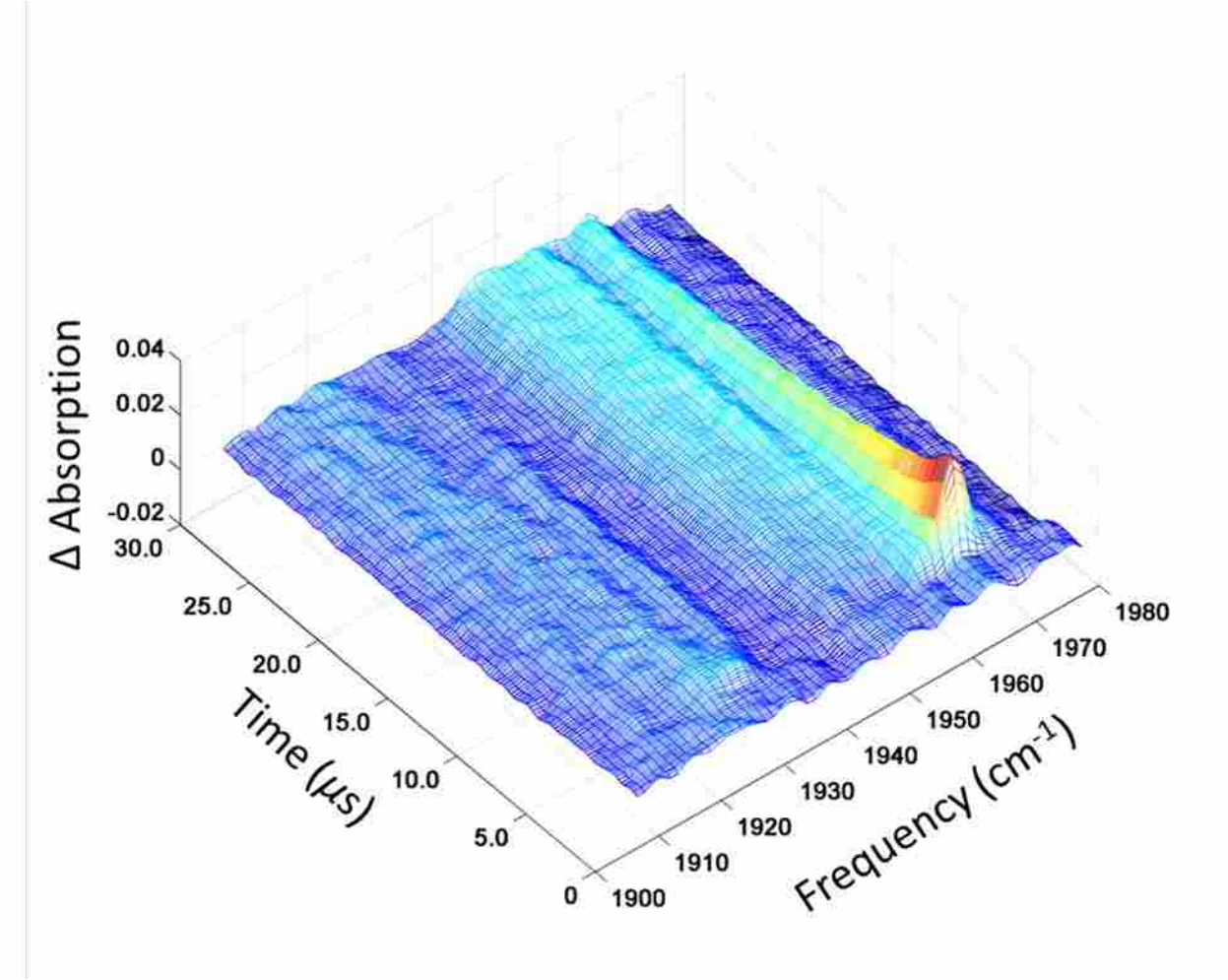

Figure 4.3. Decay of Photogenerated $Mo(CO)_5$(methylcyclohexane) at 1963 cm-1 from 2.5 mM Mo(CO)6 in methylcyclohexane to form an Mo dimer complex in 5 to 10 μs.

$$E_{bond} = E_{complex} - \Sigma\, E_{fragments} \qquad \textbf{Equation 4.4}$$

4.3 Results

4.3.1 SS FTIR Spectra

To observe the reaction between methylcyclohexane and group 6 metal hexacarbonyls, SS-FTIR spectra were first taken in methylcyclohexane. Within the time resolution of our detector, the photogenerated coordinatively unsaturated

$Cr(CO)_5$,[13] $W(CO)_5$ (see **Figure 4.2**) and $Mo(CO)_5$ (see **Figure 4.3**) each formed solvated intermediates with methylcyclohexane. For chromium[13] and tungsten these intermediates last for microseconds. Molybdenum, however, is more reactive and decays more quickly, see **Figure 4.3**. Step Scan FTIR spectra of samples of 2.5 mM and 5.0 mM $Mo(CO)_6$ in neat cyclohexane yielded a rates of reaction with a ratio of three, suggesting that the reaction is second order in $MO(CO)_5$(solv) concentration and that there may be a formation of a molybdenum dimer. Further investigation is required in order to fully understand the kinetics of this reaction.

All $M(CO)_6$ (M = Cr, W, Mo) in organic solvents, with low concentrations of a secondary ligand, follow similar reaction pathways. There is a loss of a carbonyl upon photolysis of $M(CO)_6$ to form $M(CO)_5$; however, due to the response time of our detector, we were unable to observe this intermediate. Wang et al.[14] observed the formation of naked $Cr(CO)_5$ within 200 fs of the photolysis of the parent $Cr(CO)_6$. We observed bleaching of the parent to occur at 1984 cm^{-1} for $Cr(CO)_6$, 1981 cm^{-1} for $W(CO)_6$ and 1987 cm^{-1} for $Mo(CO)_6$. These frequencies are not included in the SS FTIR plots because the parent absorption is very strong in comparison to the absorptions of the intermediates. Bleaching of the parent peak is followed by the formation of a solvated transient within 25 ps.[15] We observed absorptions at 1957 cm^{-1} and 1932 cm^{-1} for $Cr(CO)_5C_6H_{12}$,[13] 1953 cm^{-1} and 1926 cm^{-1} for $W(CO)_5$(methylcyclohexane) (see **Figure 4.4**) and 1963 cm^{-1} and 1929 cm^{-1} for $Mo(CO)_5$(methylcyclohexane) (see **Figure 4.5**). Within the 4 cm^{-1} resolution of our experiments, the frequencies for complexes with cyclohexane and

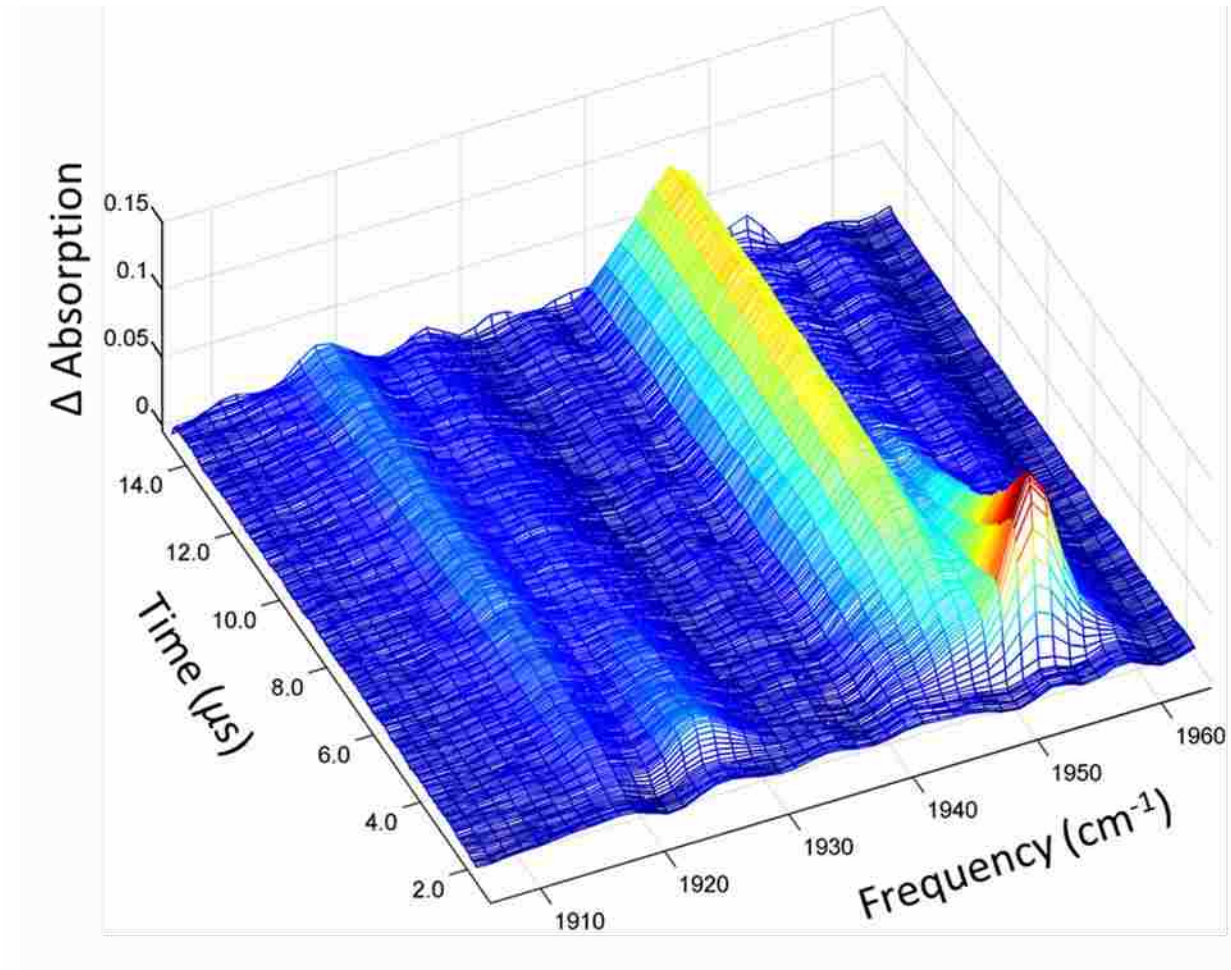

Figure 4.4 Decay of $W(CO)_5$(methylcyclohexane) in a solution of 4% benzene and methylcyclohexane to form $W(CO)_5$(benzene).

methylcyclohexane are indistinguishable, for a given metal center. These solvated complexes are the statistical products of the reaction of the "naked" $M(CO)_5$ with the solvent cage. The solvent cage around the "naked $M(CO)_5$ is primarily composed of the solvent, because the ligand or secondary solvent is in such low concentrations, therefore, the product of reacting with the solvent cage is the statistical product. The exchange of solvents for the more thermodynamically stable product takes place in the nanosecond time scale and follows pseudo-first-order kinetics.[5j, 5l] The

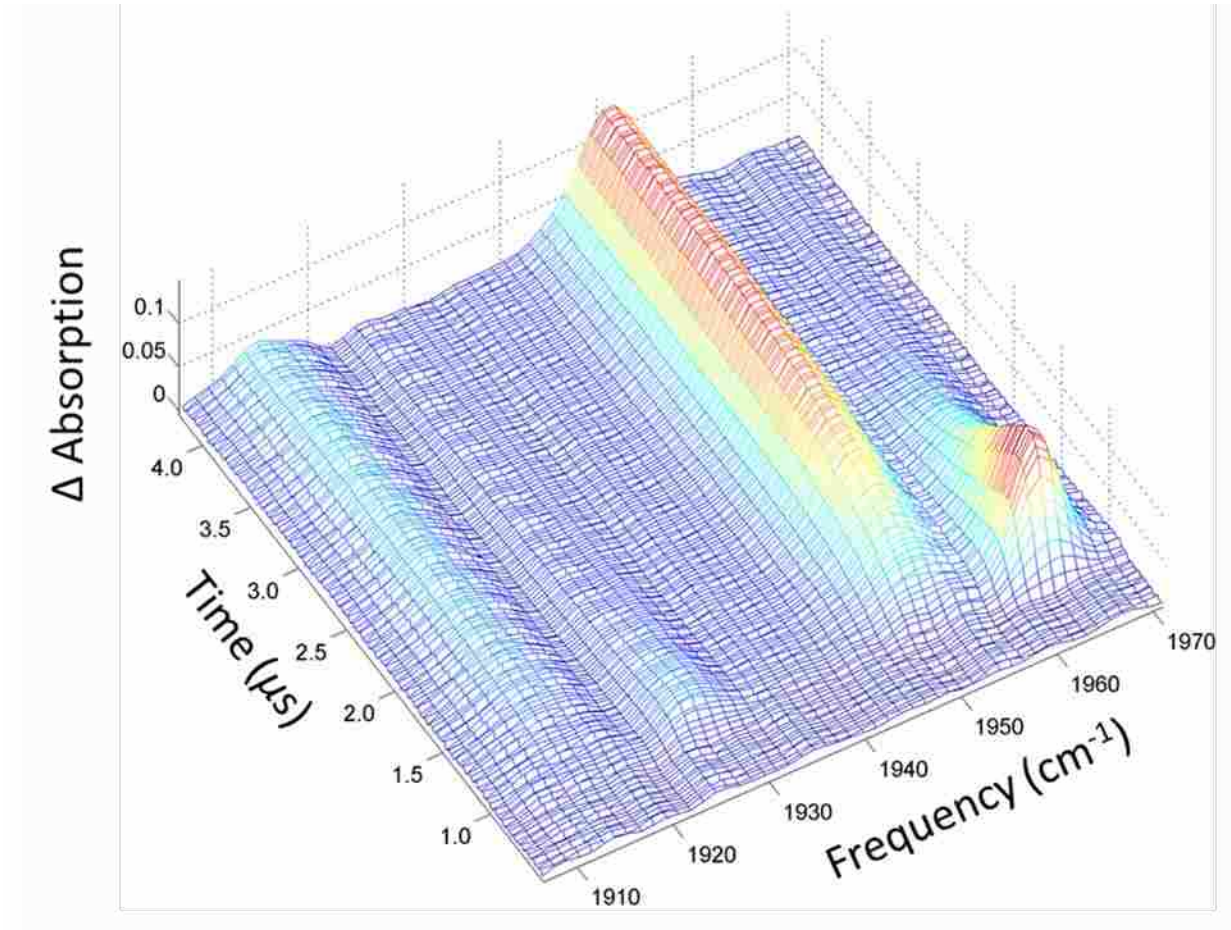

Figure 4.5 Decay of $Mo(CO)_5$(methylcyclohexnae) in 4% mesitylene and methylcyclohexane to form $Mo(CO)_5$(mesitylene).

formation of $Cr(CO)_5C_6H_6$ was identified by peaks at 1950 cm^{-1} and 1925 cm^{-1},[13] $W(CO)_5C_6H_6$ peaks at 1953 cm^{-1} and 1926 cm^{-1} (see **Figure 4.4**), $Mo(CO)_5C_6H_6$ peaks at 1963 cm^{-1} and 1929 cm^{-1} and $Mo(CO)_5$(mesitylene) with peaks at 1952 cm^{-1} and 1916 cm^{-1} (see **Figure 4.5**). The final product observed in our studies, appearing in the microsecond to millisecond time scale, is due to a contaminant complex $M(CO)_5(H_2O)$. This complex is also the final product in the photolysis of $M(CO)_6$ (M = Cr and W) in neat cyclohexane. This complex was first observed by Kelly et al.[16] with absorptions of 1943 cm^{-1}, 1913 cm^{-1} for $Cr(CO)_5(H_2O)$.[3b, 5j]

Single frequency slices from the decay of the methylcyclohexane solvated metal carbonyl complexes were fit to a single exponential (see 2.6 Data Analysis for further details). An Arrhenius plot (see **Figure 4.6**) was produced from the temperature dependent rate constants (summarized in). Activation energies were calculated from the slope of a linear least squares fit to the data. In addition to these Arrhenius plots, an Eyring analysis (including the kinetic data taken by Sheffield[13] for M=Cr and L=benzene) was performed, and enthalpies and entropies of reaction were calculated from the slope and y-intercept, respectively. These thermodynamical calculations are summarized in **Table 4.1**. Note that the order of reactivity of the three transition metals in this study goes as: Mo > Cr > W which is consistent with the findings by Goff and coworkers.[4b]

Table 4.1. Temperature Dependent Rate Constants for the Solvent Exchange Reaction with M = Mo, W, solv = Methylcyclohexane and L = Benzene, Mesitylene.

Metal	Molybdenum				Tungsten			
Solvent	Methylcyclohexane				Methylcyclohexane			
Ligand	Benzene		Mesitylene		Benzene		Mesitylene	
Temperature Dependent Rate Constants	T (^{0}C)	k (μs^{-1} M^{-1})	T (^{0}C)	k (μs^{-1} M^{-1})	T (^{0}C)	k (μs^{-1} M^{-1})	T (^{0}C)	k (μs^{-1} M^{-1})
	7.1	0.00223			4.9	0.000180	9.5	0.000102
	11.2	0.00281	11.7	0.00148	13.0	0.000216	12.3	0.000095
	16.2	0.00309	16.6	0.00168	17.0	0.000271	16.1	0.000123
	21.0	0.00356	20.8	0.00194	22.8	0.000427	21.9	0.000174
	25.6	0.00464	25.4	0.00260	26.5	0.000393		
	30.1	0.00501	30.4	0.00312	30.6	0.000454		
	35.0	0.00559	34.1	0.00358	36.1	0.000665	36.3	0.000313
	38.9	0.00631	38.1	0.00411	39.0	0.000885	39.2	0.000395
	43.6	0.00792	44.1	0.00501	44.4	0.001177		

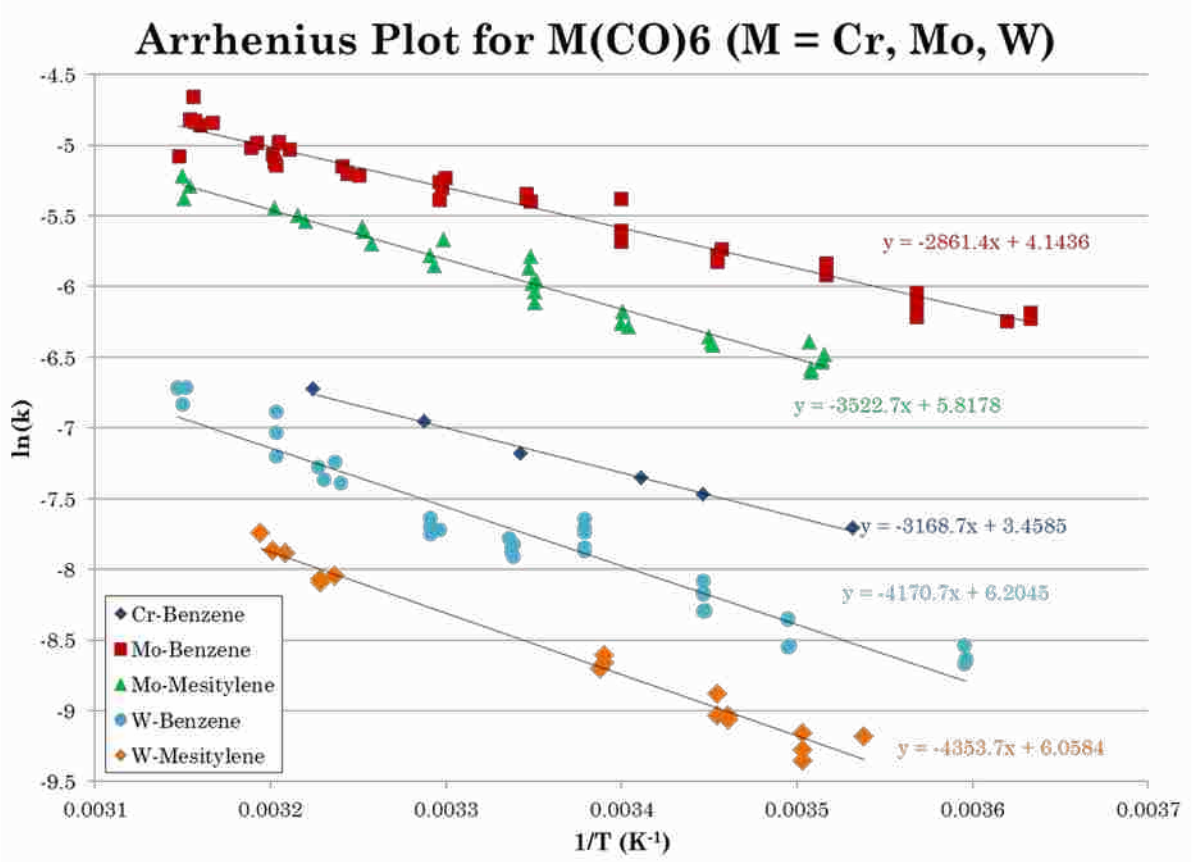

Figure 4.6 Arrhenius plot of pseudo-first-order decay of $M(CO)_5$(methylcyclohexane) M = Cr, Mo, W and L = benzene, mesitylene at temperatures of 4 to 44 ^{0}C.

Dobson and Zhang noticed that values of $\Delta S^{\ddagger}$ steadily increased as values of $\Delta H^{\ddagger}$ increased (R = 0.953) for **Equation 4.1** with M = Cr, solv = n-heptane using a series of trapping nucleophiles, piperidine, tetrahydrofuran, pyridine, acetonitrile, 2-picoline, ethanol, l-hexene, chlorobenzene and 2,6-lutidine).[6] Following this work, Schultz[5b, 5e] and coworkers plotted the enthalpies of reaction vs. entropies of reaction for both M = Cr, L = cyclohexane and M = W, L = cyclohexane. **Figure 4.7** is a plot of data measured by the Schultz group and our measurement of the enthalpy and entropy of activation for the $W(CO)_5$(benzene) complex. The linear

least squares fit for both the Schultz set and the entire set is shown in the plot. While there is a slight difference in the linear fit of the two sets of data, including our measurement slightly increases the R^2 of the fit. This is evidence that, even though our experiments were performed with different instruments, sample preparation and in different primary solvents, the results are in good agreement. A plot of $\Delta H^{\ddagger}$ vs. $\Delta S^{\ddagger}$ for molybdenum hexacarbonyl was not possible as a search of the literature yielded few studies of the $\Delta H^{\ddagger}$ for these complexes exists and none which also include values for $\Delta S^{\ddagger}$ could be found.

Table 4.2. Thermodynamic Properties of Solvent Exchange Reaction for Group Six Transition Metal Carbonyls.

Metal	Solvent	Ligand	Ea (kJ/mol)	$\Delta H^{\ddagger}$ (kcal/mol)	$\Delta S^{\ddagger}$ (cal/mol K)	References
Cr	Cyclohexane	Benzene	26.3	6.89	-0.195	Sheffield[13]
Mo	Methylcyclohexane	Benzene	23.7	6.26	-0.194	This Work
W	Methylcyclohexane	Benzene	35.1	8.98	-0.191	This Work
Mo	Methylcyclohexane	Mesitylene	29.8	7.70	-0.191	This Work
W	Methylcyclohexane	Mesitylene	38.9	9.30	-0.190	This Work

4.3.2 Computational Binding Energies

Density Functional Theory was used to calculate binding energies of $M(CO)_5$(methylcyclohexane) (M = Cr, Mo, W) were 18.8, 20.2 and 28.1 kJ/mol for the density functional B3LYP and 44.8, 45.8 and 54.3 for the density functional M06 and 41.2, 41.9 and 48.7 for the density functional M06-L, respectively. All computations were ran using the 6-31G* basis set. As expected the density functional B3LYP under predicted the binding energy; it does not make sense that the binding energy for the solvated metal carbonyl is lower than the activation

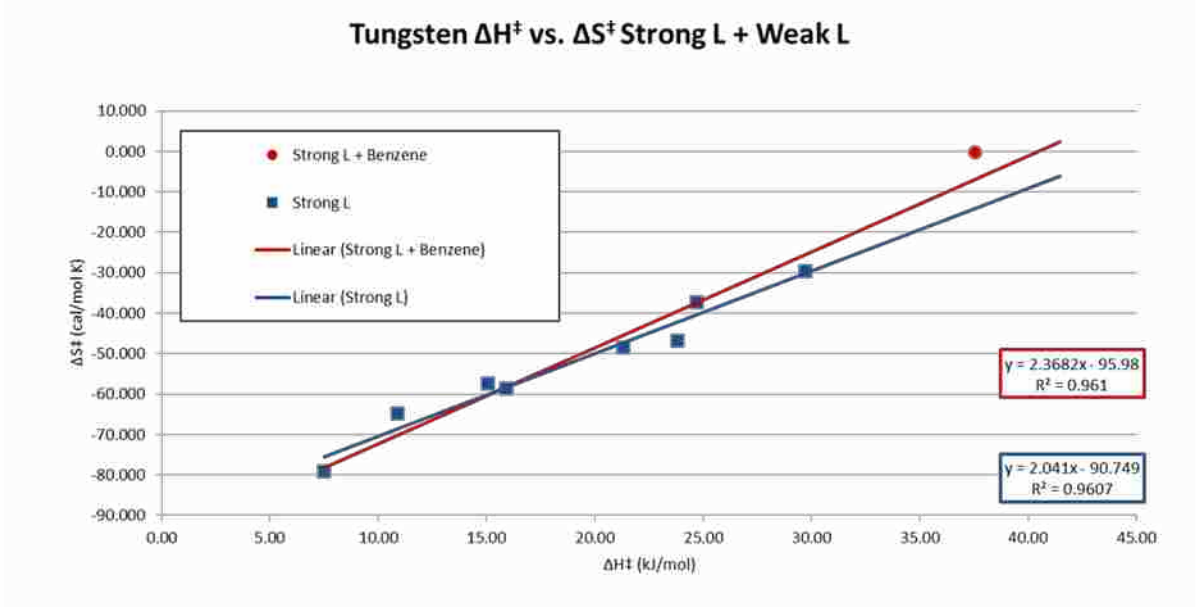

Figure 4.7 Linear relationship of ΔH‡ and ΔS‡ for moderate to weakly binding ligands to tungsten pentacarbonyl.

energy for the solvent exchange reaction. We also see that the binding energies using the density functionals M06 and M06-L are close to twice that of the measured activation energies, suggesting that the solvent exchange reaction proceeds through an associative type mechanism. The order of reactivity for the solvent exchange mechanism is not predicted correctly with either M06 or M06-L. A DFT study by Ziegler et al.[17] predicted the order of reactivity to be Cr ≈ W > Mo for the loss of the first carbonyl by the addition of more relativistic effects in the basis set and density functional.

4.3.3 Exchange Mechanism for Weakly Bound Ligands

If the reaction proceeds through a dissociative mechanism, the transition state species would be $M(CO)_5$ and the enthalpies of reaction calculated from the measured kinetics would be the bond dissociation energy for $M(CO)_5$(solv).

However, if the exchange takes place by way of an associative mechanism, the enthalpies of reaction would depend on the strength of the exchanging ligand. The transition state would be stabilized by electron density donated into the metal center by both the solvent and the entering ligand. This enthalpy of reaction would depend on the strength of the entering ligand; strong ligands would stabilize the transition state more than weak ligands. The energy of activation would decrease as the strength of the entering ligand increases. Therefore, the most probable ligands to follow an associative pathway would be the strongest binding, while those to most likely follow a dissociative pathway would be the weakest binding.

Sterics would also play a role in the enthalpy of activation; more bulky ligands and metals with smaller radii would increase this barrier. Chromium, the smallest of the group 6 metals, would be most likely to proceed through a dissociative pathway and thus have a transition state that would be most dissociative in character. A large bulky ligand like mesitylene (1,3,5-trimethylbenzne) would also cause the exchange reaction to behave more dissociative than benzene.

The solvent-ligand exchange reaction for the formation of $Cr(CO)_5C_6H_6$ in a solution of cyclohexane and positive pressure of CO was first proposed by Kelly et al.[16] to follow an associative mechanism; however, this was based on the measurement of only the room temperature rate constant for **Equation 4.1**.

Dobson and Zhang[6] measured the kinetics and deduced the mechanism for the displacement of *n*-heptane from photogenerated $Cr(CO)_5$(n-heptane) with

secondary ligands of piperidine, tetrahydrofuran, pyridine, acetonitrile, 2-picoline, ethanol, 1-hexene, chlorobenzene and 2,6-lutidine with pulsed laser flash photolysis and UV detection. They observed that the reaction takes place with a competition of associative interchange and dissociative mechanisms and that the overall mechanism is dependent on the identity of solvent and entering ligand. Ligands with greater sterics proceed by a dissociative mechanism, whereas less sterically hindered ligands proceed through an associative interchange pathway, and the upper limit in which the reaction switches is the bond dissociation energy of Cr-*n*-heptane of 8 kcal/mole. This energy was also measured by Burkey to be 11.62 kcal/mole using time resolved photoacoustic calorimetry.[5w]

Using SS FTIR, Krav-Ami and Shultz[5i] measured the rates of reaction of the solvent exchange reaction on $W(CO)_5$ in cyclohexane for a series of ligands. The rate of reaction was observed to linearly increase with a larger red shift in the IR spectrum of $W(CO)_5L$ for L = pyrrolidine to furan. Increased backbonding from the metal center into the CO π antibonding orbitals weakens the CO bond strength, creating a red shift in the CO vibrational spectra. This in turn can be interpreted as an increase in electron donating ability of the ligand. The larger the CO red shift, the greater the electron donating ability of the ligand and, therefore, the better able it is to stabilize the transition state. This analysis leads Krav-Ami and coworkers to an associative mechanism with a transition state that has the solvent cyclohexane still within the coordination sphere of tungsten.

Paur-Afshari et al.[5d] studied the exchange kinetics of (1) with L = tetrahydrofuran (THF) and observed an entropy of activation for $W(CO)_5THF$ in cyclohexane solution considerably lower than the bond dissociation energy of $W(CO)_5C_6H_{12}$ of 15 kcal/mole. If the solvent exchange reaction were purely dissociative, the reaction would proceed first by the leaving or dissociation of cyclohexane, and second by the entering of the secondary solvent (in Paur-Afshari's studies this would be THF). Because the enthalpy of activation is much smaller than the literature value of the bond dissociation energy, there must be a more energetically favorable transition state. They also observed that the reaction proceeds more slowly in C_6D_{12} even though $\Delta H^{\ddagger}$ is smaller than for cyclohexane. This observation points to the solvent having a large entropic contribution to the reaction kinetics, possibly due to low frequency metal solvent hindered rotations.

In continuation of the work in the Schultz group with THF, Lugovskoy and coworkers[5f] measured enthalpies of reaction of the solvent exchange reaction with ligands; furan, 2,3-dihydrofuran and 2,5-dihydrofuran, using step scan FTIR spectroscopy. The low values of enthalpies of activation support the findings for the THF data. They also observed large negative values for the entropies of activation, providing evidence that the rate determining step is not solvent dissociation. Lacking evidence of an intermediate with an increased coordination sphere around the central metal, Lugovskoy explains the solvent exchange reaction group 6 transition metal carbonyls with moderately binding ligands to occur through and associative process with a late transition state.

Observations by the Schultz group of the solvent exchange reaction for strong to moderately binding ligands aided in the determination of this mechanism to proceed through an associative pathway; however, if the entering group is weakly binding and therefore less likely to persuade the solvent to leave, would the reaction still be considered associative? We have measured the activation energies for the exchange of the solvent cyclohexane by weakly binding benzene to the group 6 transition metals Cr, Mo and W to be 26.3 kJ/mol, 23.7 kJ/mol and 35.1 kJ/mol, and the enthalpy of reaction to be 6.89 kcal/mol, 6.26 kcal/mol and 8.98 kcal/mol, respectively. The upper limit for the enthalpy of reaction for an associative pathway would be the bond dissociation energy for the metal and primary solvent. Using PAC, Yang et al.[18] measured the bond dissociation energy of $Cr(CO)_5C_6H_{12}$ to be 15 kcal/mole in the solution phase. Therefore, the solvent exchange process with weakly binding ligands must also proceed through a similar associative interchange pathway spoken of by Lugovskoy.[5f] However the very small negative of the entropy of reaction values (-0.194 cal mol^{-1} $K^{-1}$for M=Mo and L =benzene, -0.191 cal mol^{-1} K^{-1} for M=Mo and L=mesitylene, -0.191 cal mol^{-1} K^{-1} for M=W and L=benzene, and -0.191 cal mol^{-1} K^{-1} for M=W and L=mesitylene) must mean that the transition state has more solvent metal bond breaking than ligand bond forming than with more strongly binding ligands like THF.

We do not, however, have binding energies for $Mo(CO)_5$(cyclohexane) and $W(CO)_5$(cyclohexane) and therefore cannot draw the same hard conclusions. Reactions with tungsten precede much slower, implying ligands bond much slower

than they do with chromium. Therefore, we would expect the binding energy to be larger than 15 kcal/mol. The ligand exchange reaction with tungsten must therefore also follow an associative interchange mechanism, though it appears to have more dissociative character. The data for molybdenum suggests that the bond dissociation energy would be lower than 15 kcal/mol, and a further analysis would depend on how much lower this is.

In addition, we have studied the ligand exchange with L =mesitylene (1,3,5-trimethylbenzne) and M = Mo. Mesitylene will be more sterically hindered then L = benzene, which is confirmed in that the activation energy increases to 29.8 kJ/mole from 23.7 kJ/mol. This series of experiments needs to continue to measure the activation energy for the formation of $Cr(CO)_5$(mesitylene) and $W(CO)_5$(mesitylene). This will allow for a better understanding of the role of sterics down the entire group 6 metal carbonyls in the ligand exchange reaction.

4.4 Conclusions

The rate of the ligand exchange reaction has been measured for the weakly binding ligands benzene and mesitylene giving activation energies of 26.3 kJ/mol (M = Cr, L = benzene), 23.7 kJ/mol (M = Mo, L = benzene), 35.1 kJ/mol (M = W, L = benzene) and 29.8 kJ/mol (M = Mo, L = mesitylene). An Eyring analysis yielded enthalpy and entropy of reaction values. The enthalpy of reaction values were all less than the bond dissociation energy of $Cr(CO)_5C_6H_{12}$, implying the reaction takes place through an associative pathway. Entropy of reaction values were only slightly

negative. Therefore, the transition state has more metal solvent bond breaking than metal ligand bond formation.

4.5 References

1. Asplund, M. C.; Yang, H.; Kotz, K. T.; Bromberg, S. E.; Wilkens, M. J.; Harris, C. B., Femtosecond Infrared Studies of Chemical Bond Activation. *Laser Chem.* **1999,** *19*, 253–262.

2. Ishikawa, Y.; Hackett, P. A.; Rayner, D. M., Coordination of Molecular Hydrogen and Nitrogen to Coordinatively Unsaturated Tungsten Carbonyls in the Gas Phase. *J. Phys. Chem.* **1989,** *93*, 652–657.

3. (a) Turner, J. J.; Simpson, M. B.; Poliakoff, M.; Maier, W. B., Synthesis and Decay Kinetics of Tricarbonyldinitrogennickel ($Ni(CO)_3N_2$) in Liquid Krypton: Approximate Determination of the Nickel-Dinitrogen ($Ni\text{-}N_2$) Bond Dissociation Energy. *J. Am. Chem. Soc.* **1983,** *105*, 3898–3904; (b) Turner, J. J.; Simpson, M. B.; Poliakoff, M.; Maier, W. B.; Graham, M. A., Mixed Carbonyl-Dinitrogen Compounds: Synthesis and Thermal Stability of $Cr(CO)_{6-x}(N_2)_x$ in Liquid Xenon Solution and Low-Temperature Matrixes. *Inorg. Chem.* **1983,** *22*, 911–920.

4. (a) Burdett, J. K.; Downs, A. J.; Gaskill, G. P.; Graham, M. A.; Turner, J. J.; Turner, R. F., Characterization by Infrared and Raman Spectroscopy of Matrix-Isolated $M(CO)_5N_2$ (M = Chromium, Molybdenum, or Tungsten) Produced by Photolysis of $M(CO)_6$. *Inorg. Chem.* **1978,** *17*, 523–532; (b) Goff, S. E. J.; Nolan, T. F.; George, M. W.; Poliakoff, M., Chemistry of Reactive Organometallic Compounds at Low Temperatures and High Pressures: Reactions of $M(CO)_6$ (M = Cr, Mo, W),

(η^6-$C_6H_3Me_3$)$M(CO)_3$ (M = Cr and Mo), and $W(CO)_5CS$ with H_2 and N_2 in Polyethylene Matrices. *Organometallics* **1998,** *17*, 2730–2737.

5. (a) Shagal, A.; Schultz, R. H., Steric and Electronic Effects in Linkage Isomerization Reactions of $M(CO)_5(L)$ (M = Cr, Mo, W; L = 2-methyl-2,3-dihydrofuran, 2,3-dihydropyran). *Organometallics* **2007,** *26*, 4896–4903; (b) Schultz, R. H.; Biber, L.; Reuvenov, D.; Revzin, T.; Sinai, T.; Zahavi, A., Reactions of the Transient Species $Cr(CO)_5$(cyclohexane) with C_4H_nE (n=4, 8; E = O, NH, S) studied by Time-Resolved IR Absorption Spectroscopy. *J. Chem. Soc., Dalton Trans.* **2007**, 41–51; (c) Schoonover, J. R.; Strouse, G. F., Time-Resolved Vibrational Spectroscopy of Electronically Excited Inorganic Complexes in Solution. *Chem. Rev.* **1998,** *98*, 1335–1356; (d) Paur-Afshari, R.; Lin, J.; Schultz, R. H., An Unusual Solvent Isotope Effect in the Reaction of $W(CO)_5$(solv) (solv = Cyclohexane or Cyclohexane-d12) with THF. *Organometallics* **2000,** *19*, 1682–1691; (e) Lugovskoy, A.; Shagal, A.; Lugovskoy, S.; Huppert, I.; Schultz, R. H., Reaction of the Transient Species $W(CO)_5$(Cyclohexane) with Pyrrolidine and with Pyrrole. *Organometallics* **2003,** *22*, 2273–2278; (f) Lugovskoy, A.; Paur-Afshari, R.; Schultz, R. H., Reaction of the Transient Species $W(CO)_5$(Cyclohexane) with Cyclo-C_4H_nO (n = 4, 6, 8) Studied by Time-Resolved Infrared Absorption Spectroscopy†. *J. Phys. Chem. A* **2000,** *104*, 10587–10593; (g) Lees, A. J.; Adamson, A. W., Reaction Kinetics of the Intermediate Produced in the Laser Pulse Photolysis of Tungsten Hexacarbonyl in Fluid Solution. *Inorg. Chem.* **1981,** *20*, 4381–4384; (h) Krishnan, R.; Schultz, R. H., Electronic and Steric Effects in Ligand Substitution at a Transient Organometallic Species: The

Reaction of $W(CO)_5$(Cyclohexane) with $(CH_3)_n$THF and $(CH_3)_n$Furan (n = 1, 2). *Organometallics* **2001,** *20*, 3314–3322; (i) Krav-Ami, S.; H. Schultz, R., When the Ligands Go Marching in: A Step-Scan Fourier Transform Infrared Spectroscopic Study of Ligand Attack at the Transient Species $W(CO)_5$(CyH). *J. Chem. Soc., Dalton Trans.* **1999**, 115–118; (j) Hermann, H.; Grevels, F. W.; Henne, A.; Schaffner, K., Flash Photolysis with Infrared Detection. The Photochemistry and Secondary Thermal Reactions of $M(CO)_6$ [M = Cr, Mo, and W]. *J. Phys. Chem.* **1982,** *86*, 5151–5154; (k) Grills, D. C.; Huang, K.-W.; Muckerman, J. T.; Fujita, E., Kinetic Studies of the Photoinduced Formation of Transition Metal-Dinitrogen Complexes Using Time-Resolved Infrared and UV-vis Spectroscopy. *Coord. Chem. Rev.* **2006,** *250*, 1681–1695; (l) Church, S. P.; Grevels, F. W.; Hermann, H.; Schaffner, K., Fast Infrared Detection of Pentacarbonyldinitrogenchromium ($Cr(CO)_5N_2$) in Room-Temperature Solution. *Inorg. Chem.* **1984,** *23*, 3830–3833; (m) Barré, C.; Boudot, P.; Kubicki, M. M.; Moiese, C., Synthesis, Spectroscopy, Bonding and Structure in Phosphido Bridged Bimetallics Derived from Bent Metallocenes of Molybdenum and Tungsten and from Group 6 Metal Carbonyls. *Inorg. Chem.* **1995,** *34*, 284–291; (n) Banno, M.; Iwata, K.; Hamaguchi, H.-o., Intra- and Intermolecular Vibrational Energy Transfer in Tungsten Carbonyl Complexes $W(CO)_5(X)$ (X = CO, CS, CH_3CN, and CD_3CN). *J. Chem. Phys.* **2007,** *126*; (o) Zhang, S.; Bajaj, H. C.; Zang, V.; Dobson, G. R.; Vaneldik, R., Volumes of Acitvation for Solvent Displacement-Reactions on Pentacarbonyl Chromium(0) - Comparison of Data for Pure and Mixed-Solvents. *Organometallics* **1992,** *11*, 3901–3903; (p) Yang, G. K.; Vaida, V.;

Peters, K. S., Application of Time-Resolved Photoacoustic Calorimetry to Cr---L Bond Enthalpies in $Cr(CO)_5$---L. *Polyhedron* **1988,** *7*, 1619–1622; (q) Shulin, Z.; Dobson, G. R., Octahedral Metal Carbonyls. 74. Estimates of Solvent-Metal Bond Strengths in (Solvent)$M(CO)_5$ Complexes (Solvent = benzene (M = Mo, W) and Tetrachloromethane (M = Cr)). *Inorg. Chim. Acta* **1991,** *181*, 103–109; (r) Rudzki, J. E.; Goodman, J. L.; Peters, K. S., Simultaneous Determination of Photoreaction Dynamics and Energetics Using Pulsed, Time-Resolved Photoacoustic Calorimetry. *J. Am. Chem. Soc.* **1985,** *107*, 7849–7854; (s) Rothberg, L. J.; Simon, J. D.; Bernstein, M.; Peters, K. S., Pulsed Laser Photoacoustic Calorimetry of Metastable Secies. *J. Am. Chem. Soc.* **1983,** *105*, 3464–3468; (t) Morse, J. M.; Parker, G. H.; Burkey, T. J., Enthalpy of Carbonyl Dissociation from Metal Hexacarbonyls $M(CO)_6$ (M = Chromium, Molybdenum, Tungsten) in Alkane Solvent: Determination of Intermolecular Agostic Bond Strengths. *Organometallics* **1989,** *8*, 2471–2474; (u) Jiao, T.; Leu, G.-L.; Farrell, G. J.; Burkey, T. J., Photoacoustic Calorimetry and Quantum Yields of $Mo(CO)_6$ Ligand Exchange in Linear Alkanes: Determination of Volume of Reaction, Energetics, and Kinetics of Nucleophile Displacement of Alkane from $Mo(CO)_5$(Alkane). *J. Am. Chem. Soc.* **2001,** *123*, 4960–4965; (v) Gittermann, S. M.; Letterman, R. G.; Jiao, T.; Leu, G.-L.; DeYonker, N. J.; Webster, C. E.; Burkey, T. J., Bond Energies, Reaction Volumes, and Kinetics for σ- and π-Complexes of $Mo(CO)_5L$. *J. Phys. Chem. A* **2011**, 9004–9013; (w) Burkey, T. L., *Energetics of Organometallic Species*. Kluwer Academic Publishers: Drodrecht, The Netherlands, 1992; (x) Shimoi, M.; Nagai, S.-i.; Ichikawa, M.; Kawano, Y.; Katoh,

K.; Uruichi, M.; Ogino, H., Coordination Compounds of Monoborane−Lewis Base Adducts: Syntheses and Structures of [$M(CO)_5(\eta^1\text{-}BH_3\text{-}L)$] (M = Cr, Mo, W; L = NMe_3, PMe_3, PPh_3). *J. Am. Chem. Soc.* **1999,** *121*, 11704–11712; (y) Matthews, S. L.; Pons, V.; Heinekey, D. M., Dihydrogen Complexes of Electrophilic Metal Centers: Observation of $Cr(CO)_5(H_2)$, $W(CO)_5(H_2)$ and $[Re(CO)_5(H_2)]+$. *J. Am. Chem. Soc.* **2004,** *127*, 850–851.

6. Dobson, G. R.; Zhang, S. L., Mechanism of Displacement of Alkanes from Photogenerated (Alkane) $Cr(CO)_5$ Complexes. *J. Coord. Chem.* **1999,** *47*, 409–416.

7. Dobson, G. R.; Spradling, M. D., Reactions of 4-Acetylpyridine with $(RH)W(CO)_5$ Intermediats (RH = Cyclohexane, Methylcyclohexane) Produced via Pulsed Laser Flash Photolysis. *Inorg. Chem.* **1990,** *29*, 880–882.

8. Zhang, S. L.; Dobson, G. R., Octahedral Metal-Carbonyls. 79. Mechanism of the Reaction of Photogenerated (solvent)$Cr(CO)_5$ Intermediates with Lewis-Bases (L) in Binary and Ternary Solvent/L Mixtures (Solvent = Fluorobenzene, Chlorobenzene, Normal-heptane - L = 1-hexene, piperidine). *Organometallics* **1992,** *11*, 2447–2452.

9. Breheny, C. J.; Kelly, J. M.; Long, C.; O'Keeffe, S.; Pryce, M. T.; Russell, G.; Walsh, M. M., Photochemistry of (η^6-arene)$Mo(CO)_3$ and the Role of Alkane Solvents in Modifying the Reactions of Coordinatively Unsaturated Metal Carbonyl Fragments. *Organometallics* **1998,** *17*, 3690–3695.

10. Valiev, M.; Bylaska, E. J.; Govind, N.; Kowalski, K.; Straatsma, T. P.; Van Dam, H. J. J.; Wang, D.; Nieplocha, J.; Apra, E.; Windus, T. L.; de Jong, W. A.,

NWChem: A comprehensive and Scalable Open-Source Solution for Large Scale Molecular Simulations. *Comput. Phys. Commun.* **2010,** *181*, 1477–1489.

11. Frisch, M. J.; Trucks, G. W.; Schlegel, H. B.; Scuseria, G. E.; Robb, M. A.; Cheeseman, J. R.; Scalmani, G.; Barone, V.; Mennucci, B.; Petersson, G. A.; Nakatsuji, H.; Caricato, M.; Li, X.; Hratchian, H. P.; Izmaylov, A. F.; Bloino, J.; Zheng, G.; Sonnenberg, J. L.; Hada, M.; Ehara, M.; Toyota, K.; Fukuda, R.; Hasegawa, J.; Ishida, M.; Nakajima, T.; Honda, Y.; Kitao, O.; Nakai, H.; Vreven, T.; Jr., J. A. M.; Peralta, J. E.; Ogliaro, F.; Bearpark, M.; Heyd, J. J.; Brothers, E.; Kudin, K. N.; Staroverov, V. N.; Kobayashi, R.; Normand, J.; Raghavachari, K.; Rendell, A.; Burant, J. C.; Iyengar, S. S.; Tomasi, J.; Cossi, M.; Rega, N.; Millam, J. M.; Klene, M.; Knox, J. E.; Cross, J. B.; Bakken, V.; Adamo, C.; Jaramillo, J.; Gomperts, R.; Stratmann, R. E.; Yazyev, O.; Austin, A. J.; Cammi, R.; Pomelli, C.; Ochterski, J. W.; Martin, R. L.; Morokuma, K.; Zakrzewski, V. G.; Voth, G. A.; Salvador, P.; Dannenberg, J. J.; Dapprich, S.; Daniels, A. D.; Farkas, Ö.; Foresman, J. B.; Ortiz, J. V.; Cioslowski, J.; Fox, D. J. *Gaussian 09*, Gaussian, Inc.: Wallingford CT, 2009, 2009.

12. G.Black; Chase, J.; Chatterton, J.; Daily, J.; Elsethagen, T.; Feller, D.; Gracio, D.; Jones, D.; Keller, T.; Lansing, C.; Matsumoto, S.; Palmer, B.; Peterson, M.; Schuchardt, K.; Stephan, E.; Sun, L.; Swanson, K.; Taylor, H.; Thomas, G.; Vorpagel, E.; Windus, T.; Winters, C. *ECCE, A Problem Solving Environment for Computational Chemistry*, Software Version 6.0 Pacific Northwest National Laboratory: Richland, Washington 99352-0999, USA, 2009.

13. Sheffield, C. Time-Resolved Infrared Spectroscopy and Density Functional Theory Study of Weak Interactions of Metal Carbonyls and Organic Solvents. Brigham Young University, Provo, 2010.

14. Wang, L.; Zhu, X.; Spears, K. G., Unsaturated Transition-Metal Complexes in Solution: Naked $Cr(CO)_5$ in Cyclohexane Solution Observed by Picosecond IR Transient Absorption. *J. Am. Chem. Soc.* **1988,** *110*, 8695–8696.

15. Welch, J. A.; Peters, K. S.; Vaida, V., Medium Effects on the Photodissociation of Hexacarbonylchromium ($Cr(CO)_6$). *J. Phys. Chem.* **1982,** *86*, 1941–1947.

16. Kelly, J. M.; Bent, D. V.; Hermann, H.; Schultefrohlinde, D.; von Gustorf, E. K., Pentacarbonylchromium-Solvent Complexes : Flash-Spectroscopic Determination of Rate Constants of Formation and of Stability Constants and Their Application as Solvent Parameters to Catalytic Butadiene Oligomerisation. *J. Organomet. Chem.* **1974,** *69*, 259–269.

17. Ziegler, T., Approximate density functional theory as a practical tool in molecular energetics and dynamics. *Chem. Rev.* **1991,** *91*, 651–667.

18. Yang, G. K.; Vaida, V.; Peters, K. S., Application of Time-Resolved Photoacoustic Calorimetry to Cr-L Bond Enthalpies in $Cr(CO)_5$-L. *Polyhedron* **1988,** *7*, 1619–1622.

Chapter 5: Dynamics of the $Mo(CO)_6$ Mediated Pauson-Khand Reaction; Cyclization of 1,3-Enynes to Fused Bicyclic Cyclopentenones.

5.1 Introduction

The Pauson-Khand reaction is a (2 + 2 + 1) cobalt-mediated cycloaddition of an alkyne, an alkene and carbon monoxide to form a cyclopentanone. This reaction is useful in synthetic chemistry[1] and in the field of natural products.[2] It is initiated by the addition of the alkyne to $Co_2(CO)_8$, which bridges the two cobalt atoms, oriented perpendicular to the Co-Co bond.[3] To test our ability to measure the products of these solvated intermediates with secondary ligands we turned our attention to understanding the reaction dynamics of the Pauson-Khand reaction.[1f]

In 1973 Ihsan U. Khand, with Peter L. Pauson and others as coauthors, published a two-part article[4] on the reactions of organocobalt complexes including the complexation of alkynes to dicobaltoctacarbonyl through the loss of CO. The second of these papers reports a (2 + 2 + 1) cycloaddition between an alkyne, an alkene and carbon monoxide.[4b] These complexes are very stable and can be isolated. In 1977, Pauson and Khand published "Uses of Cobalt-Carbonyl Acetylene Complexes in Organic Synthesis.[1f]" Included in this paper are further reactions of alkenes and carbon monoxide with these alkyne dicobaltoctacarbonyl complexes to form new cyclopentanones. A reaction from this article denotes the addition of an alkyne to $Co_2(CO)_8$ and a further reaction with ethene to produce a cyclopentanone. A search of the literature only turned up studies of the reaction kinetics after the addition of the alkyne.[5] However, upon further investigation, we discovered the

addition of 1-octyne resulted in a thermal reaction of dicobaltoctacarbonyl at room temperature. Having discovered that $Co_2(CO)_8$ reacts thermally with alkynes, we began the search for a test molecule for our studies and found a reference to a very similar reaction using $Mo(CO)_6$ mediated Pauson-Khand reaction in the "Encyclopedia of Reagents for Organic Synthesis."[6] Jeong and coworkers[7] studied the use of metal hexacarbonyls as catalysts in the cyclization of 1,3-enynes with DMSO and at 100 ^{0}C to form a fused bicyclic cyclopentanone.

5.2 Methods

5.2.1 Reagents

Metal carbonyls were obtained from Aldrich with purities of 97% for $W(CO)_6$, 99% for Cr(CO)6 and 98% for Mo(CO)6 and were stored as received. Solvents were obtained from; Sigma Aldrich, reagent plus 99% methylcyclohexane, Alfa Aesar, 97% diethyl allylmalonate and propargyl bromide 97%, 80% w/w in toluene, Decon Laboratories, Inc., 200 proof ethanol and CCI, ACS grade sodium metal lumps. All solvents were also stored with added molecular sieves and back filled with argon upon opening and after each use. Sodium metal lumps were stored under argon. For temperature resolved experiments methylcyclohexane was used in place of cyclohexane to obtain kinetic data over a broader temperature range.

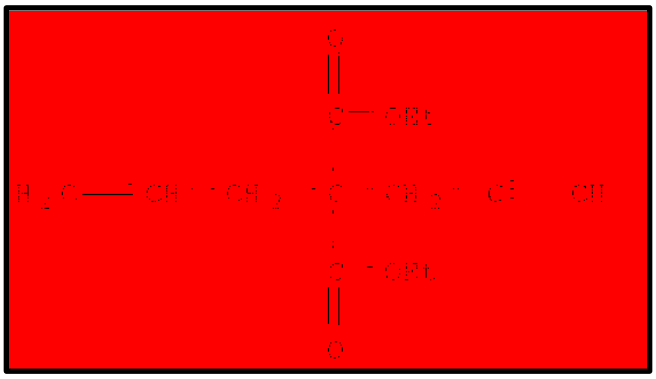

Figure 5.1 Lewis Structure of the Synthesized Enyne.

5.2.2 Synthesis of Enyne

A detailed procedure for the synthesis of 2-(2-propen-1-yl)-2-(2-propyn-1-yl)-, 1,3-diethyl ester (see **Figure 5.1**) solution can be found in **Appendix A**. Sodium ethoxide is prepared by adding equal molar quantities of sodium metal and 100% ethanol. Sodium metal lumps are carefully trimmed of any sodium hydroxide and cut into small pieces. A solution of diethyl allylmalonate in diethyl ether is prepared and the previously prepared sodium ethoxide is added dropwise to this solution. The sodium ethoxide removes the acidic hydrogen from the diethyl allylmalonate, turning the solution to a pale yellow color. Addition of propargyl bromide will slowly, over the course of about an hour, add to the open site on the diethyl allylmalonate. The remaining organics are extracted with a sodium chloride brine solution and washed with ether to remove the product. The product is then dried with magnesium sulfate to remove the aqueous layer and rotovaped to remove excess ether and ethanol. NMR was used to identify the products as 2-(2-propen-1-yl)-2-(2-propyn-1-yl)-, 1,3-diethyl ester (referred from here forward as enyne).

5.2.3 Step Scan FTIR

Samples where continuously flowed through an IR cell to a lower return cell where a peristaltic pump (Masterflex Easy-load II) returned the sample back to the upper holding cell. Return and holding glass cells were produced in-house with an outer jacket to facilitate flowing ethylene glycol from a temperature bath through both cells and IR sample cell. Reactions were photo-initialized by pumping the Metal to Ligand Charge Transfer (MLCT) bands on the metal carbonyls with a

tripled YAG (Coherent Precision II) pumped OPO (Optical Parametric Oscillator, Continuum Panther). Transient species were followed with SS FTIR spectroscopy using a Bruker model IFS/66S FTIR equipped with a Mercury Cadmium Telluride (MCT) detector modified for step scan experiments. A band pass IR filter (1600 to 2600 cm^{-1}) was placed in front of the MCT detector to reduce the number of interferometer points needed to complete each step scan measurement. The timing pulse from the Precision II was sent through a Stanford Research Digital Delay Pulse Generator (model DG535) to sync the FTIR with the laser pulse. Sample preparation and experiments were carried out under positive argon pressure.

5.3 Results and Discussion

The addition of the enyne to the metal center in $Mo(CO)_5$ could proceed through as many as three separate pathways. First, the enyne could add through the ester group. Using DFT calculations we have ruled out this possibility as we could not find a stable minimum energy structure. Second, the enyne could add through the π cloud of the alkene group. To observe the addition of an alkene to photogenerated $Mo(CO)_5$, we performed SS FTIR experiments (**Figure 5.2**) with 2.5 mM $Mo(CO)_6$ and 4% 1-hexene in cyclohexane (see **Figure 5.2**). We observed peaks at 1963 cm^{-1} and 1928 cm^{-1} from $Mo(CO)_5C_6H_{12}$ decay and three new peaks form with the same time constant at 1955 cm^{-1}, 1946 cm^{-1} and 1924 cm^{-1}, which we assign as $Mo(CO)_5(\eta^2$-1-hexene). The third possible point of attachment is through the π cloud of the alkyne bond. We also observed this attachment by using 1-heptyne in replacement for 1-hexene in the above experiment (see Figure 5.2). We observed a

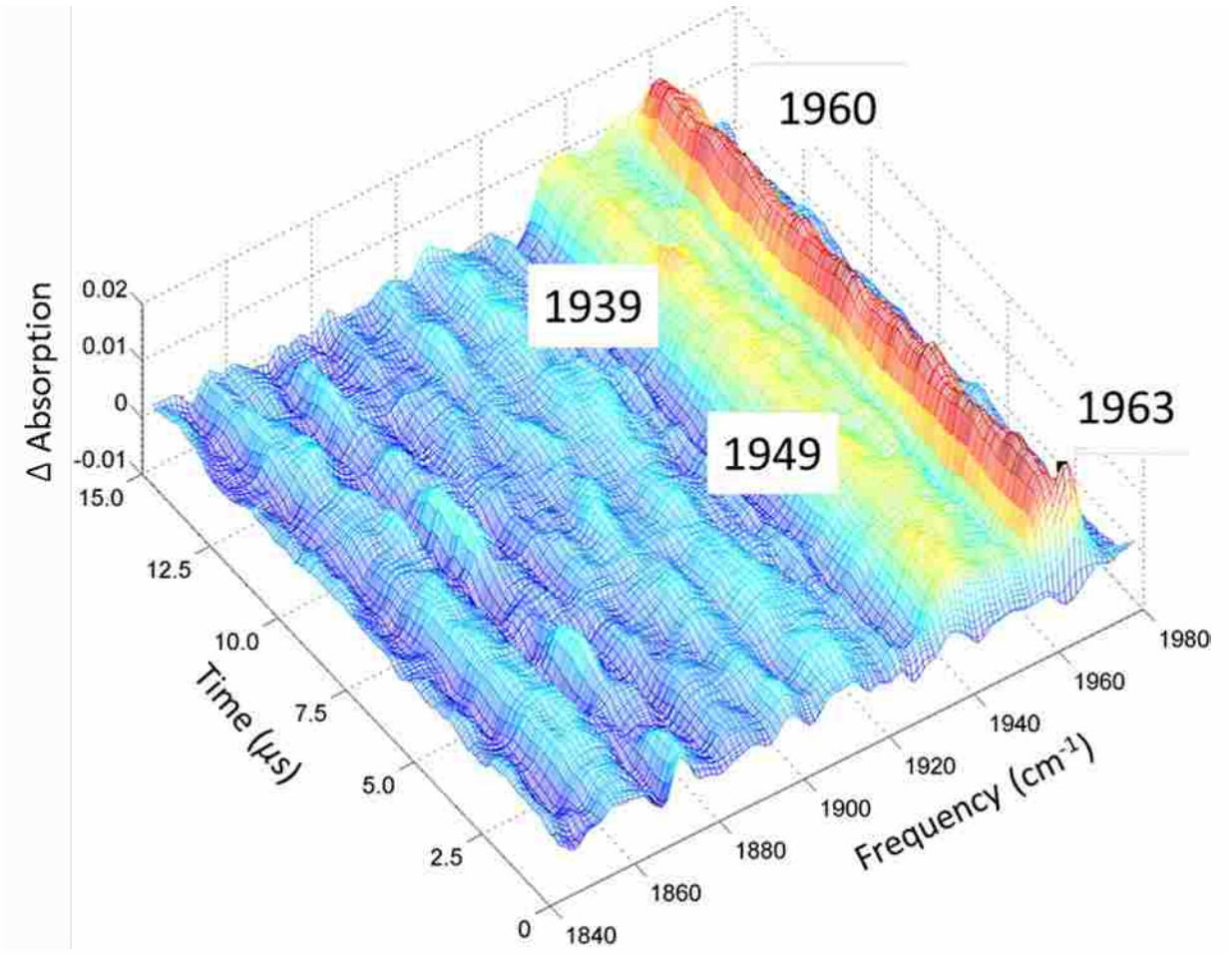

Figure 5.2. Ligand Exchange Reaction with M = Mo and L = 1-heptyne in methylcyclohexane.

similar red shift of the cyclohexane complex peak at 1963 cm-1 and the growth of new peaks at 1949 cm^{-1} and 1939 cm^{-1} with the same time constant; however we were not able to observe the decay of the cyclohexane complex at 1928 cm^{-1}. In our observations of the ligand exchange kinetics in Chapter 4, we observed the doubly degenerate (E) $Mo(CO)_5(C_6H_{12})$ peak at 1963 cm^{-1} decay and a single frequency peak grow in; with the addition of 1-hexene or 1-heptyne, we observe the growth of two peaks after the decay of the metal-methylcyclohexane complex. We believe the

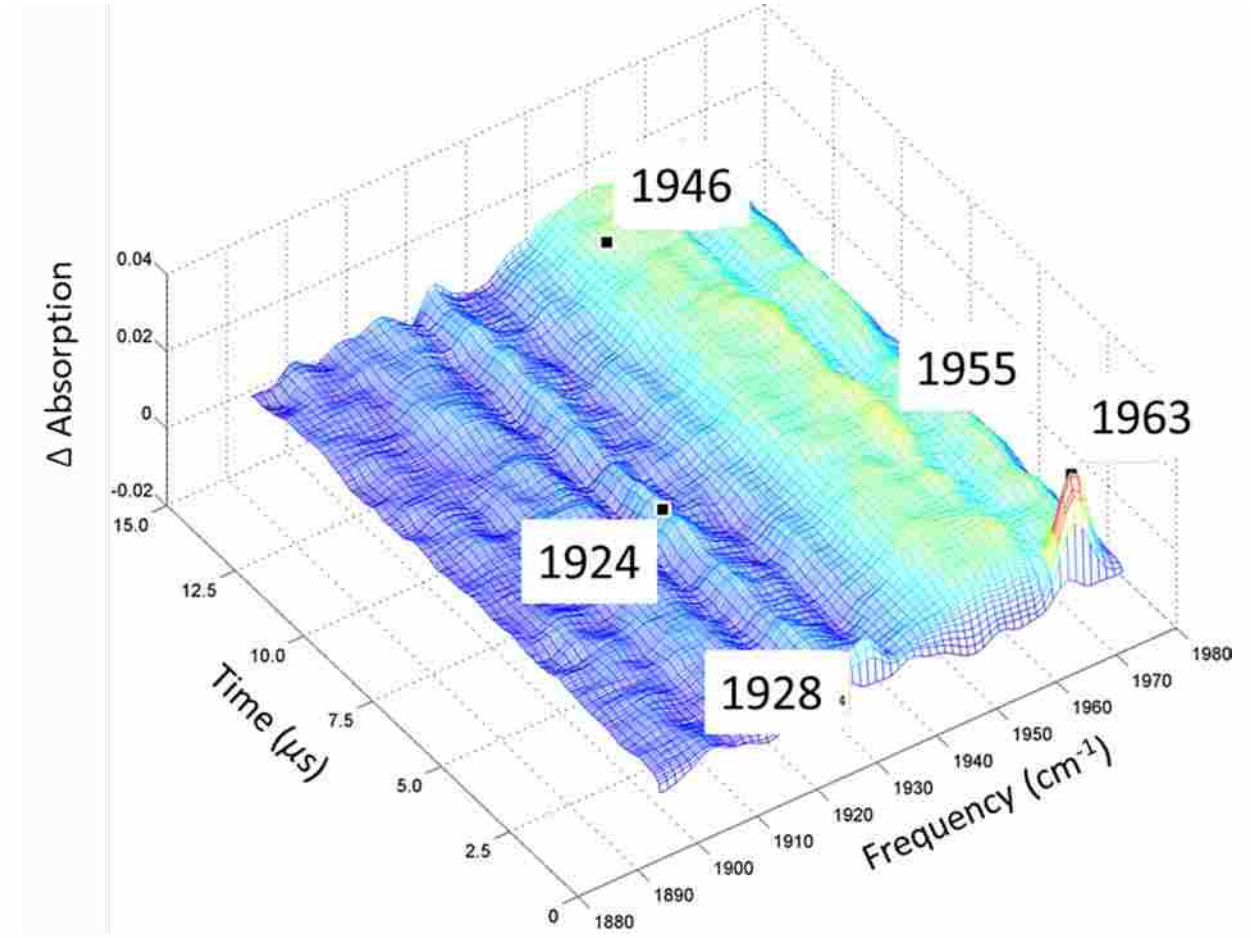

Figure 5.3. Ligand Exchange Reaction with M = Mo and L = 1-hexene in methylcyclohexane.

reason we no longer see a single peak from the doubly degenerate E vibrational frequency is due a sufficient breaking of the square pyramidal geometry of the carbonyls surrounding molybdenum by the addition of 1-hexene or 1-heptyne. Comparison of these two spectra will aid us in understanding the spectra taken with the addition of enyne.

In experiments performed with 2.5 mM $Mo(CO)_6$ and 3% enyne in methylcyclohexane, the SS FTIR spectrum (**Figure 5.3**) shows the same cyclohexane complex peaks at 1963 cm^{-1} and 1928 cm^{-1}. The exchange products of

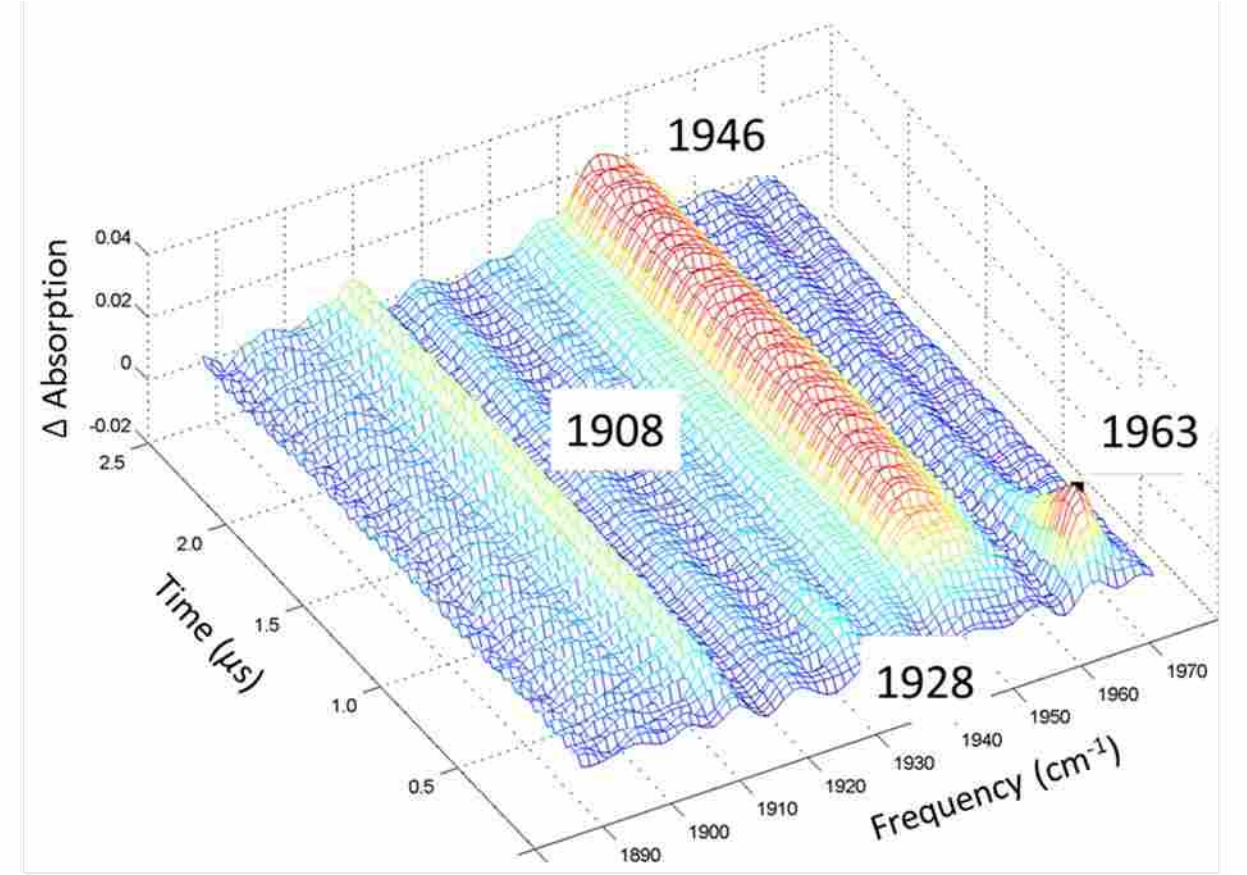

Figure 5.4. Decay of $Mo(CO)_5$(methylcyclohexane) to form $Mo(CO)_5$(Enyne)

this reaction are different from either the alkene or alkyne experiments, which both had a very broad absorption with two peaks. The initial enyne exchange product has one broad peak at 1946 cm^{-1} with a small shoulder on the lower frequency side at 1908 cm^{-1}. We must ask, is the enyne complexing through the alkyne, alkene or ether? The red shift in the E frequency is greater for 1-heptyne than 1-hexene, due to greater π backbonding from the metal to the carbonyl; an alkyne has greater electron density then an alkene. The difference between the vibrational frequencies for the enyne and 1-heptyne are only 3 cm^{-1}, the enyne is a much larger molecule and is more electron rich than a strait-chain alkyne, which is less than the 4 cm^{-1}

resolution of our spectrum. We are confident that the enyne binds through the alkyne first with no evidence of the addition through the alkene.

Temperature resolved data for this reaction were taken from -8 to 30 ^{0}C. The pseudo-first-order decay of the $Mo(CO)_5$(methylcyclohexane) peak at 1963 cm^{-1} was fit using jfit with a single exponential for the instrument response function, a single exponential for the decay, time zero and an offset. An Arrhenius plot of the natural log of the rate constants versus T^{-1} gave an activation energy of 15.68 kJ mol^{-1} and an Eyring analysis yielded $\Delta H^{\ddagger}$=4.34 kcal mol^{-1} and $\Delta S^{\ddagger}$ = -0.836 cal mol^{-1} K^{-1} (at T = 298 K).

Conducting SS FTIR experiments at 2.5 microsecond time slices with 2.5 mM $Mo(CO)_6$ and 3% enyne in cyclohexane, we have observed a second shift in the carbonyl peaks that we believe to be the addition of the alkene side of the enyne. This complex remains lasts longer then the length of this scan, 750 μs. This addition would occur through the loss of another carbonyl and association through the π cloud of cloud of the C-C double bond. We have not yet conducted the temperature resolved experiments; therefore, we cannot calculate the activation energy, enthalpy of reaction, or entropy of reaction.

5.4 Conclusions

The molybdenum mediated Pauson-Khand reaction proceeds following pseudo-first-order kinetics for the addition of alkyne portion of the enyne. An Arrhenius plot of the rates of decay of the Mo methylcyclohexane complex over a temperature range of -8 to 20 ^{0}C gave an energy of activation of 15.6 kJ/mol. The

ligands 1-hexene, 1-heptyne or enyne interact through the metal such that the square pyramidal-like geometry of the metal carbonyls we have previously studied is broken. This breaking of the square pyramidal-like geometry of the carbonyls bonded to the metal causes their vibrations, previously doubly degenerate E, to split. Further studies of the addition of the alkene portion of the enyne and longer time resolutions are needed to finish the full description of this mechanism.

5.5 References

1. (a) Abel, E. W.; Stone, F. G. A.; Wilkinson, G., *Comprehensive Organometallic Chemistry II : A review of the Literature 1982–1994*. 1st ed.; Pergamon: Oxford ; New York, 1995; Vol. 12; (b) Pauson, P. L.; Khand, I. U., USES OF COBALT-CARBONYL ACETYLENE COMPLEXES IN ORGANIC SYNTHESIS*†. *Annals of the New York Academy of Sciences* **1977,** *295*, 2-14; (c) Peter L, P., The Khand Reaction : A Convenient and General Route to a Wide Range of Cyclopentenone Derivatives. *Tetrahedron* **1985,** *41*, 5855–5860; (d) Schore, N. E., The Pauson–Khand Cycloaddition Reaction for Synthesis of Cyclopentenones. In *Organic Reactions*, John Wiley & Sons, Inc.: 2004; (e) Trost, B. M.; Fleming, I., *Comprehensive Organic Synthesis: Selectivity, Strategy, and Efficiency in Modern Organic Chemistry*. 1st ed.; Pergamon Press: Oxford, England ; New York, 1991; Vol. 5; (f) Pauson, P. L.; Khand, I. U., Uses of Cobalt-Carbonyl Acetylene Complexes in Organic Synthesis*†. *Ann. N.Y. Acad. Sci.* **1977,** *295*, 2–14.

2. Donkervoort, J. G.; Gordon, A. R.; Johnstone, C.; Kerr, W. J.; Lange, U., Development of Modified Pauson-Khand Reactions with Ethylene and Utilisation in the Total Synthesis of (+)-Taylorione. *Tetrahedron* **1996,** *52*, 7391–7420.

3. (a) Abel, E. W.; Stone, F. G. A.; Wilkinson, G., *Comprehensive organometallic chemistry II : a review of the literature 1982-1994*. 1st ed.; Pergamon: Oxford ; New York, 1995; Vol. 8; (b) Anderson, A. B., Theoretical Study of Structures and Binding Properties of Nickel Tetracarbonyl, Iron Pentacarbonyl, and Diiron and Dicobalt

Hexacarbonyl Acetylenes. *Inorg. Chem.* **1976,** *15*, 2598–2602; (c) Dickson, R. S.; Fraser, P. J., Compounds Derived from Alkynes and Carbonyl Complexes of Cobalt. In *Advances in Organometallic Chemistry*, Stone, F. G. A.; Robert, W., Eds. Academic Press: 1974; Vol. Volume 12, pp 323-377; (d) Wilkinson, G.; Stone, F. G. A.; Abel, E. W., *Comprehensive Organometallic Chemistry: The Synthesis, Reactions, and Structures of Organometallic Compounds.* 1st ed.; Pergamon Press: Oxford Oxfordshire ; New York, 1982; Vol. 5.

4. (a) Khand, I. U.; Knox, G. R.; Pauson, P. L.; Watts, W. E., Organocobalt Complexes. Part I. Arene Complexes Derived from Dodecacarbonyltetracobalt. *J. Chem. Soc., Perkin Trans. 1* **1973**, 975–977; (b) Khand, I. U.; Knox, G. R.; Pauson, P. L.; Watts, W. E.; Foreman, M. I., Organocobalt Complexes. Part II. Reaction of Acetylenehexacarbonyldicobalt Complexes, $(R^1C_2R^2)Co_2(CO)_6$, with Norbornene and its Derivatives. *J. Chem. Soc., Perkin Trans. 1* **1973**, 977–981.

5. Gordon, C. M.; Kiszka, M.; Dunkin, I. R.; Kerr, W. J.; Scott, J. S.; Gebicki, J., Elucidating the Mechanism of the Photochemical Pauson-Khand Reaction: Matrix Photochemistry of Phenylacetylenehexacarbonyldicobalt. *J. Organomet. Chem.* **1998,** *554*, 147–154.

6. Paquette, L. A., *Encyclopedia of Reagents for Organic Synthesis*. 2nd ed.; Wiley: Hoboken, N.J., 2009.

7. Jeong, N.; Lee, S. J.; Lee, B. Y.; Chung, Y. K., Molybdenium Mediated Preparation of Cyclopentenones. *Tetrahedron Lett.* **1993,** *34*, 4027–4030.

Chapter 6: Conclusions

Many organometallic reactions are solvent dependent, suggesting solvent molecules interact with reaction intermediates. Group 6 metal carbonyls act as good test molecules to observe these kinds of reactions, because they are relatively unreactive until perturbed, and carbonyl absorptions are very strong and mostly isolated in the IR spectra. Following the time trace of these carbonyl frequencies with SS FTIR, we have studied the solvent exchange reaction of group 6 metal carbonyls. This reaction begins with the photolysis of the Metal to Ligand Charge Transfer (MLCT) band of $M(CO)_6$ (M = Cr, Mo, W) in the solution phase, which results in the loss of a CO. Coordinatively unsaturated metal carbonyls are solvated within the time resolution of our spectrometer. In neat solvent cyclohexane solutions, chromium or tungsten solvated complex lasts for microseconds to milliseconds until reacting with H_2O, a contaminant, to form $M(CO)_5(H_2O)$, whereas molybdenum reacts to form a dimer. In solutions with 4% of a more strongly binding (than the primary solvent) secondary solvent, the primary solvent is replaced within microseconds. The order of reactivity follows Mo > Cr > W. An Arrhenius plot of the kinetic measurements over the temperature range of 4 to 44 ^{0}C yielded activation energies of 23.7 kJ/mol (M = Mo, L = benzene), 35.1 kJ/mol (M = W, L = benzene), 29.8 kJ/mol (M = Mo, L = mesitylene) and 36.2 kJ/mol (M = W, L = mesitylene) in methylcyclohexane. An Eyring analysis yielded enthalpy of reaction values lower than calculated binding energy of metal-methylcyclohexane, and slightly negative entropy of reaction values. Lower enthalpy of reaction values

suggests the mechanism follows an associative pathway, and slightly negative values of the entropy of reaction (these are an order of magnitude smaller than most of the moderately binding secondary ligands) denote that the ligand exchange reaction occurs through an associative reaction with an earlier transition state than more strong to moderately binding ligands. The enthalpy of reaction values increase from Mo to Cr to W, while there is little change in the entropy of reaction values.

Many of these organometallic transients are very reactive and cannot be isolated for further study; therefore, they are difficult to identify. One option is to use computational chemistry to calculate molecular properties, including the vibrational frequencies of the carbonyl ligands. The carbonyl ligand vibrational frequencies are dependent on the chemical environment around the metal due to metal to carbon π backbonding. An increase in the electron density on the metal, will result in weakening of the CO triple bond, and a red shift in the IR frequency will occur. Furthermore, carbonyl vibrational frequencies are easily identifiable in the IR spectra, as they are strong and well isolated. Using NWCHEM and the Extensible Computational Chemistry Environment (ECCE), we calculated the carbonyl vibrational frequencies of metal carbonyl transients measured in our lab, and those found in the literature. Measured and computational frequencies were compared; scaling factors were found to be 0.9519±0.0095 for B3LYP, 0.9429 ± 0.0087 for M06 and 0.9565 ± 0.0095 for M06-L with overall shifts of 102 ± 16, 121 ± 15, 93 ± 17 cm^{-1}, respectively. The accuracy or standard deviation of the overall shift is more important than the overall shift itself. The density functional M06 is the

best functional, as would be expected, while all functionals do a good job at predicting carbonyl frequencies. Factoring in the decreased computational cost of B3LYP over M06, and they would be comparable in effectiveness.

We applied the knowledge we gained in the study of the solvent exchange reaction to better understand the mechanism of the Pauson-Khand reaction, a [2+2+1] cycloaddition reaction that uses $Co_2(CO)_8$ to mediate the reaction. Unfortunately, the addition of an alkyne to dicobalt octacarbonyl reacts thermally, and so we were not able to use SS FTIR to study this reaction. However, a quick search of the literature found molybdenum hexacarbonyl a viable test molecule for this reaction. Identical to the solvent exchange reaction, the molybdenum mediated Pauson-Khand reaction also begins with the solvation of the coordinatively unsaturated $Mo(CO)_5$. The initial product is the solvated complex, which decays away with pseudo-first-order kinetics and is displaced by the C-C triple bond in 2-(2-propen-1-yl)-2-(2-propyn-1-yl)-1,3-diethyl ester on the nanosecond time scale. The IR frequencies match very well with those we observed for the addition of 1-heptyne. An Arrhenius plot over the temperature range of -8 ^{0}C to 20 ^{0}C yielding an energy of activation of 17.8 kJ/mol; suggesting the mechanism also occurs through an associative reaction, with a later transition state then with the solvent exchange reaction with benzene and mesitylene ligands. Another shift in the carbonyl frequencies, presumably the loss of another carbonyl and the addition of the alkene, can be observed with a time resolution of 2.5 μs; however, more experiments must be performed to calculate the energy of activation for this step.

In addition to continuing work on the molybdenum mediated Pauson-Khand reaction, there are additional experiments which need or could to be done. The solvent exchange reaction with metals chromium and tungsten and the entering secondary ligand mesitylene are currently in the process of being done. These experiments would provide an overall trend for group 6 metal carbonyls with a more sterically hindered ligand than benzene. Another project could involve looking at the solvent exchange reaction with a primary solvent other than methylcyclohexane/cyclohexane or n-heptane to better understand the effects of the primary solvent. Although the computational work on the carbonyl vibrational frequencies and binding energies of these transients is finished, additional calculations could be conducted to identify the energy, and geometry of the transition state for the solvent exchange reaction would give further insight into this reaction mechanism. Understanding the interaction of reaction intermediates with their surrounding solvent molecules is key to a correct understanding of the reaction mechanism. This work provides important information on these interactions and on the dynamics of formation and dissociation of these complexes, and it will help in further understanding organometallic reactions.

Appendix A Standard Operating Procedures

A.1 **Sample Preparation.**

1) Pull out dry glassware; 250 ml two necked round bottom flask, 30 ml graduated syringe and CaF windows and 10 inch, 16 gauge syringe needle from the oven. Replace any round bottom two neck flasks for next researcher.

2) Back fill the round bottom flask with Argon (inert gas) until cool. Allow glass syringes and CaF windows to cool.

3) Weigh out sample and add it to the two necked round bottom flask. (The masses of solute and volumes of solvent need to prepare a given sample are stored in Excel files stored in the S:\mcalab folder on the research drive.)

4) The diffusion pump works by super heating oil under low pressures, created using a mechanical pump, in order to boil the oil. When gaseous oil condenses it creates a vacuum able to get down to approximately 10^{-6} torr verses 10^{-3} for the mechanical pump. The diffusion pump has two sets of manifolds connected to it. The manifold on the left belongs to our lab. Our manifold consists of pump and argon compartments and valves on the manifold can be used to open either of these.

5) Argon from a tank located in the closet outside C370 can be made to flow by opening the Swagelok needle value on inside top left of the hood. You can control the flow by the degree you open the needle valve; watch the bubbler behind the valve to observe the flow. As long as there the bubbler is

producing bubbles of argon the pressure inside the argon manifold is greater than atmospheric pressure.

6) Remove the glass adapter connected to the rack on the diffusion pump and grease it and where it attaches to the manifold with vacuum grease, reconnect it using the yellow clip.

7) While flowing argon through the adapter in step 6 connect larger ground glass neck of the two necked round bottom flask to the adapter, use the blue clip to hold the flask in place.

8) Place a small neoprene stopper in the other neck.

9) Solvents are stored under the hood in the flammable only cabinet. Remove cyclohexane/methylcyclohexane and secondary ligand from this cabinet.

10) Because oxygen reacts with the intermediates in our reactions, we need to minimize the amount of air we introduce during the sample preparation procedure. One step we take is to rinse the 30 ml graduated syringe by pulling approximately 1 ml of solvent into the syringe, invert the syringe and pull the plunger almost out of the syringe body. This will help form a barrier between the body and plunger when measuring out the solvent. Any solvent leftover in the syringe should be placed in the waste container.

11) The volume in the syringe needle may now contain small amounts of oxygen from the air which will need to be replaced by argon. This is done by flowing argon into the solvent bottle. Insert the syringe needle above the solvent

and pull up on the plunger, remove the syringe needle from the solvent bottle and compress the plunger. Repeat this process three times.

12) Now pull up the desired volume of solvent for the sample you are preparing and insert it into the round bottom flask.

13) Repeat the steps in **10.)** through **12.)** to add a secondary solvent/ligand if desired.

14) Blow off all solvents with argon for approximately 60 seconds and return to their proper storage places.

15) Follow the steps in **Appendix A.2 Freeze, Pump, Thaw.**

16) Turn on argon to the sample pumping system next to the FTIR before freeze, pump, thawing the sample. If the argon is able to purge longer then you will have better signal to noise ratio in your AC scans.

A.2 **Freeze, Pump, Thaw.**

1) <u>It is very important that you read and understand the contents of this standard operating procedure prior to using the pumping system.</u>

2) The freeze, pump, thaw process consist of repeating the following steps at least three times. We use this process to eliminate any gasses dissolved into the solvents used in preparing a sample.

3) The first step is to freeze the sample connected to the manifold. Place the small round bottom dewar under the two necked round bottom flask and raise the ring stand to support it. Slowly fill the round bottom dewar with

liquid nitrogen to freeze the sample. Once the sample is frozen fill the round bottom dewar with liquid nitrogen.

4) The second step is to pump out the gasses above the frozen sample, the round bottom dewar must remain full of liquid nitrogen during this process so that the sample remains frozen. While pumping on with the diffusion pump any thawed sample will quickly evaporate and contaminate the expensive diffusion pump oil.

5) The pumping system consists of a mechanical pump, located under the hood, a diffusion pump and a series of four valves. One valve clearly opens the pumping system up to the atmosphere and is not used except when shutting down the system for maintenance (see appendix **A.6 Mechanical Pump Maintenance**). The remaining three valves are used control pumping system. The bottom valve opens the mechanical pump to pump on the diffusion pump. The middle valve opens the mechanical pump to pump on the system. The top valve opens the diffusion pump to pump on the system. The system consists of the two manifolds connected to the pumping system. <u>One should **NEVER** open all three of the control valves at once.</u>

6) Because the pressure in the flask is unknown we must always change over to the mechanical pump first. This is done by closing the top control valve; this process closes the diffusion pump from the system. Next close the bottom valve; this closes the mechanical pump off to the diffusion pump. Finally open the system up to the mechanical pump by opening the middle

valve. Never leave the mechanical pump off the diffusion pump for more than five minutes; this will cause the diffusion pump to stop refluxing.

7) If the diffusion pump ever stops refluxing you need to take precautionary measures in order that you do not break the glass "christmas tree" located inside of the diffusion pump. First turn off the temperature control unit located at the rightmost side of the hood. Second lower the heating element under the diffusion pump using the stage below it. Third close off all three control valves. Fourth let the diffusion pump cool to room temperature. Follow the steps included in appendix **A.6 SOP: Mechanical Pump Maintenance** for instructions to restart the diffusion pump.

8) Keeping the sample frozen open the valve to the sample and pump the system down to below 25 mTorrs

9) Only once you have pumped below 25 mTorrs switch to the diffusion pump by first closing the middle valve and opening the bottom valve. Watch to see the diffusion pump is refluxing well; a good measure of this is being able to see oil droplets form and fall off the upper portion of the christmas tree. If the pump is not refluxing wait to open the top valve to the system. You may have to switch back and forth between the mechanical pump and the diffusion pump if the pressure in the system goes above 25 mTorrs during this process.

10) Once the diffusion pump is refluxing properly and the system/sample is pumped down below 25 mTorr open the top valve.

11) While continuing to keep the sample frozen pump the system/sample down to approximately 1 mTorr.

12) Close the valve connecting the sample to the manifold.

13) Remove liquid nitrogen dewar.

14) Thaw the sample by partially submersing the two necked round bottom flask in a beaker of warm tap water. Support the beaker with the same ring stand as before.

15) Repeat the freeze, pump, thaw cycle three times. The signal to noise ratio in our step scan data is adversely effected by not pumping down to approximately 1 mTorr three times If you cannot reach 1 mTorr an addition freeze, pump, thaw step must be added to the preparation of the sample.

A.3 **LASER Start Up and Shut Down.**

1) Before using the Precision II/Panther LASER you must first be trained and pass an oral exam. This standard operating procedure is only to act as a quick reference of the startup and shut down protocol.

2) Open Water Source and Return located above the Precision II.

3) Switch on electronics on bottom right of power supply.

4) Turn keyswitch on top center of power supply counter-clockwise to the **ON** position. It will take ~15 seconds for the control unit to complete its system check.

5) Record date, name, lab group and shot count in Precision II log book.

6) To start the lamps flashing press **auto/manual** and **start** on remote box. The lamps need to warm up by flashing before they can begin lasing.

7) Wait 30 minutes without Q-switching to thermally stabilize the system

8) Press **program up** button on remote box until the desired mode; the MCA Lab uses program 3.

9) Press **activate** button on remote box.

10) Turn the key on seeder clockwise to **ON** position.

11) Press **shutter** and **Q-switch** on the remote box (you will need to press the **Q-switch** button twice), until all four LEDs are lite on the remote box.

12) Refresh PC connected to Panther; the computer will crash if it is not refreshed before laser light is opened into the Panther.

13) Check to make sure movable mirror mounts and prisms are oriented correctly for UV LASER light.

14) Open desired ports. For experiments in the MCA lab open the center port between the Precision II and Panther.

15) Select desired wavelength on PC.

16) Using power meter positioned after 2nd prism, maximize power output (as seen on oscilloscope) by adjusting SHG1 on PC and 2nd and 3rd harmonic crystals by using 1 and 1 and 2 and 2 on the remote box. Record average max power and frequency in Precision II log book.

17) When you are ready to shut down the laser follow steps 9 through 13.

18) Press stop on the remote box.

19) Turn keyswitch on the seeder to the standby position

20) Turn keyswitch on the main power supply unit to the off position

21) Switch off electronics on the bottom right of the main power supply unit.

22) Turn off cooling water located above the Precision II laser.

A.4 **LASER and FTIR Alignment**

1) The FTIR must be aligned prior to the alignment of the LASER.

2) Start up the laser according to **Appendix A.3 Laser Start up and Shut Down.** Remember the laser must warm up for thirty minutes, if you are going to run a sample the same day you are aligning the LASER and FTIR it would be most efficient to turn on and warm up the laser while you freeze, pump, thaw the sample.

3) Cool down the MCT detector in the FTIR by inserting the funnel into the detector and adding approximately two funnels full of liquid nitrogen. Once the detector is cooled add an additional funnel full of liquid nitrogen. During data collection a funnel full of liquid nitrogen should be added to the detector approximately every hour.

4) Open OPUS on the computer. Go to measure tab and then align mode. This will bring up a graph of the interferogram. If the plot of the interferogram is too small to see press

5) Use the adjustment knobs, all three one at a time, on the back of the parabolic mirror just prior to the MCT detector to maximize the counts on the plot of the interferogram.

6) Insert the alignment FTIR sample cell in a way that maximizes the interferometer counts. This maximum may be less than the previous one with no cell in.

7) Once the startup protocol for the laser is finished we must first guide the laser to the FTIR and through the alignment FTIR cell. Unless something ot the laser optics table has been moved the laser should already be close to aligned. Place a rubber stopper in the optics port running through the wall separating the FTIR and main laboratory room in the MCA lab. It is easiest align the laser if you cover the larger, outer side of the rubber stopper with a sticky note or label. On the laser optics table there are two alignment prisms used to center the laser on the rubber stopper; use the top adjustment nob on the first prism to align the laser in the vertical direction and the bottom adjustment nob on the second prism to align the laser in the horizontal direction.

8) Place a paper card on the exiting side of the third prism, located just inside the FTIR room. Remove the rubber stopper and check the alignment on this prism. You may have to repeat step 3 multiple times to get this alignment on just right.

9) Guide the laser through the pinhole and to the first turning mirror on the FTIR optics table by using the alignment nobs on the third prism.

10) Being careful to not let the laser beam inter the detector or source/interferometer cavities of the FTIR (You will have to use cards to

block/guide the laser into the sample compartment of the FITR), use the alignment nobs on this first aluminum turning mirror to direct the laser beam off the second aluminum turning mirror and through the FTIR alignment cell.

11) Mark the position of the laser beam on sticky note on the sample cavity. During measurements you can use the first aluminum turning mirror to adjust the alignment of the laser beam back to this position on the sticky note if the optics table was slightly bumped.

12) The sample is now ready to place inside the upper sample chamber by following the steps in sample preparation.

A.5 **DC offset**

1) After the MCT detector is cooled with liquid nitrogen, the FTIR cell is placed in the sample compartment and the sample solution is flowing through the FTIR cell take the DC output from the TM 501 Power Module and connect it to the oscilloscope.

2) The settings for the channel on the oscilloscope will need to be set to: 50Ω DC and the trigger will need to be set to this channel and the oscilloscope set to normal trigger.

3) Use the adjustment knobs on the upper right of the TM 501 Power Module to center the offset on the oscilloscope to zero. This may require you to change the y-axis to a lower mv per division by turning the y-axis adjustment knob.

A.6 **DC Scan**

1) On the computer attached to the FTIR there are two ISO cards, one card is for the computer and FTIR communications and the second for taking Step Scan data. On the second card there are four BNC cable connections. Starting from the top, the first and second connections (referred as first and second channels from here forward) will change depending upon the type of Step Scan experiment you want to perform, the third connection is for the laser trigger pulse and the last connection should always have a 50Ω nub on it.

2) At this point in the DC output should be connected into the input for the TM 501 Power Module and the AC output should be connected into the second input on the left side of the FTIR.

3) For a DC scan place the output from TM 501 Power Module in the upper BNC connection on the PC.

4) Leave the third connection empty.

5) If it is not already open, start OPUS by selecting the icon at the bottom center of the screen.

6) Select "Measure" from the left panel in OPUS.

7) Select "Special Measurements" followed by "Transient Recorder TRS"

8) Within the Transient Recorder TRS screen select

a. Device: PAD1232 40 Mhz Spectrum

b. Number of Time Slices: 300

c. Time Resolution: Depends upon Reaction being measured

d. Co addition Repeat Count: 10, if using Panther

e. Delay Before Experiments: 0

f. Trigger delay: 0

g. Stabilization Delay: 40 msec

9) In addition to these settings deselect both "Use Second Channel for Weighing" and "Use Second Channel for phase correction"

10) Select "Internal" under "Experimental Time Base" and "Internal" under "Experimental Trigger"

11) Press "Start Measurement".

12) Quietly leave the back FTIR room and silently close the door.

13) You can observe the progress of the DC scan on the computer monitor in the lab office.

A.7 **Raw AC Scan**

1) Remove the output of the AC channel from the FTIR and connect it in the first channel. The DC cable should be inserted into the second channel.

2) Select "Measurement" from the left panel in OPUS.

3) Select "Setup Experiment"

4) Deselect "Single Channel", select "Interferogram" and "OK"

5) Select "Special Measurements" followed by "Transient Recorder TRS"

6) Within the Transient Recorder TRS screen select

a. Device: PAD1232 40 Mhz Spectrum

b. Number of Time Slices: 300

c. Time Resolution: Depends upon Reaction being measured

d. Co addition Repeat Count: 1

e. Delay Before Experiments: 0

f. Trigger delay: 0

g. Stabilization Delay: 40 msec

7) In addition to these settings deselect both "Use Second Channel for Weighing" and "Use Second Channel for phase correction"

8) Select "Internal" under "Experimental Time Base" and "Internal" under "Experimental Trigger"

9) Press "Start Measurement".

10) Quietly leave the back FTIR room and silently close the door.

11) You can observe the progress of the DC scan on the computer monitor in the lab office.

A.8 **AC scan**

1) To ensure that the MCT detector does not warm up during data collection it should be filled with liquid nitrogen prior to each AC scan.

2) Remove the BNC cables from both channels 1 and 2.

3) Place the DC BNC into channel 2 and AC BNC into channel 1.

4) Select "Measurement" from the left panel in OPUS.

5) Select "Setup Experiment"

6) Deselect "Interferogram", select "Single Channel" and "OK"

7) Select “Special Measurements” followed by “Transient Recorder TRS”

8) Within the Transient Recorder TRS screen select

a. Device: PAD1232 40 Mhz Spectrum

b. Number of Time Slices: 300

c. Time Resolution: Depends upon Reaction being measured

d. Co addition Repeat Count: 10

e. Delay Before Experiments: 0

f. Trigger delay: 0

g. Stabilization Delay: 40 msec

9) In addition to these settings deselect “Use Second Channel for Weighing” and select “Use Second Channel for phase correction”

10) Select “Internal” under “Experimental Time Base” and “Ext. Positive Edge” under “Experimental Trigger”

11) Press “Start Measurement”.

12) Quietly leave the back FTIR room and silently close the door.

13) You can observe the progress of the DC scan on the computer monitor in the lab office.

A.9 **Synthesis of 2-(2-propen-1-yl)-2-(2-propyn-1-yl)-, 1,3-diethyl ester (Enyne) used in Pauson-Khand Reaction**

1) See PropanedioicAcid excel spreadsheet for calculations and volumes. The excel sheet is programmed to give percent yield also.

2) Cut and weigh out the .3649 grams of Na metal. Make sure to remove as much of the NaOH outer layer.

3) Add 15 ml EtOH and allow the base to form.

4) Place 30 ml of diethyl ether in a round bottom flask on ice. Add 2.95 ml of diethyl allylmalonate to the diethyl ether.

5) Slowly add the sodium ethoxide dropwise to the ether. When the base is added stir vigorously for 10 min. The solution should turn pale yellow.

6) Add 1.61 ml of propargyl bromide slowly to the solution, and stir for an hour until room temperature is reached.

7) Add about equal volume brine to the solution to create layers. Extract the organic layer and wash the aqueous layer three times with 100 ml of ether.

8) Dry with magnesium sulfate and filter. Use the filter paper and plastic funnel, and filter into rotovap flask.

9) Run on the rotovap at about 40 celsius until the ether and ethanol are both evaporated.

A.10 **Figures in Matlab for publication**

1) Create figure in Matlab using plot or mesh (See **Appendix B Data Analysis**)

2) On the figure created go to File, Export Setup.

3) Export Setup has several types of Properties which need editing. Other settings can be adjusted as needed.

a. Size. Maximum width of 3.25 in by maximum length of 9.5 in.

b. Rendering. For grayscale use 600 dpi and 300 dpi for color.

c. Fonts. Minimum font size of 4.5 points, Helvetica or Arial.

d. Lines. Select Use fixed line width. Minimum 0.5 pt lines.

4) Click “Apply to Figure”

5) Click “Export”

6) You can also store and load Export Styles.

A.11 **Mechanical Pump Maintenance**

1) Turn off the heat to the diffusion pump by turning the dial of the powerstat to zero and lowering the heating element.

2) Let the oil in the diffusion pump cool to room temperature.

3) Vent the system to atmosphere.

4) Turn off the mechanical pump.

5) Drain oil into large shallow pan by first opening the upper and then the lower screw caps

6) When drained replace the lower screw cap and fill to optimum level with mechanical pump oil.

7) Replace the upper screw cap.

8) Turn on diffusion pump and pump down the entire system to below 25 mTorr.

9) Replace heating element and turn the powerstat dial to 60. The oil in the diffusion pump will heat up but not start to reflux.

10) Slowly ramp up the dial on the powerstat to 75 while paying careful attention to the pressure in the system and that the diffusion pump is refluxing properly.

11) The diffusion pump is ready once it is fully refluxing and the pressure inside the system is below 25 mTorr.

Appendix B Data Analysis

B.1 **OPUS**

1) We should first make a copy of all data files to be analyzed. This is done to protect the original raw data files form accidentally saving over them in opus. This is best done by creating a folder for each DC, AC pair in the same folder as the raw unprocessed data and copying the pair into it. You should also place a folder labeled average if you want to average the raw data in OPUS.

2) Start OPUS in windows to begin the data analysis. The OPUS program is password protected; the password is "OPUS".

3) Using 'Open" under "File" load the DC and AC for the data being analyzed. Alternatively you may drag and drop the files into left side panel in OPUS under "Display default.ows".

4) In order to view 3 dimensional graphs of the collected files you will need to double click the box which reads "SSC" under each file name within OPUS. This will create a new display window with loaded 3 dimensional data files within it.

5) A single click on "SSC" box below each file name in this new display will load the 3 dimensional spectra collected for each file name.

6) Examine each file. Unload all files that are mislabeled or not useable data.

7) Change the names of mislabeled filenames.

From this point there are two different options to proceed, first you can average the raw data sets and extract the files for further analysis in Matlab. Second, extract each data set individually to analyze in Matlab. For the first option use the Spectrum Calculator to Average data sets as explained in **B.2 Using the Spectrum Calculator to Average Data in OPUS** before continuing.

8) All DC files are static measurements where AC files are dynamic measurements and therefore must be extracted from OPUS data differently

9) Select "SSC" box under the DC file that you are going to extract.

10) Go to **Data Extraction** under **Measure**.

11) Change the path length to the folder containing the copied AC and DC files.

12) Change the name to dc.0, there is no reason other than tradition why this name could not be something else.

13) Under extraction mode you want to check; From: beginning of file, To: end of file, Coadd all to one block, If file already exists: increment name and Extracted files: load.

14) Now click **Extract**.

15) Select the newly created dc.0 file.

16) Select **Save File As** under **File**.

a. Name file: dc.asc

b. Path: same as above

c. Mode: Data Point Table

d. Data Point Table: 5,5 (comma is necessary to load into Matlab)

e. All Data Points

17) Now we will use a Macro to extract every time slice from the AC file the same way we just saved the two dimensional dc.0 file.

18) First if you do not remember the number and length of each time slice, right click on AC file name. Click "Show Parameters". In the side window, click "Acquisition Parameters". Note number next to "Tr.Rec. Slices" (should be something like 300). This is the number of time slices. Later, the length of each slice will also be needed. This is the number next to "Tr.Rec. Resolution".

19) Select the "SSC" box corresponding to the AC file you wish to extract.

20) Click **Run Macro** under **Macro**. We have already set up macros with some of the most used number of time slices. Select the appropriate macro.

21) Change to path to same as above, the one with the copied AC/DC files in. Click "Continue", and again "Continue". Check path. If not correct, select "Incorrect Directory". If correct path, select "Continue".

22) Check path folder to ensure all asc files (same number as above) are there. You may want to open some of these files with notepad to verify that they include extracted data and are not just blank documents.

23) Repeat this process for each pair of DC and AC files.

B.2 **Using the Spectrum Calculator to Average Data in OPUS**

1) The Spectrum Calculator is used like a regular calculator to perform mathematical operations in OPUS on spectra; each calculation is temporarily saved as the originally selected file. Because of this you must first create a copy of the raw data files to average. If we ever need to reanalyze these files we need a copy of the untouched raw data.

2) Load the desired files as previously explained in **B.1 OPUS**.

3) Select a DC file, and go to "Measure", "Spectrum calculator".

4) Press "C" on the Spectrum Calculator to clear.

5) Press "("

6) Separating each DC file with a "+" double click each file

7) Press ")"

8) Press "/" to divided by the number of spectra.

9) Press "="

10) The filename will now have a red file icon next to it.

11) To save changes, calculation performed in Spectrum Calculator, right click on the filename and press "save." The filename selected will now be the average of all of the other DC files.

12) Unload all other DC files and delete them in the average folder.

13) Repeat steps for AC files.

B.3 **Matlab**

1) Open Matlab, you may want to just minimize OPUS as it is easier to look up information about the files you just extracted and view two and three dimensional plots.

2) If this is the first time you are using Matlab to analyze data there are some scripts called m files used to quickly load and process the files extracted from OPUS. You can do this one of two ways. You should become more familiar with the code that Matlab uses to import data but, because there is a bit of a learning curve it is best to start by using these files.

3) Copy and paste **loaddc.m**, **loadac.m** and unzip **jfit.zip** located in **S:\mcalab\Matlab files** into your **U:\Documents\MATLAB** folder. In addition you may want to copy and paste "msread4.m" for analysis of rapid scan data, which is not discussed in this work.

4) Alternatively you can add the **S:\mcalab\Matlab files** folder into your Matlab search path by going to **Set Path** under **File.**

5) Press **Add Folder**.

6) Find the **S:\mcalab\Matlab files** folder and press **OK**.

7) Press **Close**.

8) Press **Yes**.

9) When you open Matlab you will see many other folders open under the main program. The **Workspace** is where all the scalars, vectors and matrices you are currently working on are listed. The **Command History**

lists a History of all the commands you have typed into the **Command Window**. The **Command Window** is where you type the code that you want Matlab to perform. The **Current Folder** is where Matlab is going to look for any file names you use in the code. If you do not see one of these windows you can add them by checking next to the window you want to show up under **Desktop** in the menu bar. You can also adjust the size and position and unlock these windows from the main program view.

10) Change the current folder to the folder you exported your AC and DC data to using OPUS. Often this is most easily done by copy and pasting into the folder location under **Current Folder**.

11) In the Command Window type **loaddc**, Matlab will ask you the number of time slices? If you do not know how many time slices use OPUS as discussed in step 18 of **B.1 OPUS**. Type in the number and hit enter. This will import a vector called **dc** and create a matrix called **dc3**, note that the scalar called **nslice** which is equal to the number of time slices you entered.

12) In the Command Window type **loadac**. You will be asked to give the length in time of each slice, which you use step 18 of **B.1 OPUS** to look up. Matlab will then ask for the amplification which is 4 unless you are using an amplifier box. You will now have scalars called **tslice** and **amp**, vectors called **freq** and **time** and a matrix called **ac**. The **loadac** m file also calculates a matrix called **absorb** from the **ac** and **dc** matrices and smoothed matrix called **smabs** from **absorb**.

13) The **loadac** m file also saves the previously mentioned scalars, vectors and matrices in the **Workspace** to a file called **matlab.mat** inside the **Current Folder**. If for some reason you need to go back and look at this data again there you can just load this file into Matlab by clicking **Import Data** under **File**. If you need to save your work to continue at another time you can type **save** in the **Command Window** and the current workspace will be saved to **matlab.mat** inside of the **Current Folder**. Alternatively typing open will import **matlab.mat** into the **Workspace** if it exists inside the **Current Folder**.

14) The next steps to analyze your data will depend more upon what experiment you are doing.

15) We want to create a three dimensional plot of the data. This is done by using mesh. Typing **mesh(smabs)** will produce a three dimensional plot of the smoothed absorbance however, the changes in absorption we are dealing with are very small and unlikely to appear on this plot.

16) Using OPUS find the frequency of one of the peaks you want to plot.

17) Typing **min(find(freq<"that frequency"))** will give back the slice in **freq** that corresponds to that frequency, let's say 993 for this tutorial.

18) Using a range of say ±25 freq slices around 993 we can use mesh to plot a much more narrow (in the frequency) range.

19) We also need to add in the time range, using a colon (:) will include all slices. Type **mesh(smabs(:, 968:1018))**. You will have to continue to adjust

the frequency range to include the desired portion of the smoothed absorption.

20) Notice that the labels of the axis are not correct the correct values. To add this dimension to the plot we need to include the **freq** and **time** vectors to the mesh. This is done by adding them before **smabs** in the opposite order they appear in **smabs**, **freq** first followed by **time**, i.e. **mesh(freq(968:1018), time, smabs(:, 968:1018))**. Notice that we included the same frequency slices in **freq** as are in **smabs** and since we include all time slices in **smabs** we do not need to denote which slices to include in **time**. If you only wanted to plot the first 100 time slices you would use **mesh(freq(968:1018), time(1:100), smabs(1:100, 968:1018))**.

21) The mesh command is useful to look at the final processed data but we only want to look at a single frequency trace in order to fit our data to a rate constant. We already know the **freq** slice we want to plot, 993. To plot this frequency slice use the command plot, i.e. **plot(smabs(:, 993)**.

22) Continue to analyze the data by one of two methods: jfit or cftool.

B.4 **Using jfit to Fit Data**

1) Create a vector for the time data, xx=time'. The prime is important because jfit needs a vector of 300 by 1 and time is a vector of 1 by 300. A semicolon at the end of your code will not show each data point, i.e. xx=time';.

2) Create vector for the absorption, yy=smabs(:,993);. We continued to use frequency slice 993 however, this may be different for your data.

3) Jfit requires a string of guess variable to begin fitting your data. This string is composed of (instrument response time constant, ratio of the exponentials, peak decay time constant, offset, time zero) and looks like (107, .5, 290, 0.12, 600).

4) To begin the jfit m file type: [A, B, C] = jfit(xx, yy, 'jmexp',[107, 0.5, 290, 0.12, 600],[1,1,1] into the Command Window. You will need to adjust these parameters until you get an approximate fit. Changing the string of ones at the end to zeroes will auto fit the data but, an approximate fit is needed first.

5) You can also hold a single parameter constant and let the jfit program fit the remaining parameters. To hold the peak decay constant change the second and third "1" to "0". To hold the offset constant, change the first and third "1" to "0" and to hold time zero constant change the first and second "1" to "0".

B.5 **Using cftool to Fit Data**

1) To use Matlab's curve fitting tool we first need to create the time and absorption vectors we want to fit.

2) First plot the data set using plot(time, smabs(:,497)) where 497 is equal to the frequency slice you wish to plot.

3) At the top of the figure window is a row of tools, if you move your curser over the boxes it will revile the tool's name. Select the zoom tool and zoom into time zero of the peak decay (the maximum).

4) Select the data curser tool and select the top of the peak. Note the position in time (for this tutorial we will use 875). It looks like a plus sign on top of a curve.

5) Create a new vector for both time and absorption which only contain the points from there forward. To create the time vector you will use: t=0:tslice:(nslice*tslice -875);. This will create vector that starts at 0 and steps by factors of tslice until it reaches nslice*tslice-875. The absorption vector will be x=smabs(875/tslice:nslice, 497);. This will create a vector along the frequency slice 497 that starts that the peak and goes to the end of the time trace.

6) Now open Matlab's curve fitting tool, type cftool in the Command Window.

7) Press the Data button and select xx as the X Data and yy as the Y Data, name the data set and press Create data set.

8) Press Close.

9) Pressing the Fitting button will open up Fitting window. In the fitting window you will create a new fit equation and use this equation to fit your data.

10) Press New fit, it will auto name your fit as fit 1. Additional fits will increase numerically. Select your data set and Custom Equations as the type of fit.

11) On the right center of the Fitting window will be a button named New, press it. This will allow you to create a customized equation to fit your data.

12) Click the General Equations tab. The equation we want to use (y=a*exp(-b*x) +c) is already typed into the equation field. If not, you will need to enter it.

13) Below the equation is a list of starting guesses at the values of a, b and c. Change these values to 0, 1e-4 and 0.

14) Use the fit options window (click on the Fit options button in the Fitting window) to optimize the R-square of the fit. Most often changing Robust to LAR with any of the Algorithms gives the best fit.

Appendix C Experimental Parameters

C.1 **Bruker IFS 66/S FTIR Settings**

Set Optical Parameters

Source Setting	MIR-Source
Optical Filter Setting	OPEN
Aperture Setting	10 mm
Measurement Channel	Front
Detector	MCT
Scanner Velocity	4; 5.0 Hz
Stablization Delay	0
Delay Before Measurement	0
Gain Switch Gain	ON
Gain Switch Window	300
Signal Gain, Sample	Automatic
Signal Gain, Background	Automatic

Acquisition Parameters

Wanted High Frequency Limit	2600.0
Wanted Low Frequency Limit	1500.0
Low Pas Filter	1; 16 kHz
Acquisition Mode	Single Sided Fast Return
Correlation Test Mode	No

FT Parameters

Start Frequency Limit for File	2600.0
End Frequency Limit for File	1500.0
Phase Resolution	32
Phase Correction Mode	Mertz
Apodization Function	Four Point
Zero Filling Factor	2

Transient Recorder TRS

Device	PAD1232 40MHz SPECTRUM
Number of Time Slices	(depends upon experiment)
Time Resolution	(depends upon experiment)
Coaddition Repeat Count	(usually 10, depends upon exp.)
Delay Before Experiments	0
Trigger Delay	0
Stabilization Delay	40
Experiment Time Base	Always Internal
Experiment Trigger	Internal for DC, rawAC
	Ext. Positive Edge for AC

C.2 **TM 501 Power Module**

Input: 1mΩ 47p F, connected with a T with 50Ω nub.

Gain: 100

Output: ±5V, 20mA Max

C.3 **Stanford Scientific Digital Delay Pulse Generator**

These settings are for general use only. When switching to a new time slice length they should be checked by using the procedures explained in Appendix A.

For experiments with 25 and 50 ns time slices

TRIG settings
- Term = 50 Ω
- EXT
- Threshold = +0.60 V
- Slope = -

DELAY
- A = T + 137.7 μs
- B = A + 100 ns

OUTPUT
- AB
- LOADS = 50 Ω
- TTL

For experiments with 100 ns time slices

TRIG settings
- Term = 50 Ω
- EXT
- Threshold = +0.60 V
- Slope = -

DELAY
- A = T + μs
- B = A + 100 ns

OUTPUT
- AB
- LOADS = 50 Ω
- TTL

For experiments with 2.5us time slices

TRIG settings
- Term = 50 Ω
- EXT
- Threshold = +0.60 V
- Slope = -

DELAY
- A = T + 98.4 μs
- B = A + 100 ns

OUTPUT
- AB
- LOADS = 50 Ω
- TTL

Appendix D OPUS scripts

D.1 **Extract AC**

```
VARIABLES SECTION
FILE <Ffilename> = ScSm/Multiple;
NUMERIC <filenumber> = 1;
STRING <filename> = '1';
FILE <Sfilename> = ScSm;
*STRING <outfile> = '300.asc';
FILE <$ResultFile 1> = Spec;
*STRING <finaldir> = 'U:\Desktop\Work Space for 28 Sep 11 Moco6';
FILE <$ResultFile 2> = Spec;
*STRING <tmpdir> = 'c:\data\TEMP';
BUTTON <IncorrectDirectory> = Goto (FinalDirectory);
*STRING <finalDirBase> = 'U:\Desktop\Work Space for 28 Sep 11 Moco6';
NUMERIC <scanno> = 1;
PROGRAM SECTION
UserDialog ('Enter destination directory', STANDARD,
EDIT:'<finalDirBase>', BLANK, BLANK, BLANK, BLANK, BLANK, BLANK,
BLANK, BLANK, BLANK, BLANK, BLANK, BLANK, BLANK, BLANK);
<scanno>=0;
<scanno>=<scanno>+1;
```

```
PostrunExtract ([<Ffilename>:ScSm/Multiple], {EXS=0, EXE=1, ENT=0,
ENE=10, ECO=0, XTP='<tmpdir>', XTN='0.ext', XTI=1});
<finaldir>='<finalDirBase>';
Label (FinalDirectory);
UserDialog ('FIles will be written to', STANDARD, TEXT:'<finaldir>',
BUTTON:'<IncorrectDirectory>', BLANK, BLANK, BLANK, BLANK, BLANK,
BLANK, BLANK, BLANK, BLANK, BLANK, BLANK, BLANK, BLANK);
<filenumber>=1;
StartLoop (300, 1);
<outfile> = '<filenumber>.asc';
<filename> = '<filenumber>.ext';
[<Sfilename>:ScSm] = LoadFile ('<tmpdir>\<filename>', WARNING |
ABORT);
If (MACROERROR, .EQ., TRUE);
Goto (end);
Endif ();
SaveAs ([<Sfilename>:ScSm], {DAP='<finaldir>', OEX='1', SAN='<outfile>',
COF=64, INP='C:\OPUS_NT\METHODS', IFP='C:\OPUS_NT\METHODS',
INM='DEFAULT', IFN='DEFAULT', DPA=5, DPO=5, SEP=', ', YON=, YON='0',
ADP='1'});
Unload([<Sfilename>] , {});
Delete ('<tmpdir>\<filename>');
```

<filenumber> = <filenumber> + 1;

EndLoop (1);

Label(end);

PARAMETER SECTION

ELF=0;

EAB=0;

ECO=0;

ENE=1;

ENT=0;

XTI=1;

XTN=1.ext;

XTP=F:\TEMP;

EXE=0;

EXS=0;

Appendix E Matlab Scripts

E.1 **loaddc.m**

```
nslice=input('Number of time slices ?')
fid=fopen('dc.asc');
ddd=fscanf(fid,'%f, %f',[2,inf]);
fclose(fid);
dc=ddd(2,:)./nslice;
%We divide by the number of time slices %because when we use OPUS to coadd to %one block it adds all time slices.
dc3=ones(nslice,1)*dc;
clear ans
clear ddd
clear fid
save
%This command saves the Matlab %workspace to the current folder as %matlab.mat
```

E.2 **loadac.m**

```
tslice=input('Length of each slice ?')
amp=input('Amplification ?')
%This is always 4 unless you are %using an amplifier box due to the %preamp in digitizer board, preamp = %4.
for i=1:nslice,
```

```
filename=[num2str(i),'.asc'];
fid=fopen(filename);
ddd=fscanf(fid,'%f,%f',[2,Inf]);
ac(i,:)=ddd(2,:);
fclose(fid);
end
freq=ddd(1,:);
time=0:tslice:((nslice-1)*tslice);
absorb=real(-log(1+ac./(dc3*amp)));
%Some scans end up containing %negative values in parts of the raw
%spectrum and since taking the %natural log of a negative number %results in an
imaginary number we %added 'real' to this calculation
[M,N]=size(freq);
for i=1:N,
smabs(:,i)=smooth(absorb(:,i),7);
end
clear ddd
clear fid
clear ans
clear filename
clear i
clear M
```

```
clear N
save
```

E.3 **jfit.m**

```
function [p1,yfit,F]=jfit(x,y,fstring,iniguess,held)
% JFIT Nonlinear curve fitting and plotting routine with convolutions
%
%      JFIT(X,Y,FSTRING,GUESS) is a front end to the FMINS function
%      of the Matlab Toolkit.  It performs a convolution with a gaussian
%      of width GUESS(1) against the model function FSTRING.  Guess(2)
%      is assumed to be the overall amplitude (this speeds it up) The rest
%      of GUESS is passed to the function file.  JMFIT uses 1024 points
%      for calculating the convolution, because then it can use FFT methods
%      that require a vector of length 2^n.
%
%      FSTRING should be a function of the form
Y=FSTRING(X,GUESSPARMS)
%      where X is the vector for with the function should be evaluated
%      with the functional parameters GUESSPARMS, returning a vector Y.
%
%      JFIT(X,Y,FSTRING,GUESS,HELD) allows the caller to hold certain
%      "guess" values constant.  HELD is a vector of ones and zeroes
%      the same length as GUESS - 2, since it is assumed that fwhm
```

```
%       does not vary, and that amplitude does.  It should look like
%       [1 0 1] (hold the first and third parameter values
%       and fit the second).  If HELD is all ones, then the routine
%       just plots and exits.  This is useful when you are trying to
%       pick starting values.  The function also returns YFIT,
%       the fit curve, if required.
%
%       By default, the convolution is done with 1024 points, this can
%       be edited.  Also, by default, each pass at fitting the data
%       takes 40 iterations (40 iterations between plots), this too
%       can be edited.  Also, the tolerance, i.e., the level after
%       which the routine judges that the fit isn't getting improved
%       by FMINS, can be edited.
%
%       Jason McNeill, Feb 1996, styled after CURVEFITNL, J. Rees

replot=30; %number of iterations before a replot
stptol=.000001; %stop if chisq has improved by less than stptol percent
maxits=20; %max number of loops before quitting
options=zeros([1 14]);
%options(1)=1;
options(14)=replot;
```

```
conpts=1024; %number of points in convolution
global AMP FTx FTif HeldP VaryI Fstring
disp('(you probably dont need to pay attention to warnings)');
if nargin<5,
   error('usage: jfit(x,y,fstring,[fwhm amp params],holdstr)');
end

HeldP=iniguess(3:length(iniguess));
VaryI=find(held==0);
Fstring=fstring;
%save parameters so we can fix select parameters
fwhm=iniguess(1); %full width half-max used to convolve
AMP=iniguess(2);
%now calculate FTx, instrument function FTif
FTx=(0:(conpts-1))/conpts*(max(x)-min(x))*1.1+min(x)-.05*(max(x)-min(x));
% the above assumes 5% padding.  You may want more.
FTif=(jmgauss(FTx-FTx(1),fwhm)+jmgauss(FTx-(FTx(conpts)+FTx(conpts)...
  -FTx(conpts-1)),fwhm)); %fixed as per NHGe's suggestion.
FTif=fft(FTif);
FTif=FTif(:);
%now to define what parameters to send to FMINS
pfm=HeldP(VaryI);
```

```
[F,yfit]=jfit_fun(pfm,x,y);
figure(1)
plot(x,y,'x',x,yfit)
title(['square error=' num2str(F)]),xlabel([sprintf(' %f',[AMP HeldP])])
drawnow
if length(pfm)==0, disp('just plotting, no fitting'),return, end
OF=F*10;
numits=0;
userstop=0;
while numits < maxits & abs((OF-F)/OF)>stptol & userstop==0,
 %repeat until no improvement
 pfm=fminsearch('jfit_fun',pfm,[],x,y);
 numits=numits+1;
 %reconstruct parameters
 p1=HeldP;
 p1(VaryI)=pfm;
 p1=[AMP p1];
 OF=F;
 [F,yfit]=jfit_fun(pfm,x,y);
 %for plotting intermediate results
 figure(2)
 plot(x,y,'x',x,yfit,x,yfit(:)-y(:)-(.15*AMP),'o')
```

```
 title(['square error=' num2str(F)])
 xlabel([sprintf(' %f',[fwhm p1])])
 drawnow
 if numits==1,
   disp('drawing "Quit" button');
%   if get(0,'terminalprotocol') == 'x',
     QuitButton=uicontrol(2,'Style','push','Position',[100 300 100 25],...
       'String','Good Enough','callback','set(2,"userdata","done")');
     drawnow
 %  end
 else
   if length(QuitButton) == 1,
     if isempty(get(2,'userdata')) == 0 %'done'
       set(2,'userdata',[]);
       delete(QuitButton);
       userstop=1;
       QuitButton=[];
     end
   end
 end
end
if length(QuitButton) == 1,
```

```
  delete(QuitButton);
  QuitButton = [];
end
disp('The best fit is: ')
disp(p1)
```

E.4 **jmexp.m**

```
function yval=jmexp(xdat,pp)
%function yval=jmexp2(xdat,[a1,b1,c1,t0])
%
%jmexp2: "bi exponential "
%
%       finds a1*exp(-t/b1)+c1
%


%calculate exponential
yval1=exp(-1/pp(2)*(xdat-pp(4)))+pp(3);
%
%force exponential to zero for negative x
yval=yval1 .* ((xdat-pp(4)) >= 0);
yval=pp(1)*yval/max(yval);
```

```
endfunction yval=jmexp(xdat,pp)
%function yval=jmexp2(xdat,[a1,b1,c1,t0])
%
%jmexp2: "bi exponential "
%
%       finds a1*exp(-t/b1)+c1
%


%calculate exponential
yval1=exp(-1/pp(2)*(xdat-pp(4)))+pp(3);
%
%force exponential to zero for negative x
yval=yval1 .* ((xdat-pp(4)) >= 0);
yval=pp(1)*yval/max(yval);
end
```

Appendix F Sample DFT Input files

F.1 NWCHEM BQX Input File

The addition of "bq" before atoms denotes it as a "ghost atom" in which the only the basis sets from and not the element itself is included in the calculation. A calculation of the entire metal carbonyl ligand complex as well as the metal carbonyl with "ghost" ligand and the ligand with "ghost" metal carbonyl are needed to calculated the strength of the metal-ligand interaction.

```
Title "Total-1-ligand"

Start  Total-1-ligand

echo

Memory 300 mw

charge 0

geometry autosym units angstrom
 bqMo     0.000303823     -1.05982     0.154168
 bqC     1.44091     -1.85905     -1.09457
 bqC     1.48013     -0.307265     1.39282
 bqC     -1.45039     -0.291546     1.41778
```

bqC 0.000731492 -2.74405 1.18234

bqO 2.30807 0.0829237 2.09318

bqO 0.00101627 -3.73372 1.78757

bqO -2.26185 0.107535 2.13222

bqO 2.23902 -2.34260 -1.77262

bqC -1.46945 -1.84590 -1.06887

bqO -2.28359 -2.32351 -1.73188

C 1.22757 1.79646 -1.04441

C 1.20543 2.79101 -0.0603792

C 0.00157943 3.29442 0.446671

C -1.20434 2.79465 -0.0595450

C -1.23024 1.80003 -1.04314

H -0.00378813 0.605613 -2.36362

C -0.00228036 1.28358 -1.51271

C -2.54685 1.36300 -1.64403

H -2.14455 3.19812 0.310955

C 0.00326567 4.34602 1.53088

H 2.14717 3.19158 0.309354

C 2.54236 1.35740 -1.64784

H -3.03438 2.20579 -2.14951

H -2.41489 0.564603 -2.37901

H -3.24105 1.00429 -0.875454

H 0.896134 4.97738 1.47645

H -0.878559 4.99176 1.46510

H -0.00709533 3.88055 2.52538

H 2.40893 0.552865 -2.37582

H 3.02542 2.19726 -2.16252

H 3.24094 1.00686 -0.879518

end

ecce_print /fslhome/rgates2/compute/ecce/Mo/Mo-Met-B3LYP-correct/Total-1-ligand/ecce.out

basis "ao basis" spherical print

H S

18.73113700 0.03349500

2.82539400 0.23472700

0.64012200 0.81375700

H S

0.16127800 1.00000000

O S

5484.67170000 0.00183100

825.23495000 0.01395000

188.04696000 0.06844500

52.96450000 0.23271400

16.89757000 0.47019300

5.79963500 0.35852100

O SP

15.53961600 -0.11077800 0.07087400

3.59993400 -0.14802600 0.33975300

1.01376200 1.13076700 0.72715900

O SP

0.27000600 1.00000000 1.00000000

O D

0.80000000 1.00000000

bqO S

5484.67170000 0.00183100

825.23495000 0.01395000

188.04696000 0.06844500

52.96450000 0.23271400

16.89757000 0.47019300

5.79963500 0.35852100

bqO SP

15.53961600 -0.11077800 0.07087400

3.59993400 -0.14802600 0.33975300

1.01376200 1.13076700 0.72715900

bqO SP

0.27000600 1.00000000 1.00000000

bqO D

0.80000000 1.00000000

C S

3047.52490000 0.00183500

457.36951000 0.01403700

103.94869000 0.06884300

29.21015500 0.23218400

9.28666300 0.46794100

3.16392700 0.36231200

C SP

7.86827200 -0.11933200 0.06899900

1.88128800 -0.16085400 0.31642400

0.54424900 1.14345600 0.74430800

C SP

0.16871400 1.00000000 1.00000000

C D

0.80000000 1.00000000

bqC S

3047.52490000 0.00183500

457.36951000 0.01403700

103.94869000 0.06884300

29.21015500 0.23218400

9.28666300 0.46794100

3.16392700 0.36231200

bqC SP

7.86827200 -0.11933200 0.06899900

1.88128800 -0.16085400 0.31642400

0.54424900 1.14345600 0.74430800

bqC SP

0.16871400 1.00000000 1.00000000

bqC D

0.80000000 1.00000000

Mo S

2.36100000 -0.91217600 0.81392600

1.30900000 1.14774500 -1.13600800

0.45000000 0.60971100 -1.16115900

0.16810000 0.00000000 1.00647900

Mo S

0.04230000 1.00000000

Mo P

4.89500000 -0.09082600 0.00000000

1.04400000 0.70429000 0.00000000

0.38770000 0.39731800 0.00000000

0.49950000 0.00000000 -0.10819400

0.07800000 0.00000000 1.03680900

Mo P

0.02470000 1.00000000

Mo D

2.99300000 0.05270600

1.06300000 0.50039100

0.37210000 0.57940200

Mo D

0.11780000 1.00000000

bqMo S

2.36100000 -0.91217600 0.81392600

1.30900000 1.14774500 -1.13600800

0.45000000 0.60971100 -1.16115900

0.16810000 0.00000000 1.00647900

bqMo S

0.04230000 1.00000000

bqMo P

4.89500000 -0.09082600 0.00000000

1.04400000 0.70429000 0.00000000

0.38770000 0.39731800 0.00000000

```
      0.49950000        0.00000000       -0.10819400
      0.07800000        0.00000000        1.03680900
bqMo    P
      0.02470000        1.00000000
bqMo    D
      2.99300000        0.05270600
      1.06300000        0.50039100
      0.37210000        0.57940200
bqMo    D
      0.11780000        1.00000000
END
ECP
Mo nelec 28
 Mo ul
   0       537.96678100        -0.04694900
   1       147.89829400       -20.20800800
   2        45.73589000      -106.21163000
   2        13.29114700       -41.81073700
   2         4.70599600        -4.20541000
 Mo s
   0       110.29917600         2.80637200
   1        23.20146500        44.51620100
```

```
   2         5.35301300         82.77852300
Mo p
   0        63.29014000          4.94208800
   1        23.33153000         25.86049800
   2        24.67594200        132.47087400
   2         4.64930400         57.31497900
Mo d
   0       104.48399800          3.00545900
   1        66.23072400         26.36378500
   2        39.12831800        183.38492000
   2        13.11644400         98.44530700
   2         3.62802600         22.49013800
END


dft
 mult 1
 direct
 noio
 XC b3lyp
 iterations 200
 mulliken
end
```

task dft energy

F.2 **NWCHEM Input File**

An NWCHEM input file would look like the previous input with the exception that all the atoms that are labeled with a "bq" before them would not.

F.3 **Gaussian 09 Counterpoise Input File**

A copy of the Gaussian 09 input file[1] used to calculate the Basis Set Superposition Error (BSSE) using the "Counterpoise=2" keyword. Note the addition of "(fragment=1)" and "(fragment=2)" directly after each atom to denote the metal carbonyl and ligand portions of the complex.

```
%nprocshared=12
%Mem=200000000
%Chk=W-mesitylene-cp.chk
#P rB3LYP/GEN 5D Pseudo(Read) Opt=(MaxCycle=100 )  Freq=()
SCF=(MaxCycle=100)  Punch=(MO) Pop=() Counterpoise=2

W-mesitylene-cp

0 1 ! charge and multiplicity
 Mo(fragment=1)     0.301670     -0.996306     0.101570
 C(fragment=1)     2.30811     -1.30133     -0.306016
 C(fragment=1)     0.255595     -2.76084     0.980757
 C(fragment=1)     -0.183481     -1.92420     -1.68334
```

C(fragment=1)	-1.70870	-0.752108	0.536549
C(fragment=1)	0.789205	-0.129796	1.91929
O(fragment=1)	-2.82793	-0.658764	0.795900
O(fragment=1)	0.228268	-3.79980	1.49938
O(fragment=1)	3.42083	-1.52660	-0.512726
O(fragment=1)	1.05939	0.308856	2.95042
O(fragment=1)	-0.447153	-2.49252	-2.65213
C(fragment=2)	0.501732	1.50380	-1.32630
C(fragment=2)	-0.891083	1.69033	-1.46304
C(fragment=2)	-1.54411	2.54057	-0.558853
H(fragment=2)	-2.61908	2.68470	-0.650104
C(fragment=2)	-0.844486	3.22122	0.443937
C(fragment=2)	0.546128	3.05176	0.530576
H(fragment=2)	1.10199	3.59812	1.29102
C(fragment=2)	1.23771	2.20941	-0.345121
H(fragment=2)	1.03958	0.948649	-2.09265
C(fragment=2)	-1.65815	1.07454	-2.61128
H(fragment=2)	-2.08092	1.86093	-3.24940
H(fragemnt=2)	-1.01963	0.446285	-3.23870
H(fragment=2)	-2.49718	0.462613	-2.25929
C(fragment=2)	-1.56449	4.12396	1.41870
H(fragment=2)	-1.05806	5.09175	1.51477
H(fragment=2)	-2.59731	4.30911	1.10701

H(fragment=2) -1.59432 3.67424 2.41985

C(fragment=2) 2.74627 2.12293 -0.285273

H(fragment=2) 3.09214 1.73034 0.678539

H(fragment=2) 3.14867 1.48062 -1.07393

H(fragment=2) 3.19179 3.11825 -0.404948

H 0

S 3 1.00

18.73113700 0.03349500

2.82539400 0.23472700

0.64012200 0.81375700

S 1 1.00

0.16127800 1.00000000

****

O 0

S 6 1.00

5484.67170000 0.00183100

825.23495000 0.01395000

188.04696000 0.06844500

52.96450000 0.23271400

16.89757000 0.47019300

5.79963500 0.35852100

SP 3 1.00

```
     15.53961600     -0.11077800      0.07087400
      3.59993400     -0.14802600      0.33975300
      1.01376200      1.13076700      0.72715900
SP  1  1.00
      0.27000600      1.00000000      1.00000000
SP  1  1.00
      0.08450000      1.00000000      1.00000000
D   1  1.00
      0.80000000      1.00000000
****
C  0
S   6  1.00
   3047.52490000      0.00183500
    457.36951000      0.01403700
    103.94869000      0.06884300
     29.21015500      0.23218400
      9.28666300      0.46794100
      3.16392700      0.36231200
SP  3  1.00
      7.86827200     -0.11933200      0.06899900
      1.88128800     -0.16085400      0.31642400
      0.54424900      1.14345600      0.74430800
SP  1  1.00
```

```
     0.16871400      1.00000000      1.00000000
SP  1  1.00
     0.04380000      1.00000000      1.00000000
D   1  1.00
     0.80000000      1.00000000
****
MO  0
S   3  1.00
     2.36100000     -0.91217600
     1.30900000      1.14774500
     0.45000000      0.60971100
S   4  1.00
     2.36100000      0.81392600
     1.30900000     -1.13600800
     0.45000000     -1.16115900
     0.16810000      1.00647900
S   1  1.00
     0.04230000      1.00000000
P   3  1.00
     4.89500000     -0.09082600
     1.04400000      0.70429000
     0.38770000      0.39731800
P   2  1.00
```

```
      0.49950000     -0.10819400
      0.07800000      1.03680900
P   1  1.00
      0.02470000      1.00000000
D   3  1.00
      2.99300000      0.05270600
      1.06300000      0.50039100
      0.37210000      0.57940200
D   1  1.00
      0.11780000      1.00000000
****

MO  0
MO-ECP   3   28
f potential
 5
0      537.96678100     -0.04694900
1      147.89829400    -20.20800800
2       45.73589000   -106.21163000
2       13.29114700    -41.81073700
2        4.70599600     -4.20541000
s-f potential
 3
```

0 110.29917600 2.80637200

1 23.20146500 44.51620100

2 5.35301300 82.77852300

p-f potential

4

0 63.29014000 4.94208800

1 23.33153000 25.86049800

2 24.67594200 132.47087400

2 4.64930400 57.31497900

d-f potential

5

0 104.48399800 3.00545900

1 66.23072400 26.36378500

2 39.12831800 183.38492000

2 13.11644400 98.44530700

2 3.62802600 22.49013800

F.4 **Gaussian 09 Input File**

See Gaussian 09 Counterpoise Input File, they only differ by the addition of the keyword “Counterpoise=2” and “(fragment=N)”.

F.5 **References**

1. Frisch, M. J.; Trucks, G. W.; Schlegel, H. B.; Scuseria, G. E.; Robb, M. A.; Cheeseman, J. R.; Scalmani, G.; Barone, V.; Mennucci, B.; Petersson, G. A.; Nakatsuji, H.; Caricato, M.; Li, X.; Hratchian, H. P.; Izmaylov, A. F.; Bloino, J.; Zheng, G.; Sonnenberg, J. L.; Hada, M.; Ehara, M.; Toyota, K.; Fukuda, R.; Hasegawa, J.; Ishida, M.; Nakajima, T.; Honda, Y.; Kitao, O.; Nakai, H.; Vreven, T.; Jr., J. A. M.; Peralta, J. E.; Ogliaro, F.; Bearpark, M.; Heyd, J. J.; Brothers, E.; Kudin, K. N.; Staroverov, V. N.; Kobayashi, R.; Normand, J.; Raghavachari, K.; Rendell, A.; Burant, J. C.; Iyengar, S. S.; Tomasi, J.; Cossi, M.; Rega, N.; Millam, J. M.; Klene, M.; Knox, J. E.; Cross, J. B.; Bakken, V.; Adamo, C.; Jaramillo, J.; Gomperts, R.; Stratmann, R. E.; Yazyev, O.; Austin, A. J.; Cammi, R.; Pomelli, C.; Ochterski, J. W.; Martin, R. L.; Morokuma, K.; Zakrzewski, V. G.; Voth, G. A.; Salvador, P.; Dannenberg, J. J.; Dapprich, S.; Daniels, A. D.; Farkas, Ö.; Foresman, J. B.; Ortiz, J. V.; Cioslowski, J.; Fox, D. J. *Gaussian 09*, Gaussian, Inc.: Wallingford CT, 2009, 2009.